Title

Monitoring Change in Urban Forests: Remote Sensing Methods for Evaluating Canopy Cover, Removals, and Fire Recovery

ISBN

9798186172796

Author

Pawlak, Camille Christine

Publication Date

2026-07-30

Peer reviewed|Thesis/dissertation

UNIVERSITY OF CALIFORNIA

Los Angeles

Monitoring Change in Urban Forests:
Remote Sensing Methods for Evaluating Canopy Cover, Removals, and Fire Recovery

A dissertation submitted in partial satisfaction of the

requirements for the degree Doctor of Philosophy

in Geography

by

Camille Christine Pawlak

2026

ABSTRACT OF THE DISSERTATION

Monitoring Change in Urban Forests:
Remote Sensing Methods for Evaluating Canopy Cover,
Removals, and Fire Recovery

By

Camille Christine Pawlak
Doctor of Philosophy in Geography
University of California, Los Angeles, 2026
Professor Thomas W. Gillespie, Chair

Urban forests provide essential infrastructure for managing the urban heat island effect. As climate change progresses and many cities get hotter, well-planned urban forests have the potential to prevent hundreds of heat-related deaths annually. Urban trees are difficult to manage because they are continually changing. Trees grow, decline, are planted and removed, and can be vulnerable to rapid and broad-scale loss through development, storms, drought, and fire. Cities are increasingly setting canopy cover goals, including California's statewide goal to increase urban canopy cover by 10% by 2035, but evaluating progress towards that goal requires methods to track and monitor change that can account for uncertainty and identify when and where canopy is lost.

This dissertation develops remote sensing methods to monitor urban forest canopy cover changes, phenology, removal, and post-fire recovery across California. I combine high-resolution National Agriculture Imagery Program aerial imagery, repeated PlanetScope satellite observations, tree inventory data, parcel information, and field and image-based validation to examine urban forest change across multiple spatial and temporal scales.

First, I developed a four-year canopy cover time series for all California census-designated places from 2016 to 2022 using 60-cm aerial imagery and a deep learning classification model. I estimated canopy cover and change using an error-adjusted area estimation, which showed apparent statewide canopy decline was not statistically distinguishable from no change once mapping uncertainty was considered. Residential parcels consistently contained more than half of the canopy within incorporated urban areas, showing that statewide canopy goals will depend on engaging with private landowners.

Second, I combined biannual canopy maps with monthly PlanetScope time series to identify likely individual tree removals and estimate when they occurred. Seasonal PlanetScope data classified broad foliage types with 84% accuracy across two California cities. NAIP-derived canopy change identified removals over a two-year interval with 91.7% accuracy, while a PlanetScope-based classifier identified removals from time-series data with 81.0% accuracy. For 36 of 49 manually validated removals, PlanetScope estimated a removal date within a validated removal window. These results show that aerial imagery can identify canopy loss between image dates, while repeated satellite observations can provide more information about when that loss occurred.

Finally, I applied these methods to measure individual-tree canopy condition after the 2025 Eaton and Palisades fires. I compared post-fire canopy condition with each tree's own pre-fire seasonal baseline to distinguish trees that were returning toward typical condition from those that remained below baseline. Approximately 26.7% of large fire-affected trees were within their pre-fire range by April 2025, increasing to 38.5% by April 2026. Burn severity was the strongest and most consistent predictor of post-fire canopy condition, while foliage type, species, property type, and city were also associated with recovery patterns.

The methods developed in this dissertation make it possible to monitor urban forest change at scales that are difficult to capture through field assessment alone, both through broad spatial scales and frequent temporal updates. Although developed and applied across California, these methods provide an approach that can be extended to other cities with comparable high-resolution imagery, repeated satellite observations, and tree-location data. Cities can use this information to plan urban forest management better and to track whether canopy goals are being met by showing where canopy is being retained, lost, or recovering after disturbance.

The dissertation of Camille Christine Pawlak is approved.

Kyle C. Cavanaugh

Gregory S. Okin

G. Andrew Fricker

Matthew K. Ritter

Thomas W. Gillespie, Committee Chair

University of California, Los Angeles

2026

Table of Contents

List of Figures

List of Tables

Acknowledgments

The quality of this work owes a great deal to the many collaborators and friends who helped along the way. I am deeply grateful to my advisor, Dr. Thomas Gillespie. Tom's encouragement, support, and belief in my ideas made this process possible. Thank you for always finding time for me, being a supportive and friendly face, helping navigate funding applications and paths, and for believing I could do anything while giving me the guidance to get there.

I am grateful to my committee. To Dr. Andrew Fricker, for encouraging me to continue my education, for his generosity, and for his thorough and thoughtful advice throughout. I would not have considered a Ph.D. without him, and he and his family bring a lot of richness into my life. To Dr. Kyle Cavanaugh, my first advisor in undergrad and a continued presence since. Thank you for taking a chance on an aspiring drone pilot, for your ongoing support, and for the collaborative environment you create at UCLA. To Dr. Greg Okin, whose input made my chapter and my scientific thinking so much stronger. Thank you for always making time and pushing my work to be better. To Dr. Matt Ritter, who fostered my love of trees and applied science. Matt makes doing science fun, and I am a better writer, scientist, and person for knowing him. To Dr. Michael Shin and Dr. Park Williams, whose work and presence inspire me to keep growing as a scientist and teacher.

To my fellow graduate students: Lori Berberian, Joan Chimezie, Willow Coleman, Karina Dutko, Dr. Erica Gallerani, Khalil Ganem, Ryan Lam, Emelly Ortiz-Villa, Frida Perez, Lindsey Rogers, and Jordan Steingard. Your friendship and collaboration made this experience rich. To Dr. Kate Cavanaugh, who got me started in remote sensing research and was with me until the end. To Dr. Henry Houskeeper, for being an inspiring scientist and mentor and for believing I had something to contribute to ocean science. To the students who helped with my research: Griffen Guizen, Sara Arnold, Miles Caldwell, Jolina Hor, Cooper Bowen, Ryley Chase, Alexandra Crocker, Jessica Baiza, Katharine McDaniel, April Engelmeier, Kaviya Veerasingam, and Nico Julia. Your help was invaluable. And to the SARP students of summer 2025, who reminded me why I love science and teaching: Molly McKellar, Grace Woerner, Alex Lacayo, Melanie Lin, John Lund, and Logan Jewell. Spending the summer with you was a highlight of my Ph.D.

I am also grateful to many other wonderful mentors and collaborators. To Dr. Jenn Yost, for lifelong mentorship, constant guidance, friendship, and for making everything I do better. To Viscount May Reid-Marr, I can't express my gratitude for your help and support and for the richness you bring to my life. To Dr. Jonathan Ventura, for continuing to support, guide, and share resources long after I left the lab. To Dr. Natalie Love and Kieran Althaus, for their collaboration and many good talks about trees. To Dr. Trevor Ruiz and Dr. Julia Schedler, I would be much worse at statistics without you both. And to the Botany Bros, Dr. Reed, Dr. Jason, Jake, and Ben: thank you for the science, the good vibes, and the calendar submissions.

Beyond science, I am so grateful to my friends and family. To Jacob, who listened to every presentation many times, asked questions, and supported me always. To my parents, for reading everything I write and their unconditional support. To Robyn, Ben, Arielle, and David, for being my family in Los Angeles before it was official. To Robin B., who continually reminds me what really matters in life. To Olivia, my biology inspiration, and Diana, an excellent writer. To my grandparents Dale, Elaine, Nellie, Bob, and Great Uncle Jimmy, who always asked about the trees. My grandfather Dale took a great deal of time teaching me how to spell. Any errors remaining in this dissertation are entirely my own fault.

Camille Christine Pawlak
Department of Geography, University of California, Los Angeles

Education

California State Polytechnic University - San Luis Obispo, San Luis Obispo, CA
M.S., Biological Sciences 2023
University of California - Los Angeles, Los Angeles, CA
B.S. Environmental Science 2016 Minors, Conservation Biology & Geospatial Information Systems & Technologies

Research and Professional Experience

Urban Forest Institute
Staff Scientist September 2023 - July 2026

- Led remote sensing and large geospatial data projects to map, monitor, and analyze urban forest canopy and tree change across California.
- Co-authored CAL FIRE's statewide urban forest canopy plan, contributing canopy analysis, technical guidance, and plan writing in support of California's canopy cover goals.

National Aeronautics and Space Administration
Science Mentor – Ocean Science - Student Airborne Research Program June 2025-August 2025

- Served as a live-in science mentor for a cohort of six students during NASA's Student Airborne Research Program
- Supported students as they developed ocean-science research projects, worked with airborne and satellite data, addressed research challenges, and guided final scientific presentations.

Selected Publications

Houskeeper, H. F., Rosenthal, I. S., Cavanaugh, K. C., **Pawlak, C.**, Trouille, L., Byrnes, J. E. K., Bell, T. W., & Cavanaugh, K. C. (2022). Automated satellite remote sensing of giant kelp at the Falkland Islands (Islas Malvinas). PLOS ONE, 17(1), e0257933. https://doi.org/10.1371/journal.pone.0257933

Kenny, R., Johns, J., **Pawlak, C.**, Fricker, A., Yost, J., & Ritter, M. (2026). Urban trees and structure loss in the 2025 Eaton and Palisades fires. Urban Forestry & Urban Greening, 121, 129470. https://doi.org/10.1016/j.ufug.2026.129470

Love, N. L. R., Nguyen, V., **Pawlak, C.**, Pineda, A., Reimer, J. L., Yost, J. M., Fricker, G. A., Ventura, J. D., Doremus, J. M., Crow, T., & Ritter, M. K. (2022). Diversity and structure in California's urban forest: What over six million data points tell us about one of the world's largest urban forests. Urban Forestry & Urban Greening, 74, 127679. https://doi.org/10.1016/j.ufug.2022.127679

Pawlak, C. C., Love, N. L. R., Yost, J. M., Fricker, G. A., Doremus, J. M., & Ritter, M. K. (2023). California's native trees and their use in the urban forest. Urban Forestry & Urban Greening, 89, 128125. https://doi.org/10.1016/j.ufug.2023.128125

Rendon, P., Love, N., **Pawlak, C**., Yost, J., Ritter, M., & Doremus, J. (2024). Street tree diversity and urban heat. Urban Forestry & Urban Greening, 91, 128180. https://doi.org/10.1016/j.ufug.2023.128180

Saccomanno, V. R., Bell, T., **Pawlak, C**., Stanley, C. K., Cavanaugh, K. C., Hohman, R., Klausmeyer, K. R., Cavanaugh, K., Nickels, A., Hewerdine, W., Garza, C., Fleener, G., & Gleason, M. (2023). Using unoccupied aerial vehicles to map and monitor changes in emergent kelp canopy after an ecological regime shift. Remote Sensing in Ecology and Conservation, 9(1), 62–75. https://doi.org/10.1002/rse2.295

Vannucci, P. F., Kianmehr, A., **Pawlak, C. C.**, Faiola, C. L., Wilson, J. P., & Berelson, W. M. (2025). The role of urban forest composition in modulating summertime air quality in Los Angeles. Science of The Total Environment, 1003, 180715. https://doi.org/10.1016/j.scitotenv.2025.180715

Ventura, J., **Pawlak, C.**, Honsberger, M., Gonsalves, C., Rice, J., Love, N. L. R., Han, S., Nguyen, V., Sugano, K., Doremus, J., Fricker, G. A., Yost, J., & Ritter, M. (2024). Individual tree detection in large-scale urban environments using high-resolution multispectral imagery. International Journal of Applied Earth Observation and Geoinformation, 130, 103848. https://doi.org/10.1016/j.jag.2024.103848

Selected Presentations

2025 February. *Tracking California's Urban Forest: Big Data and Remote Sensing for Smarter Management.* Invited Talk at Climate Solutions Now – Online.

2024 December. *Harnessing Neural Networks for Broad-Scale Urban Canopy Cover Mapping: A Remote Sensing Approach in California.* Presentation at the American Geophysical Union annual conference – Washington D.C.

2024 May. *Open Canopy: mapping California's urban canopy.* Presentation at the Western Chapter of the International Society of Arboriculture annual conference – San Diego, CA.

2023 August. *Data-Driven Urban Forest: How We Can Use Data and Tools to Manage Urban Forests.* Invited talk at the Professional Tree Care Association of San Diego annual meeting – San Diego, CA.

Scholarships, Fellowships, and Awards

2024. Esri User Conference*, 3rd Place, Communicating Science Spatially* - Urban Canopy: Mapping California's Canopy Cover from 2016-2022

2024. Award of Arboriculture Research, Western Chapter of the International Society of Arboriculture (WCISA)

2022-2023. *Graduate Dean Scholarship* UCLA

UCLA Geography Department Service

Colloquium Chair, 2024-2025

Chapter 1. Introduction

As temperatures rise and urban populations grow, urban forests are a critical component of city infrastructure, helping keep cities cool and livable. Urban canopy has been found to reduce local air temperatures by 0.5- 5.8 °C, reducing urban residents' exposure to extreme heat (Yang et al., 2025). Expanding urban canopy cover could prevent hundreds of heat-related deaths annually (McDonald et al., 2024). Planning, managing, and creating policies to support canopy expansion relies on having measurable goals for canopy cover, planting, and tree retention. However, the urban forest undergoes constant change. Urban trees grow, are continually altered by development, face stressors of urban life, and are constantly being planted and replaced. These processes occur at different spatial and temporal scales, from gradual canopy growth or decline in individual trees, to large losses in canopy cover resulting from construction, storm damage, or fire. Urban forest monitoring is often based on periodic inventories or canopy assessments that provide valuable snapshots, but do not keep pace with the rate of change and decision-making in order to effectively manage this valuable resource. This mismatch in pace creates a central problem for urban forest management: cities are increasingly asked to evaluate whether canopy goals are being met, but the methods used to measure canopy change do not match the rate at which the urban forest is changing.

Because of the state's policies, diverse climate and geography, and high number of urban residents, California is an ideal setting to address this problem. California's cities span vast environmental and climatic conditions, including communities along the mild coastal areas, hot inland valleys, high-elevation mountains, and deserts (McPherson et al., 2010). The vast range of conditions supports the diverse number of urban tree species that are planted in California's urban forest, with 562 species documented with over 100 individuals, and some cities with diversity indices rivaling those of the most diverse places on earth, tropical forests (CUFI, 2026; Love et al., 2022). California's urban canopy has been affected by storms, extreme drought, heat events, and expanding urban development over the past decade (California Department of Conservation, 2020; Hulley et al., 2020; Summers et al., 2022; Williams et al., 2022). At the same time, California has committed to increasing urban tree canopy through AB 2251, which establishes a statewide goal of a 10% increase in canopy cover by 2035 (California Urban Forestry Act, 2022) and has released a plan to make that goal a reality (CAL FIRE, 2026). Evaluating progress toward such a goal requires more than estimating canopy cover at a single date or tracking losses every five years. It requires information about where canopy is located, how canopy differs across communities and property contexts, whether observed changes are real, and whether apparent gains or losses reflect persistent change rather than classification uncertainty, image-acquisition variability, or other mapping artifacts which are common errors in remote sensing classification research that examines change over time (Lehrbass & Wang, 2012; Olofsson et al., 2014; Richardson & Moskal, 2014).

Urban canopy cover alone does not fully describe urban forest condition or persistence. Large, mature trees contribute disproportionately to ecosystem services, and their removal cannot be rapidly offset by planting multiple small trees (Doick, 2021; Le Roux et al., 2014; Liang and Huang et al., 2023). Urban trees are also commonly exposed to the same stressors they help mitigate, including heat and water stress. At the same time, additional pressures such as compacted soils, limited rooting space, pollution, pests, physical damage, and development can contribute to decline or mortality (Hilbert et al., 2019; Marchin et al., 2022; Orusa and Mondino, 2021; Percival, 2023). The ecological and social functions of urban forests depend on both how much canopy exists and the condition of individual trees (Allen et al., 2021; Czaja et al., 2020). Canopy persistence is also important: a city may plant thousands of trees, while continuing to lose mature canopy elsewhere, resulting in planting totals or canopy estimates that obscure where trees are being lost and replaced versus where they persist.

These dynamics are especially difficult to observe because urban forest management is fragmented across public and private land. Cities and counties may manage street trees, parks, transportation corridors, and public facilities, but much of the urban forest occurs on residential and other privately managed properties. In California, privately managed trees account for a large share of the urban forest, and the majority of canopy within incorporated urban areas occurs on residential parcels (Chapter 2; Love et al., in press). As a result, statewide canopy goals cannot be achieved only through public planting programs. They also depend on decisions individual homeowners and private organizations make about tree maintenance, removal, replacement, redevelopment, and landscaping on private land. These decisions are not captured in municipal inventories, making it difficult to determine where canopy is being retained, where it is being lost, and whether public investments are keeping pace with removals based on field data alone.

Field-based monitoring remains essential for managing individual trees, but frequent, comprehensive surveys are resource-intensive and typically cover only a portion of municipally managed trees each year (Roman et al., 2020; Van Doorn et al., 2020). Remote sensing can complement field methods by providing repeated observations of canopy extent, vegetation condition, and structural change across all landownerships (Morales-Gallegos et al., 2023; Nazeer et al., 2024; Plowright et al., 2016; Wang et al., 2021). However, urban applications remain challenging because diverse tree species, phenology, planting contexts, and surrounding buildings, pavement, shadows, and other infrastructure can complicate interpretation of spectral signals (Chi et al., 2020; Leisenheimer et al., 2024; Xiao and McPherson, 2005).

Different forms of urban forest change require different monitoring approaches. Statewide canopy change assessment requires high-resolution imagery and explicit treatment of classification uncertainty, particularly when policy targets may be similar in magnitude to mapping error (Morgenroth et al., 2025; Olofsson et al., 2014). In contrast, detecting individual-tree decline or removal requires repeated observations that account for seasonal behavior and distinguish sustained canopy change from normal variation. Tree decline and removal are related but distinct, as trees may be removed because of mortality or canopy damage but also because of development, infrastructure conflicts, storm damage, hazard management, or landowner decisions (Hilbert et al., 2019; Song et al., 2018). This distinction becomes especially important after wildfire, when post-fire canopy condition may include foliage recovery, persistent suppression, delayed decline, or in the case of the urban forest, removal during cleanup and reconstruction (Bär et al., 2019; Goetz et al., 2006; Mitri and Gitas, 2013). A single post-fire canopy map cannot separate these outcomes, particularly in urban environments where biological recovery is shaped alongside management and rebuilding decisions.

This dissertation uses remote sensing to monitor canopy extent, tree condition, removals, and post-fire change across California's urban forests. High-resolution canopy mapping shows where canopy is distributed and how it changes across communities, while repeated satellite imagery tracks individual trees through time. Comparing post-fire condition with each tree's pre-fire baseline further allows recovery and tree loss after a major stressor to be measured.

The central goal of this dissertation is to improve urban forest monitoring across multiple spatial and temporal scales. Chapter 2 develops a statewide, high-resolution canopy time series for California census-designated places and uses error-adjusted area estimates to evaluate canopy extent and change from 2016 to 2022. Chapter 3 uses repeated PlanetScope imagery and individual-tree canopy locations to track tree phenology, condition, and identify likely removals. Chapter 4 measures tree recovery, damage, and loss after the 2025 Eaton and Palisades fires. Together, these chapters show where urban canopy is distributed, how individual trees persist or are lost through time, and how post-fire urban forests change during recovery and reconstruction.

1.1 References

Allen, M. A., Roberts, D. A., & McFadden, J. P. (2021). Reduced urban green cover and daytime cooling capacity during the 2012–2016 California drought. *Urban Climate*, *36*, 100768. https://doi.org/10.1016/j.uclim.2020.100768

Bär, A., Michaletz, S. T., & Mayr, S. (2019). Fire effects on tree physiology. *New Phytologist*, *223*(4), 1728–1741. https://doi.org/10.1111/nph.15871

CAL FIRE. (2026). *Greening the Golden State: Urban Forest Canopy Plan for California [DRAFT]*. https://experience.arcgis.com/experience/74741b4e64024df898c6b254ca226099/page/Review-The-Plan

California Department of Conservation, Division of Land Resource Protection. (2020). *California Farmland Conversion Report, 2016-2020*. Farmland Mapping and Monitoring Program. https://www.conservation.ca.gov/dlrp/fmmp/Documents/fmmp/pubs/2016-2018/FCR/FCR_1618_Report.pdf

California Urban Forest Inventory. (2025). [Computer software]. https://https://datastudio.google.com/reporting/880d448d-de26-48d3-b563-0c6317e456e4/page/jWHKB

California Urban Forestry Act of 1978, 4799.06 et seq. California Public Resources Code (1181 & 1978).

Chi, D., Degerickx, J., Yu, K., & Somers, B. (2020). Urban Tree Health Classification Across Tree Species by Combining Airborne Laser Scanning and Imaging Spectroscopy. *Remote Sensing*, *12*(15), 2435. https://doi.org/10.3390/rs12152435

Czaja, M., Kołton, A., & Muras, P. (2020). The Complex Issue of Urban Trees—Stress Factor Accumulation and Ecological Service Possibilities. *Forests*, *11*(9), 932. https://doi.org/10.3390/f11090932

Doick, K. J. (2021). *Selecting urban trees for ecosystem service provision*. Forest Rsearch. https://www.forestresearch.gov.uk/research/quantification-and-valuation-of-benefits-provided-by-urban-trees/selecting-urban-trees-for-ecosystem-service-provision/

Goetz, S. J., Fiske, G. J., & Bunn, A. G. (2006). Using satellite time-series data sets to analyze fire disturbance and forest recovery across Canada. *Remote Sensing of Environment*, *101*(3), 352–365. https://doi.org/10.1016/j.rse.2006.01.011

Hilbert, D., Roman, L., Koeser, A., Vogt, J., & Van Doorn, N. (2019). Urban Tree Mortality: A Literature Review. *Arboriculture & Urban Forestry*, *45*(5). https://doi.org/10.48044/jauf.2019.015

Hulley, G. C., Dousset, B., & Kahn, B. H. (2020). Rising Trends in Heatwave Metrics Across Southern California. *Earth's Future*, *8*(7), e2020EF001480. https://doi.org/10.1029/2020EF001480

Le Roux, D. S., Ikin, K., Lindenmayer, D. B., Manning, A. D., & Gibbons, P. (2014). The Future of Large Old Trees in Urban Landscapes. *PLoS ONE*, *9*(6), e99403. https://doi.org/10.1371/journal.pone.0099403

Lehrbass, B., & Wang, J. (2012). Urban Tree Cover Mapping with Relief-corrected Aerial Imagery and Lidar. *Photogrammetric Engineering & Remote Sensing*, *78*(5), 473–484. https://doi.org/10.14358/PERS.78.5.473

Leisenheimer, L., Wellmann, T., Jänicke, C., & Haase, D. (2024). Monitoring drought impacts on street trees using remote sensing—Disentangling temporal and species-specific response patterns with Sentinel-2 imagery. *Ecological Informatics*, *82*, 102659. https://doi.org/10.1016/j.ecoinf.2024.102659

Liang, D., & Huang, G. (2023). Influence of Urban Tree Traits on Their Ecosystem Services: A Literature Review. *Land*, *12*(9), 1699. https://doi.org/10.3390/land12091699

Love, N. L. R., Grady, E., Pawlak, C., Ventura, J., Fricker, G. A., Doremus, J., Ritter, M. K., & Yost, J. M. (In Submission). *Most urban trees occur on private land in California: A statewide mapping assessment [In Submission]*.

Love, N. L. R., Nguyen, V., Pawlak, C., Pineda, A., Reimer, J. L., Yost, J. M., Fricker, G. A., Ventura, J. D., Doremus, J. M., Crow, T., & Ritter, M. K. (2022). Diversity and structure in California's urban forest: What over six million data points tell us about one of the world's largest urban forests. *Urban Forestry & Urban Greening*, *74*, 127679. https://doi.org/10.1016/j.ufug.2022.127679

Marchin, R. M., Esperon-Rodriguez, M., Tjoelker, M. G., & Ellsworth, D. S. (2022). Crown dieback and mortality of urban trees linked to heatwaves during extreme drought. *Science of The Total Environment*, *850*, 157915. https://doi.org/10.1016/j.scitotenv.2022.157915

McDonald, R. I., Biswas, T., Chakraborty, T. C., Kroeger, T., Cook-Patton, S. C., & Fargione, J. E. (2024). Current inequality and future potential of US urban tree cover for reducing heat-related health impacts. *Npj Urban Sustainability*, *4*(1), 18. https://doi.org/10.1038/s42949-024-00150-3

McPherson, E. G. (2010). Selecting Reference Cities for i-Tree Streets. *Arboriculture & Urban Forestry*, *36*(5), 230–240. https://doi.org/10.48044/jauf.2010.031

Mitri, G. H., & Gitas, I. Z. (2013). Mapping post-fire forest regeneration and vegetation recovery using a combination of very high spatial resolution and hyperspectral satellite imagery. *International Journal of Applied Earth Observation and Geoinformation*, *20*, 60–66. https://doi.org/10.1016/j.jag.2011.09.001

Morales-Gallegos, L. M., Martínez-Trinidad, T., Hernández-de La Rosa, P., Gómez-Guerrero, A., Alvarado-Rosales, D., & Saavedra-Romero, L. D. L. (2023). Tree Health Condition in Urban Green Areas Assessed through Crown Indicators and Vegetation Indices. *Forests*, *14*(8), 1673. https://doi.org/10.3390/f14081673

Morgenroth, J., Doick, K., Hauer, R., Locke, D. H., Barona, C. O., Roman, L. A., Conway, T. M., Dobbs, C., Duinker, P., Gulsrud, N. M., Jim, C. Y., Koeser, A. K., Landry, S., Livesley, S., Nesbitt, L., Shackleton, C. M., Tan, P. Y., & Yang, J. (2025). Urban tree cover targets: The good, the bad and the SMART. *Urban Forestry & Urban Greening*, *112*, 128979. https://doi.org/10.1016/j.ufug.2025.128979

Nazeer, M., Wong, M. S., Yu, X., Kwok, C. Y. T., Peng, Q., & Dai, Y. (2024). Urban tree health assessment using multifaceted remote sensing datasets: A case study in Hong Kong. *Remote Sensing Applications: Society and Environment*, *36*, 101347. https://doi.org/10.1016/j.rsase.2024.101347

Olofsson, P., Foody, G. M., Herold, M., Stehman, S. V., Woodcock, C. E., & Wulder, M. A. (2014). Good practices for estimating area and assessing accuracy of land change. *Remote Sensing of Environment*, *148*, 42–57. https://doi.org/10.1016/j.rse.2014.02.015

Orusa, T., & Mondino, E. (2021). Exploring Short-Term Climate Change Effects on Rangelands and Broad-Leaved Forests by Free Satellite Data in Aosta Valley (Northwest Italy). *Climate*, *9*(3), 47. https://doi.org/10.3390/cli9030047

Percival, G. C. (2023). Heat tolerance of urban trees − A review. *Urban Forestry & Urban Greening*, *86*, 128021. https://doi.org/10.1016/j.ufug.2023.128021

Plowright, A. A., Coops, N. C., Eskelson, B. N. I., Sheppard, S. R. J., & Aven, N. W. (2016). Assessing urban tree condition using airborne light detection and ranging. *Urban Forestry & Urban Greening*, *19*, 140–150. https://doi.org/10.1016/j.ufug.2016.06.026

Richardson, J. J., & Moskal, L. M. (2014). Uncertainty in urban forest canopy assessment: Lessons from Seattle, WA, USA. *Urban Forestry & Urban Greening*, *13*(1), 152–157. https://doi.org/10.1016/j.ufug.2013.07.003

Roman, L. A., Van Doorn, N. S., McPherson, E. G., Scharenbroch, B. C., Henning, J. G., Östberg, J. P. A., Mueller, L. S., Koeser, A. K., Mills, J. R., Hallett, R. A., Sanders, J. E., Battles,

J. J., Boyer, D. J., Fristensky, J. P., Mincey, S. K., Peper, P. J., & Vogt, J. (2020). *Urban tree monitoring: A field guide* (NRS-GTR-194; p. NRS-GTR-194). U.S. Department of Agriculture, Forest Service, Northern Research Station. https://doi.org/10.2737/NRS-GTR-194

Song, X. P., Tan, P. Y., Edwards, P., & Richards, D. (2018). The economic benefits and costs of trees in urban forest stewardship: A systematic review. *Urban Forestry & Urban Greening*, *29*, 162–170. https://doi.org/10.1016/j.ufug.2017.11.017

Summers, J. K., Lamper, A., McMillion, C., & Harwell, L. C. (2022). Observed Changes in the Frequency, Intensity, and Spatial Patterns of Nine Natural Hazards in the United States from 2000 to 2019. *Sustainability*, *14*(7), 4158. https://doi.org/10.3390/su14074158

Van Doorn, N. S., Roman, L. A., McPherson, E. G., Scharenbroch, B. C., Henning, J. G., Östberg, J. P. A., Mueller, L. S., Koeser, A. K., Mills, J. R., Hallet, R. A., Sanders, J. E., Battles, J., Boyer, D. J., Fristensky, J. P., Mincey, S. K., Peper, P. J., & Vogt, J. M. (2020). *Urban tree monitoring: A resource guide* (PSW-GTR-266; p. PSW-GTR-266). U.S. Department of Agriculture, Forest Service, Pacific Southwest Research Station. https://doi.org/10.2737/PSW-GTR-266

Wang, Z., Fan, C., & Xian, M. (2021). Application and Evaluation of a Deep Learning Architecture to Urban Tree Canopy Mapping. *Remote Sensing*, *13*(9), 1749. https://doi.org/10.3390/rs13091749

Williams, A. P., Cook, B. I., & Smerdon, J. E. (2022). Rapid intensification of the emerging southwestern North American megadrought in 2020–2021. *Nature Climate Change*, *12*(3), 232–234. https://doi.org/10.1038/s41558-022-01290-z

Xiao, Q., & McPherson, E. G. (2005). Tree health mapping with multispectral remote sensing data at UC Davis, California. *Urban Ecosystems*, *8*(3–4), 349–361. https://doi.org/10.1007/s11252-005-4867-7

Yang, X., Li, B., Li, N., & Ma, X. (2026). A study of the cooling effect of urban trees: Influencing factors, assessment methods, planning strategies, and impacts. *Theoretical and Applied Climatology*, *157*(1), 31. https://doi.org/10.1007/s00704-025-05904-2

Chapter 2. Mapping California's Urban Forest at Scale: An Error-Adjusted Canopy Time Series for Monitoring Change

Abstract

Statewide tracking of urban tree canopy change is essential for evaluating progress toward policy targets, but detecting real change requires both high-resolution mapping and rigorous uncertainty estimation. We produced a four-year canopy cover time series for all California census-designated places using 60-cm NAIP aerial imagery and a U-Net deep learning model trained with semi-automated LiDAR-derived labels and manually annotated tiles. Canopy cover and change were estimated using stratified, error-adjusted area estimation, enabling comparisons across years. Statewide canopy cover showed a modest negative trend from 2016 to 2022 (Sen's slope: -0.60% per year). However, confidence intervals included zero across all groups and climate zones, indicating that trends were not statistically distinguishable from no change. Urban canopy cover was consistently lower than non-urban canopy by approximately six percentage points, and canopy cover was highest in the Northern California Coast and lowest in the Southwest Desert. Residential parcels accounted for 55-56% of canopy within incorporated urban areas across all years, indicating that statewide canopy increase goals will require engagement with private landowners. Error adjustment substantially altered canopy estimates relative to raw pixel-count totals, with direct implications for AB 2251 canopy tracking where baselines and targets drawn from unadjusted maps may not reflect true canopy extent. This open-source workflow is transferable to future NAIP acquisition years and other U.S. states, providing a scalable framework for long-term urban forest monitoring.

2.1 Introduction

California has committed to increasing urban tree canopy, but measuring progress toward that goal is not straightforward. Even high-resolution canopy maps are predictions, and small apparent changes in canopy cover can fall within the range of classification error, acquisition variability, or image misalignment (Lehrbass & Wang, 2012; Olofsson et al., 2014; Richardson & Moskal, 2014). This creates a central challenge for urban forest monitoring: canopy targets are often expressed as simple percent increases (Morgenroth et al., 2025), while the datasets used to evaluate them rarely propagate uncertainty into change estimates.

Urban tree canopy provides important ecological and social benefits, including cooling, carbon sequestration, reductions in air pollution and stormwater runoff, and associations with physical and mental health (Cavender-Bares et al., 2022; Giacinto et al., 2021; Hwang et al., 2023; Livesley et al., 2016). Over the past decade, California's urban tree canopy has been affected by storms, extreme droughts, heat events, and expanding urban development (California Department of Conservation, 2020; Hulley et al., 2020; Summers et al., 2022; Williams et al., 2022). Within this context, California's recent AB 2251 requires a statewide 10% increase in canopy cover by 2035 (California Urban Forestry Act, 2022). Tracking progress toward that goal requires monitoring approaches that can distinguish real canopy gains and losses from apparent changes caused by mapping errors and differences in image acquisition.

High-accuracy canopy maps are increasingly created using high-resolution optical imagery, LiDAR data, and deep learning, often with reported accuracies in the 90-97% range (Akın et al., 2023; Guo et al., 2023; Martins et al., 2021; Timilsina et al., 2020; Velasquez-Camacho et al., 2023; Wang et al., 2021; Zhang et al., 2022). Aerial imagery from programs such as the National Agricultural Imagery Program (NAIP) provides sub-meter imagery statewide and can support fine-scale canopy monitoring. However, canopy cover maps are still often produced at the city scale or for single time points, and existing multi-year analyses often rely on mapped pixel totals without propagating classification error into area estimates. This is especially important when canopy goals are small. In some cities, canopy increase targets are as small as 4% (Morgenroth et al., 2025), meaning apparent change may be similar in magnitude to mapping uncertainty.

To track urban canopy change in California, we produced a four-year (2016, 2018, 2020, 2022) 60-cm canopy cover time series for all California census-designated places (CDPs) and estimated canopy cover and change using error-adjusted areas. This research develops a scalable, open-source workflow for creating canopy cover maps and uses that methodology to answer three primary research questions: (1) How did canopy cover across California CDPs change from 2016 to 2022? (2) How do canopy levels and trends vary across climate zones and between urban and non-urban portions of CDPs? and (3) Within incorporated urban areas, how is canopy distributed across parcel/property types, and is that distribution stable through time? All code, training data, model checkpoints, and canopy raster products are publicly available (GitHub: https://github.com/camipawlak/canopy_cover; Dryad: 10.5061/dryad.rjdfn2zs9).

2.2 Methods

2.2.1 Study Site

California spans approximately 423,970 km^2 and is home to over 39 million people, with 94% of the population residing in urban areas (U.S. Census Bureau, 2020b). The state is divided into six distinct climate zones: Southwest Desert, Northern California Coast, Southern California Coast, Inland Valleys, Inland Empire, and Interior West (McPherson et al., 2010, Figure 2.2). These zones vary in temperature, precipitation, and vegetation. This study focuses on all CDPs in

California, which collectively cover an area of 39,032 km^2 (U.S. Census Bureau, 2020a; Figure 2.2). CDPs are populated areas identified by the U.S. Census Bureau for statistical purposes (U.S. Census Bureau, 2016; U.S. Census Bureau, 2018; U.S. Census Bureau, 2020a; U.S. Census Bureau, 2022). For each year, the extent of the raster data is the extent of that year's CDP (2016: 37,911.90 km^2, 2018: 38,014.60 km^2, 2020: 39,032.35 km^2, 2022: 39,074.13 km^2). Unlike many previous datasets and studies that focus only on urban areas (CAL FIRE, 2025; Kropp, 2024; MacFaden et al., 2012; Zhang et al., 2022), this research also includes non-urban CDPs.

2.2.2 Approach

We conducted a two-step process to generate an urban canopy cover map for all census-designated places in California. First, we developed a general model by creating automated training data using LiDAR-derived canopy height models (CHMs) and NAIP imagery. A U-Net (Ronneberger et al., 2015) neural network was trained on these data, with training data stratified to match the proportion of urban areas in each climate zone. Second, we used transfer learning (Bozinovski & Fulgosi, 1976) to fine-tune the LiDAR-based model once for each climate zone and statewide using manually annotated training data. The best fine-tuned model was applied to the CDPs within each climate zone across California using imagery from 2016, 2018, 2020, and 2022. Mapped canopy areas were error-adjusted using accuracy assessments (Figure 2.1).

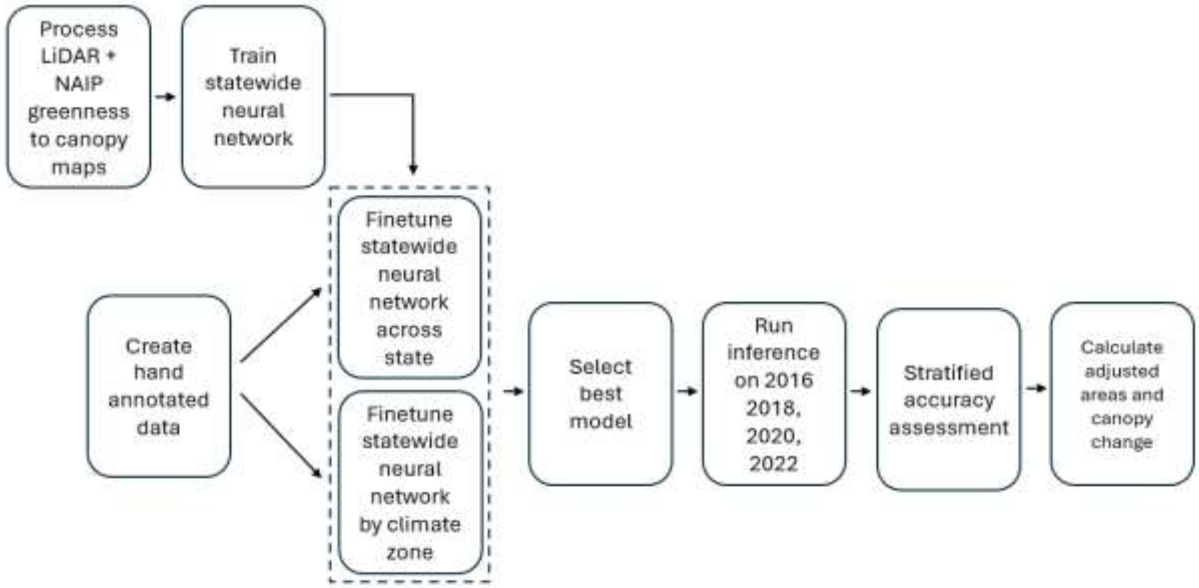

Figure 2.1 Workflow for generating California canopy cover maps and estimating canopy change from 2016 to 2022. LiDAR-derived canopy height models were paired with NAIP imagery and an NDVI-based filter to create semi-automated canopy masks for training a statewide U-Net model. Manually annotated tiles were used for two fine-tuning strategies: (1) statewide fine-tuning across all climate zones and (2) climate-zone-specific fine-tuning. The best-performing model was selected and applied to NAIP imagery from 2016, 2018, 2020, and 2022. A stratified reference sample was used to assess accuracy and to compute error-adjusted canopy area estimates and confidence intervals for canopy cover and change.

2.2.3 Data Sources

U-Net inputs were NAIP multispectral imagery, collected approximately every two years. In California, NAIP imagery has been available at 60-cm resolution since 2016. LiDAR data was sourced from the USGS 3D Elevation Program (3DEP) and included datasets for 28 cities across California from 2016 to 2021 (Figure 2.2, Appendix 2C). LiDAR datasets varied in density and coverage, ranging from 3.47 to 38.44 points per m^2.

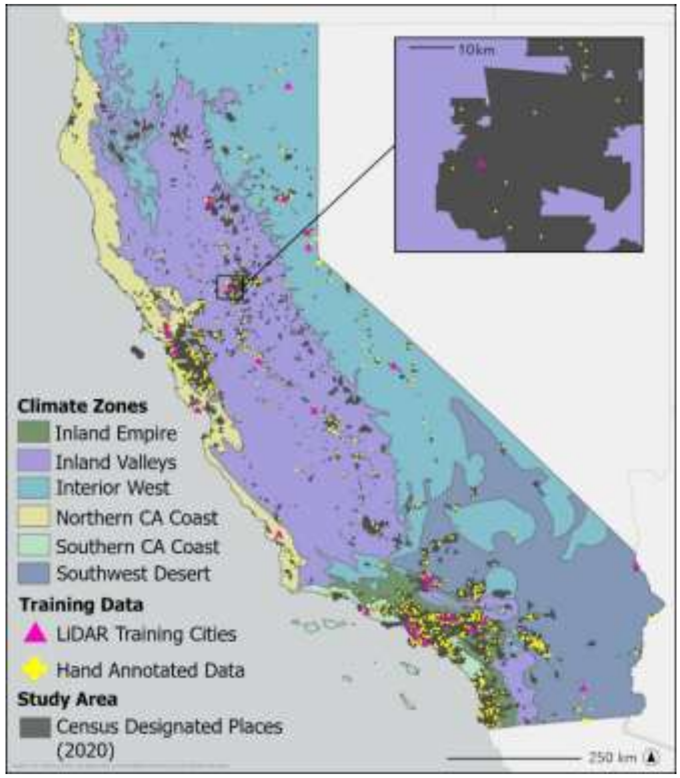

Figure 2.2 The climate zones of California, CDPs (2020), and locations of LiDAR training cities and manually annotated tiles.

2.2.4 LiDAR-Generated Training Data

In the first stage of model development, we created a semi-automated dataset of canopy-cover labels using USGS LiDAR data. Previous studies (Weinstein et al., 2019) have demonstrated the efficiency of automated training data for canopy cover prediction, which informed our methods.

Cities were selected to provide training data to represent typical urban areas within each of California's six climate zones (Figure 2.1, Appendix 2C). For each selected city, we processed the LiDAR point cloud data using the Point Data Abstraction Library (PDAL) to generate Digital Surface Models (DSMs), Digital Terrain Models (DTMs), and Canopy Height Models (CHMs). DSMs were created by filtering first-return points to capture surface elevations, including vegetation and structures, and interpolating the data using Inverse Distance Weighting. DTMs were generated by isolating ground points and interpolating bare-earth elevations using Delaunay triangulation to create a continuous surface. The CHM was calculated by subtracting the DTM from the DSM.

The resulting CHMs were paired with NAIP imagery from the nearest available year (all data within one year of the NAIP flyover). We classified all areas with heights ≥ 1.8 m as canopy (value = 1) and other areas as non-canopy (value = 0). Because urban areas include structures such as buildings, which were often misclassified as canopy, we refined the labels using Normalized Difference Vegetation Index (NDVI) values derived from NAIP imagery. Pixels with NDVI ≤ 0.05 were reclassified as non-canopy. This threshold was selected based on visual inspection of training data across multiple cities, where values at or below this level consistently corresponded to non-vegetated surfaces such as pavement, rooftops, and bare soil, with no clear cases of tree canopy falling below this value. This semi-automated process produced 30,458 training masks (448 × 448 pixels) across the state, reducing time and cost compared to manual annotation.

2.2.5 Manually Annotated Training Data

We created 645 manually annotated tiles from 2020 NAIP imagery to fine-tune models statewide and by climate zone (Figure 2.2). Tiles were 153.6 × 153.6 m, or 256 × 256 pixels. Initial tile locations were selected using stratified random sampling by climate zone, with allocation proportional to CDP area. Additional tiles were added iteratively to improve regional representation, resulting in 83-134 tiles per climate zone. Annotators delineated tree canopy using true-color and false-color infrared imagery. Uncertain areas, especially tree-shrub boundaries, were checked using Google Street View and visual cues such as shadows, crown structure, and canopy overlap with buildings. Each tile was annotated by one person and reviewed by a second annotator for consistency. The goal of the annotations was to include only canopy over 1.8 m in height, as best as possible, using visual imagery.

2.2.6 Imagery Pre-Processing

The NAIP imagery inputs consisted of four spectral bands: red, green, blue, and near-infrared, with a resolution of 60 cm, as well as a fifth band, the Normalized Difference Vegetation Index (NDVI), to help make vegetation stand out. NDVI was calculated using the formula:

$$NDVI = (NIR - Red)/(NIR + Red + 10^{-8})$$

The small constant 10^{-8} was included to prevent division by zero. NDVI values, which theoretically range from −1 to 1, were linearly scaled to 0-255 by applying the transformation $(NDVI + 1) \times 127.5$, mapping −1 to 0 and +1 to 255. The four NAIP spectral bands were then independently normalized to 0-255 using minimum-maximum normalization, with bounds pre-computed from the full California NAIP dataset for 2020 and applied as fixed values (red: 0-222, green: 0-221, blue: 0-224, NIR: 0-216). The processed data, including all five bands, was divided into 448 × 448-pixel tiles for those paired with LiDAR-generated masks and 256 × 256-pixel tiles for the manually annotated data. These tiles were split into training (80%), testing (10%), and evaluation (10%) datasets for model development.

2.2.7 Model Architecture and Training

A convolutional neural network with a U-Net architecture (Ronneberger et al., 2015) was chosen due to its ability to handle complex decision boundaries, particularly in distinguishing between trees, shrubs, and grass patches, which can have similar visual characteristics in aerial imagery. U-Net has been widely used in segmentation tasks, including tree canopy segmentation (Martins et al., 2021; Ronneberger et al., 2015; Wang et al., 2021), and has consistently outperformed or matched other deep learning architectures for tree canopy segmentation.

The model used a U-Net encoder-decoder architecture with skip connections and a ResNet-34 backbone (He et al., 2015). The decoder used four transposed-convolution blocks, and the final 1×1 convolution produced a per-pixel canopy probability map. These probabilities were converted to a binary output by applying a threshold of 0.65, selected based on visual inspection of validation outputs, which balanced commission and omission errors in canopy classification. Values above the threshold were classified as canopy (1) and those below as non-canopy (0). To handle no-data regions, areas where all input bands were zero were excluded and assigned a no-data value (255).

A masked binary cross-entropy loss function was used to optimize the model, applied to logits directly with pixels assigned a no-data value of 255 excluded from the loss calculation. The model was implemented using PyTorch and trained with the AdamW optimizer (Loshchilov & Hutter, 2019), with a learning rate of 0.0001 and a batch size of 16. Training was conducted on two Tesla V100 GPUs.

The SLM was trained for 150 epochs on 24,366 LiDAR-derived training chips, with the best checkpoint saved based on validation loss. This checkpoint was then used as the starting point for two fine-tuning runs. The SFT was trained for 147 epochs on 516 manually annotated tiles drawn from across all climate zones. The RFT produced one model per climate zone, each trained on region-specific manually annotated tiles; training set sizes ranged from 65 to 107 tiles per zone, and the number of epochs at the best checkpoint varied by zone (14- 89 epochs), reflecting differences in dataset size and convergence rate (Table 2.1). All fine-tuning used end-to-end training with data augmentation, including random 90° rotations (0°, 90°, 180°, 270°) and random horizontal flips. For all models, the best checkpoint was selected based on validation loss, alongside visual inspection of inference outputs to catch spatial artifacts or boundary errors not captured by loss alone.

Table 2.1 Number of epochs used to train selected versions of models, and number of tiles per model used for training (after 80/10/10 split for training, testing, and validation).

Model	Epochs	Training tiles
SLM	150	24,366
SFT	147	516
RFT - Inland Empire	28	85
RFT - Inland Valleys	26	99
RFT - Interior West	82	65
RFT - NorCal Coast	14	80
RFT - SoCal Coast	23	107
RFT - SW Desert	89	77

2.2.8 Accuracy Analysis and Area Estimation

We evaluated 2020 model performance using user's accuracy, producer's accuracy, and F1 scores on manually annotated data withheld from training. Validation was assessed on both the statewide and fine-tuned models. To assess the accuracy of change over time and the accuracy of each year's output, we took a stratified random sampling approach based on Olofsson et al. (2014) with the classes "canopy" and "non-canopy" as classification strata, and "urban" and "non-urban" (in 2020) as geographic strata. Urban areas were defined using yearly NLCD products developed areas (Dewitz et al., 2019). Within each CDP, we converted areas of low, medium, and high developed intensity into polygons, then filled all holes smaller than 1 km2 to ensure that urban parks were included as "urban." The remaining CDPs were classified as non-urban. Prior to the adjustment of the area, we summed mapped canopy area into groups by assigning CDPs into urban and non-urban areas, then assigning climate zones to each urban and non-urban section of the CDP. We removed all water bodies and coastline from the CDPs prior to total area calculations (areas listed in section 2.1 are for CDPs prior to water removal). The reference sample was placed using 2020 urban boundaries; for area estimation in each year, urban and non-urban areas were re-defined using that year's NLCD product to compute year-specific mapped-area weights.

Initially, 1,200 points were randomly placed within 2020 urban areas (600 on mapped canopy, 600 on mapped non-canopy). Then, 500 points were placed in non-urban areas with a 50/50 split for mapped canopy and non-canopy. Each sample point was assigned a reference classification based on the pixel it fell within; pixels were labeled by a human as canopy or non-canopy based on the dominant cover across the full pixel extent. Ambiguous pixels were labeled as NA and excluded from the analysis. Each point was validated once per year against NAIP imagery (6,800 unique validations were completed in this process). Unclear points were checked with Google Street View where available and classified as NA if uncertainty remained. This most frequently happens at the edge of a tree canopy, on shrubs where height could not be estimated, or in very dark shadows. To ensure accuracy could be assessed by climate zone, additional points were generated using simple random sampling (Python random module) for canopy and non-canopy within each climate zone to ensure no class was too rare, following Olofsson et al. (2014), who recommend increasing sample sizes for rare classes to support meaningful accuracy estimates. A minimum of 50 points per canopy and non-canopy class per climate zone was created (Appendix 2A).

To estimate canopy area for each year, we applied stratified, error-adjusted area estimation to our mapped values, following Olofsson et al. (2014). For each year, we defined two map strata based on the classified raster: canopy (mapped class 1) and non-canopy (mapped class 0). Within each reporting domain (statewide, urban vs non-urban, and climate zone), we calculated the mapped-area weight for each stratum as:

$$W_h = \frac{A_{h,map}}{A_{domain,map}}$$

where $A_{h,map}$ is the mapped area in stratum *h* and $A_{domain,map}$ is the total mapped area in that domain.

We then summarized the reference sample into error matrices for canopy and non-canopy in each domain. Reference NAs were counted for reporting but excluded from all further estimation steps; only reference points of 0 and 1 were used for accuracy calculations. Error-matrix cell counts were converted to estimated area proportion using a stratified estimator:

$$\hat{p}_{hj} = W_h \left(\frac{n_{hj}}{n_h}\right) \text{ and } \hat{p}_j = \sum_h \hat{p}_{hj}$$

where n_{hjj} is the count of reference samples in class *j* within the mapped stratum *h*, and n_h is the total number of reference points in that stratum. Overall accuracy, user's accuracy, and producer's accuracy were computed from the estimated error matrix proportions, standard errors, and 95% confidence intervals for area proportions and error-adjusted areas were calculated using the stratified variance estimators in Olofsson et al. (2014) (Appendix 2A). This approach corrects for classification error that would otherwise cause pixel-count totals to over- or underestimate true canopy area. Using adjusted areas, we compared statewide canopy percent across years, across urban and non-urban area, and across climate zones.

To understand potential drivers of canopy change, we also summed canopy area by parcel type to assess where canopy change is happening over time. Parcel data and property type classification are only for incorporated urban areas, and the layer is from 2013 (McPherson et al., 2017). For each parcel type (Residential (Muti-family, MF), Residential (Single Family, SF), Commercial/Industrial/Institutional, Open Space, Transportation Corridors, Water, and Unclassified) we built an error matrix from points in that parcel class, again excluding NAs, estimated the probability that mapped canopy and non-canopy were truly canopy, and applied the Olofsson et al. (2014) methods of adjustment described above to estimate true canopy area. We then converted our areas to the percent of the statewide canopy for each parcel type, with uncertainty summarized as 95% intervals (Appendix 2B).

2.2.9 Change Analysis

We compared adjusted canopy area estimates across the time series statewide; in urban and non-urban areas; within each climate zone; between adjacent years in each climate zone; and within urban and non-urban areas in each climate zone. Differences (for example, urban minus non-urban within a year) were evaluated with a Wald Z-test using the estimated difference in error-adjusted canopy cover divided by the standard error of that difference. We used two-sided tests with $\alpha=0.05$. To assess change over the broader time series, we calculated Sen's slope using the median of all pairwise slopes between years. Uncertainty bounds for Sen's slope were approximated using the empirical distribution of pairwise slopes (2.5th- 97.5th percentiles). Sen's slope was computed from error-adjusted canopy estimates.

2.3 Results

2.3.1 Model Accuracy 2020

Using 2020 NAIP manually annotated data withheld from the training dataset, we compared the model accuracy of the statewide LiDAR model (SLM), the regionally fine-tuned model (RFT), and the statewide fine-tuned model (SFT) across climate zones. In all cases, the SFT model had the highest F1 score and producer's accuracy (Table 2.2). User's accuracy was also the highest for SFT, except in the case of Inland Valleys, where it was slightly lower than the RFT model (Table 2.2).

Table 2.2 User's accuracy, producer's accuracy, and F1-score comparison for the Statewide LiDAR Model (SLM), Regional Fine-Tuned Model (RFT), and Statewide Fine-Tuned Model (SFT). The metrics demonstrate the performance of each model in predicting canopy cover, with RFT capturing regional specificity, SFT benefiting from broader manually annotated data, and SLM serving as the baseline trained on statewide LiDAR-derived data. These numbers are based on 2020 imagery.

Region	Model	User's	Producer's	F1
Southern California Coast	SLM	0.80	0.68	0.73
	RFT	0.89	0.76	0.82
	SFT	**0.91**	**0.83**	**0.87**
Inland Empire	SLM	0.82	0.75	0.78
	RFT	0.90	0.77	0.83
	SFT	**0.91**	**0.86**	**0.88**
Northern California Coast	SLM	0.89	0.60	0.72
	RFT	0.91	0.77	0.84
	SFT	**0.93**	**0.87**	**0.90**
Inland Valleys	SLM	0.89	0.53	0.67
	RFT	**0.92**	0.81	0.86
	SFT	0.91	**0.87**	**0.89**
Interior West	SLM	0.80	0.71	0.75
	RFT	0.86	0.84	0.85
	SFT	**0.92**	**0.88**	**0.90**
Southwest Desert	SLM	0.77	0.71	0.74
	RFT	0.89	0.75	0.82
	SFT	**0.95**	**0.87**	**0.91**

The highest statewide fine-tuned F1 score was for the Southwest Desert (F1 = 0.91) and the lowest for the Southern California Coast (F1=0.87) (Table 2.2). Among regional models, the highest F1 was for the Inland Valleys (F1=0.86), and the lowest F1 was a tie for the Southern California Coast and Southwest Desert (F1=0.82) (Table 2.2). Figure 2.3 shows example model outputs.

Figure 2.3 Example model outputs for canopy segmentation on NAIP imagery. The top panel shows the NAIP image tile, with a corresponding bottom panel with transparent model outputs overlaid together. Left: The statewide fine-tuned model (blue) overlaid under the regionally fine-tuned model (yellow). RFT has more artifacts, and under predicts canopy, but is sometimes more precise than SFT. Right: SFT (blue) overlaid on top of the output from the statewide LiDAR model (SLM, orange). SLM produces artifacts on rooftops and tends to overpredict canopy in shadows and beyond the extent of the tree compared to SFT.

2.3.2 Extrapolation to other years

Model accuracy was highest in 2020, the year the training data was created. However, model accuracy remained high across the three other applied years, with overall accuracy at or above 0.90 (Table 2.3).

Table 2.3 Error-adjusted canopy area and cover estimates for each year across all California CDPs, with accuracy metrics and urban/non-urban comparisons. Canopy area (km²) and canopy cover percent are reported with 95% confidence intervals. Overall accuracy, user's accuracy (UA), and producer's accuracy (PA) for the canopy class are reported with standard errors and are based on total reference points (excluding NAs) for that year. Urban and non-urban canopy cover percentages are error-adjusted estimates. Δ reports the difference in canopy cover percentage points between urban and non-urban areas within each year, with 95% confidence interval, Wald Z statistic, and p-value from a two-sided test marked with * for below 0.01.

Year	*Canopy Area (km2, 95% CI)*	*Canopy Percent (95% CI)*	*Overall Accuracy (SE)*	*UA (canopy, SE)*	*PA (canopy, SE)*	*Total Ref. Points*	*# Non canopy Points*	*# Canopy Points*	*Urban (%)*	*Non-Urban (%)*	*Δ %*	*95% CI (Δ)*	*z*
2016	9450.8 (8852.6-10048.9)	24.89 (23.31-26.46)	0.903 (0.008)	0.956 (0.009)	0.640 (0.020)	1615	978	637	21.8	27.9	-6.1	-9.5 to -2.7	-3.56*
2018	9188.4 (8616.2-9760.6)	24.16 (22.66-25.67)	0.915 (0.008)	0.978 (0.006)	0.662 (0.021)	1646	974	672	21	27.4	-6.3	-9.5 to -3.2	-3.92*
2020	7150.9 (6721.3-7580.5)	18.32 (17.21-19.42)	0.958 (0.006)	0.940 (0.008)	0.823 (0.025)	1719	896	823	15.2	21.3	-6.1	-8.4 to -3.8	-5.19*
2022	8433.9 (7910.6-8957.1)	21.58 (20.24-22.92)	0.930 (0.007)	0.980 (0.006)	0.690 (0.022)	1689	1062	627	18.8	24.5	-5.7	-8.5 to -2.9	-3.94*

2.3.3 Change across California

Error-adjusted statewide canopy cover was 24.9% in 2016 and 21.6% in 2022. Across all years, error-adjusted canopy cover was lower in urban than non-urban areas. Urban versus non-urban canopy cover was 21.8% vs 27.9% in 2016, 21.0% vs 27.4% in 2018, 15.2% vs 21.3% in 2020, and 18.8% vs 24.5% in 2022 (Table 2.3, Figure 2.4). Across the full time series, Sen's slope indicated a modest decline in canopy cover statewide (-0.60% per year), with similar rates of change in urban (-0.53% per year) and non-urban areas (-0.64% per year). However, confidence intervals for all three estimates were wide and included zero, indicating that these trends are not statistically distinguishable from no change over this period (Table 2.4).

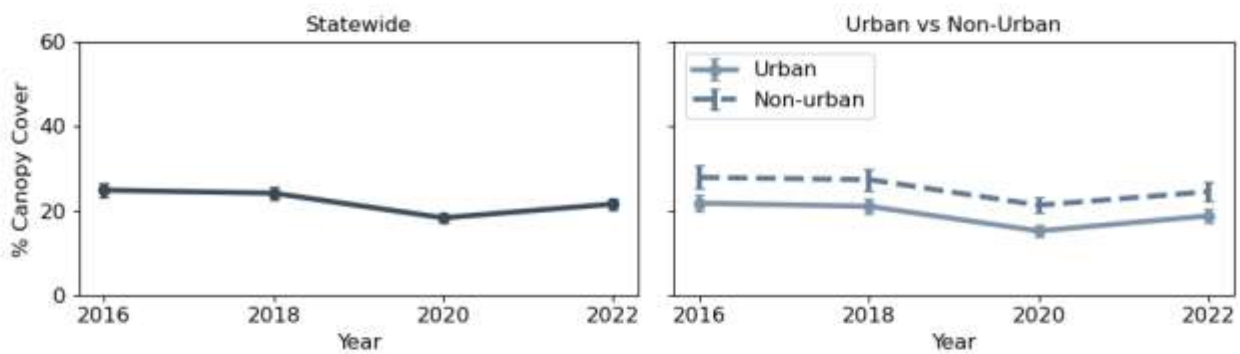

Figure 2.4 Error-adjusted canopy cover (%) across California census-designated places (CDPs) from 2016 to 2022. The statewide time series (left) summarizes canopy cover across all CDPs, and the time series (right) separates CDP area into urban and non-urban classes. Points show the error-adjusted canopy percent. Error bars indicate 95% confidence intervals (estimate ± 1.96 x SE).

When evaluated across sequential time intervals, significant changes in canopy cover were concentrated in the 2018-2020 period. During this interval, canopy cover declined significantly in the Inland Empire (-6.38%), Inland Valleys (-6.58%), and Southern California

Coast (-8.60%) (Wald Z test, $p < 0.01$). No climate zones exhibited significant changes between 2016 and 2018, and only limited recovery was observed between 2020 and 2022, with a significant increase detected in the Inland Empire (+7.80%). All other changes were not statistically distinguishable from zero ($p > 0.05$).

Table 2.4 Sen's slopes calculated using error-adjusted area estimates across the time series statewide, for urban and non-urban areas, and in each climate zone. All confidence intervals cross zero, suggesting that trends are not statistically distinguishable from no change over the study period.

Group	***Sen's Slope***	***CI low***	***CI high***
Statewide	-0.60	-2.76	1.38
Urban	-0.53	-2.77	1.52
Non-Urban	-0.64	-2.86	1.36
Inland Empire	-0.55	-3.05	3.46
Inland Valleys	-1.15	-3.10	0.51
Interior West	-0.55	-2.56	1.49
Northern California Coast	-0.53	-1.05	0.48
Southern California Coast	-0.90	-4.06	1.96
Southwest Desert	0.18	-2.01	2.20

Across climate zones, the Northern California Coast had the highest average canopy cover percent across four years at 29.7%, then Inland Valleys (27.9%), Interior West (27.6%), Southern California Coast (18.2%), Inland Empire (16.3%), and finally Southwest Desert at 7.1% (Table 2.5, Figure 2.5).

Table 2.5 The percent of CDP area in each climate zone, as well as the share (reported as percent) of total state canopy within CDPs that occurs in each climate, and the percent canopy cover within each climate zone in California. Values are reported based on 2020 only (the highest accuracy classification).

Climate Zone	***% of Total State CDP Area***	***% of Total State CDP Canopy***	***% Canopy Cover (95% CI)***
Inland Empire	17.11	9.96	10.68 (8.07-13.29); SE 1.33
Inland Valleys	33.47	44.22	24.26 (22.34-26.19); SE 0.98
Interior West	9.8	12.69	23.78 (18.72-28.84); SE 2.58
Northern California Coast	13.84	21.11	28.01 (25.52-30.50); SE 1.27
Southern California Coast	13.85	9.51	12.61 (9.53-15.70); SE 1.57
Southwest Desert	11.92	2.51	3.87 (1.16-6.57); SE 1.38

When evaluated by climate zone, Sen's slope estimates indicated generally small and uncertain rates of change in canopy cover from 2016 to 2022 (Table 2.4). Estimated trends were negative in most climate zones, including the Inland Empire (-0.55% per year), Inland Valleys (-1.15% per year), Interior West (-0.55% per year), Northern California Coast (-0.53% per year), and Southern California Coast (-0.90% per year), while the Southwest Desert showed a slight positive trend (0.18% per year). However, confidence intervals for all climate zones included zero (Table 2.4), indicating that none of these trends were statistically distinguishable from no change over the study period.

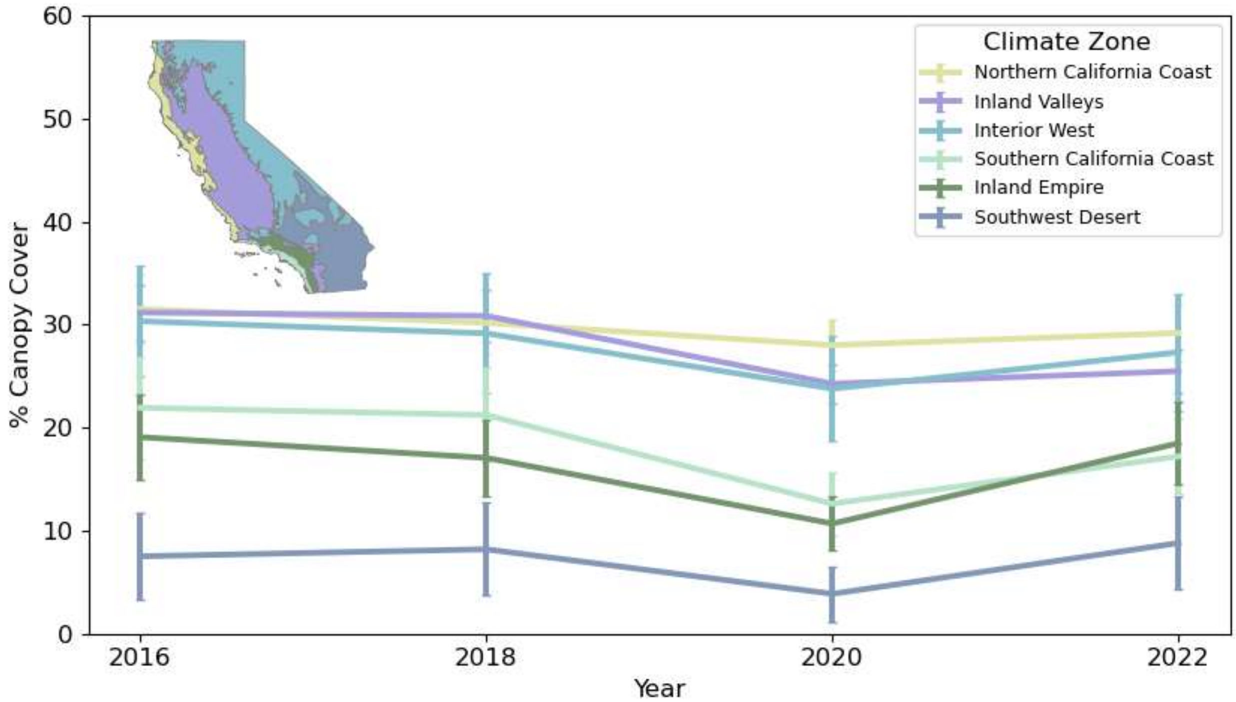

Figure 2.5 Error-adjusted canopy cover (%) by California climate zone from 2016 to 2022. Error bars indicate 95% confidence intervals (estimate ± 1.96 x SE). Climate zones are shown on the upper-left map.

Accuracy assessment points were insufficient to compute error-adjusted estimates for urban and non-urban areas within individual climate zones, so mapped canopy values are reported for these comparisons. While mapped values may over- or underestimate true canopy extent, they are sufficient to characterize relative differences across climate zones. Within each climate zone, non-urban areas in the Northern California Coast, Inland Valleys, and Interior West had higher mapped canopy cover than their urban counterparts. The Inland Empire and

Southern California Coast showed similar canopy cover in urban and non-urban areas, while the Southwest Desert had lower canopy cover outside of urban areas (Figure 2.6).

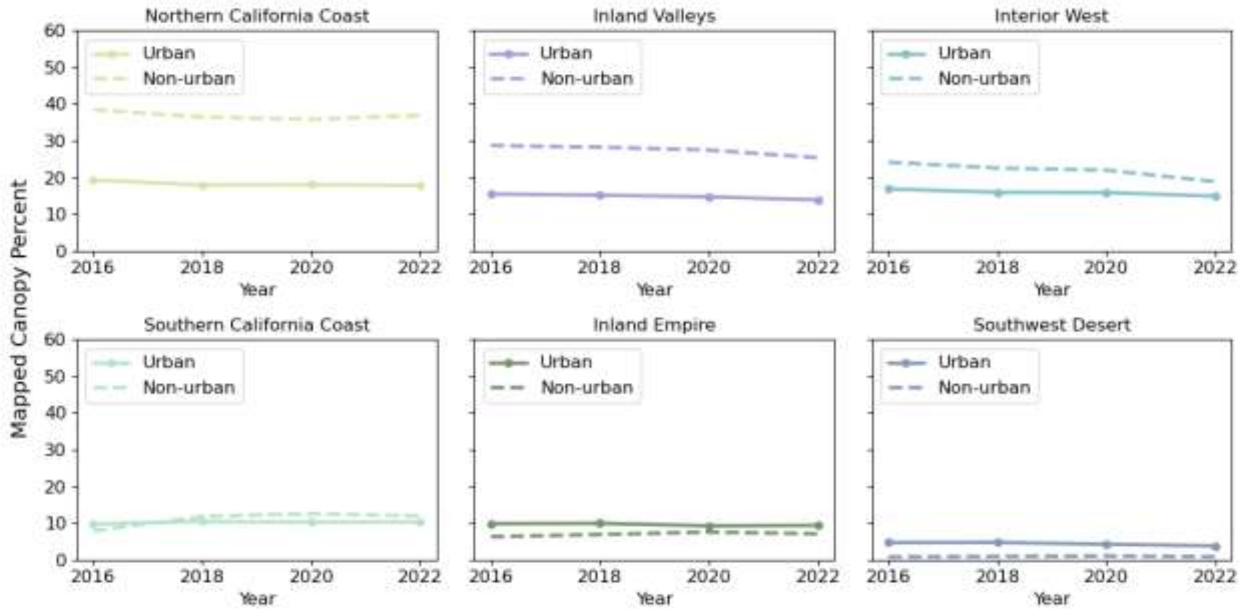

Figure 2.6 Mapped values for percent canopy cover in each climate zone's urban and non-urban areas. Most climate zones have higher canopy cover in non-urban areas.

2.3.4 Property Types with Change

The distribution of canopy cover across parcel types was largely stable across years, with each parcel type contributing a similar share of total canopy cover in each year. Residential multifamily and single-family parcels collectively made up between 55% and 56% of the canopy cover each year. Open space accounted for between 17% and 21% each year. Commercial, industrial, and institutional properties made up between 11% and 13% each year. Roadways made up between 11% and 14% each year (Figure 2.7, confidence intervals in Appendix 2B).

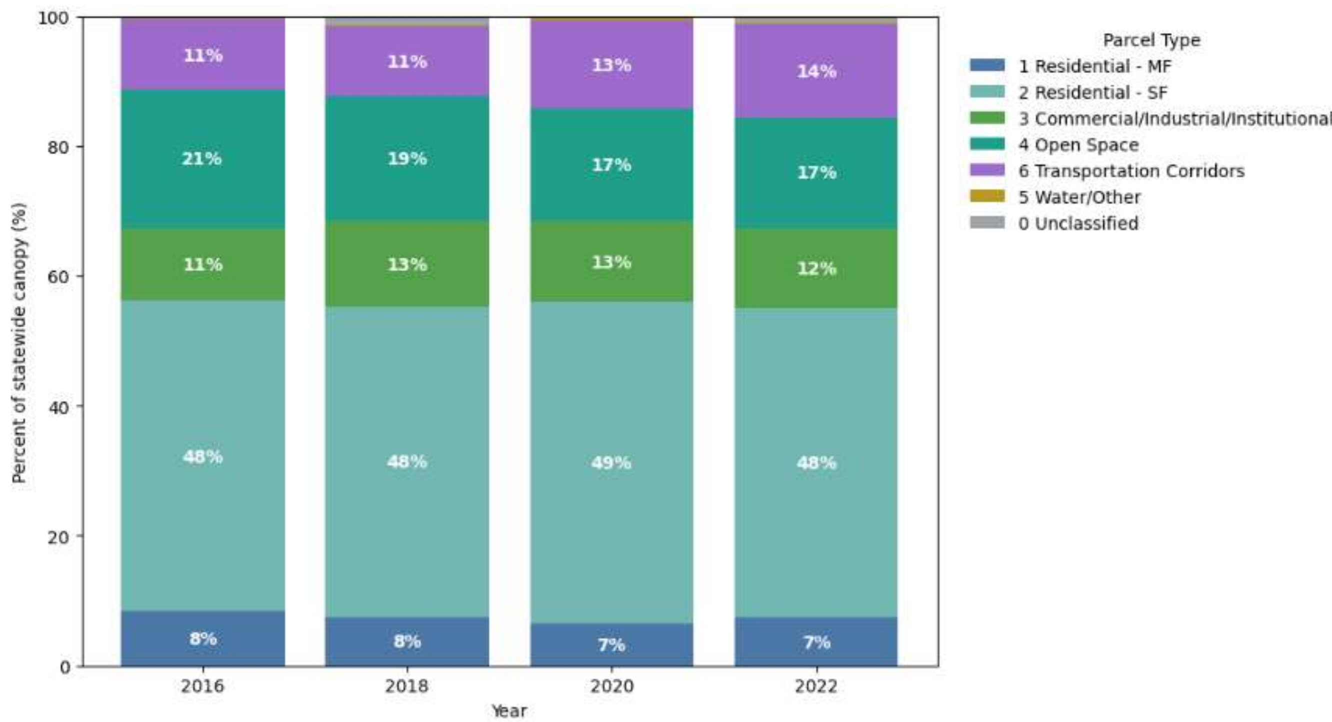

Figure 2.7 Error-adjusted parcel-type percent share of California statewide canopy by year. Stacked bars show the percent share of statewide adjusted canopy area attributed to each parcel type for 2016, 2018, 2020, and 2022.

2.4 Discussion

This study produced an error-adjusted multi-year urban canopy dataset for California census-designated places across four acquisition years at 60-cm resolution. By combining semi-automated LiDAR-derived labels with targeted manual annotation, we achieved consistently high classification accuracy across years while creating a workflow that is transferable to future NAIP acquisitions and to other states where NAIP and 3DEP LiDAR are available. Canopy area and change were estimated using stratified, error-adjusted area estimation following Olofsson et al. (2014), which we demonstrate produces substantially different estimates than raw pixel counts, a distinction with direct consequences for tracking progress toward AB 2251.

2.4.1 Canopy in California

Statewide canopy cover declined insignificantly between 2016 and 2022, with the largest decrease occurring between 2018 and 2020, followed by a partial rebound by 2022. This decline was not uniform across the state; significant decreases during 2018-2020 were concentrated in the Inland Empire, Inland Valleys, and Southern California Coast, and this was the only interval in which statistically significant declines were detected across climate zones. This canopy decrease may reflect a combination of real canopy loss and variability in view-angle acquisition. Given the two-year NAIP acquisition rate and known variability in aerial imagery geometry, longer time series are required to distinguish persistent structural canopy change from short-term imagery variability. The magnitude of observed change was small relative to total canopy extent, underscoring the importance of uncertainty-adjusted values when interpreting trends.

Spatial patterns broadly reflected California's climate gradient: canopy cover was highest in the Northern California Coast, Inland Valleys, and Interior West, and lowest in the Southwest Desert. Across all climate zones, canopy cover was lower in urban than non-urban areas, although the magnitude of this varied regionally. In the Southern California Coast, urban and non-urban canopy cover were often similar, whereas in the Inland Empire and Southwest Desert, urban canopy occasionally exceeded non-urban canopy. In these regions, shrub-dominated landscapes are common and are included in our canopy definition (woody vegetation ≥1.8 m), which can reduce contrasts between developed and non-developed areas. Except for mountainous areas and riparian corridors, the Los Angeles Basin was not historically a densely forested ecosystem, so lower canopy cover in this region should not be interpreted as forest loss (Ethington et al., 2020; Pawlak et al., 2023).

Maintaining high canopy cover percentages in urban areas will likely depend less on rapid gains from new plantings and more on preventing losses. Large, mature trees contribute disproportionately to ecosystem services (Doick, 2021; Liang and Huang et al., 2023), and the removal of a single large tree typically cannot be offset quickly by planting multiple small trees (Le Roux et al., 2014), especially within short time periods. Each year, the majority of canopy cover was on privately managed property types. This is important because tree canopy is often inequitably distributed: across 5,723 U.S. communities, low-income blocks had 15.2% less tree cover and were 1.5°C hotter than high-income blocks on average (McDonald et al., 2021). Because canopy is concentrated on private residential parcels, and because census tracts with lower income and higher proportions of non-white residents tend to have fewer and slower-growing large street trees (Velasquez-Camacho et al., 2025), achieving statewide canopy goals will require policies that actively target private landowners in disadvantaged communities. Public programs alone can only protect a small portion of the urban forest (Mincey et al., 2012).

2.4.2 Best Model Performance

The statewide fine-tuned model (SFT) consistently outperformed the regionally fine-tuned models, despite the latter's climate-zone-specific training. This suggests that, for statewide urban canopy mapping, the breadth of annotated training data may matter more than geographic specialization when urban tree structure shares common visual characteristics across regions. Regionally fine-tuned models still performed competitively with fewer annotated tiles, suggesting they may be useful when annotation resources are limited. The LiDAR-trained model exhibited greater spatial offsets and boundary artifacts, likely due to misalignment between LiDAR point clouds and NAIP imagery during label generation. Fine-tuning with manually annotated NAIP data reduced these artifacts and generalized well across acquisition years.

2.4.3 The importance of accounting for error in canopy change estimates

Canopy rasters, even when derived from high-resolution imagery and high-accuracy models, are predictions, and without propagating classification error into area estimates, comparisons across years or products can reflect mapping bias rather than true canopy change. This distinction is consequential for California, where AB 2251 mandates a 10% statewide canopy increase by 2035. If the baseline and target estimates are both based on unadjusted pixel counts, the reported progress may not reflect reality. Most large-scale canopy products do not apply error adjustment; instead, they report mapped values alongside classification accuracy metrics as separate quantities. The recent CAL FIRE (2025) statewide urban canopy dataset is a prominent example: mapped canopy cover was reported as 18.85% in 2018 and 18.78% in 2022. When we applied our reference sample to the CAL FIRE product using the Olofsson et al. (2014) framework, error-adjusted estimates increased to 28.15% (95% CI: 5,206-6,106 km^2) in 2018 and 23.98% (95% CI: 4,433-5,206 km^2) in 2022 - a difference of nearly ten percentage points in both years (Appendix 2D). A similar pattern holds for our own dataset, where error-adjusted estimates diverge substantially from mapped pixel totals. The magnitude of this divergence demonstrates that pixel-count totals can systematically misrepresent statewide canopy extent, and that changes in mapped area across years may reflect shifts in classification performance as much as real landscape change. For context, the Chesapeake Bay Land Cover dataset (one of the only other multi-year, large-scale urban canopy change products in the U.S.) reports mapped values with change classification accuracies of 75% (2013-2014) and 56% (2021-2022) without error adjustment (Bouffard et al., 2025), suggesting that this issue extends beyond California.

2.4.4 Comparison with Prior Urban Canopy Mapping Approaches

The statewide canopy cover dataset produced here extends and improves a growing body of work using deep learning and high-resolution imagery for broad-scale urban canopy mapping. Using the subset of reference points overlapping both products, our dataset achieved higher overall accuracy than CAL FIRE (2025) in urban areas (92.2% vs. 86.3% in 2018; 94.0% vs. 88.7% in 2022), with stronger canopy user's and producer's accuracies in both years, while additionally covering non-urban CDPs and a longer timeseries. Across the broader literature, U-Net architectures applied to aerial imagery have consistently achieved high accuracy for canopy segmentation. Our SFT model achieves F1 scores of 0.87-0.91 across climate zones at 60-cm resolution over a statewide domain of 39,032 km^2, exceeding the 79.3% overall accuracy reported by Erker et al. (2019) for a statewide random forest approach in Wisconsin, and comparable to the 91.52% overall accuracy of the UrbanWatch database across 22 U.S. cities (Zhang et al., 2022), while covering a larger and more diverse spatial extent.

2.4.5 Limitations and Future Work

Parallax and imperfect orthorectification can confuse canopy change estimates derived from aerial imagery (Kropp, 2024; Lehrbass & Wang, 2012; Richardson & Moskal, 2014). When acquisition geometry differs across flights or years, the apparent position and footprint of objects can shift, which can inflate or reduce mapped canopy area even when the tree itself is unchanged. Differences in sun elevation between image acquisitions can create shadows that obscure trees differently from year to year. NAIP mosaics vary in orthorectification quality and off-nadir viewing angle both spatially across California and temporally across acquisition years because imagery is collected and processed by multiple contractors and then assembled into a single statewide product. In large metropolitan areas (the Bay Area and Los Angeles Basin), flight lines tend to be denser, which reduces off-nadir effects and generally improves consistency. In many smaller or non-urban regions, flight lines are historically more widely spaced, and off-nadir angles can be larger, increasing geometric distortions (Lillesand et al., 2015).

These effects are not confined only to image seamlines that have higher view angles. Local topography, particularly hillsides, can amplify relief displacement and shape distortions even within a single flight strip, and these terrain-driven effects can vary across years depending on flight geometry and processing (Appendix 2D). The magnitude of parallax-related bias also depends on canopy form: compact, rounded crowns are less sensitive, whereas tall, conical or vertically layered crowns can have larger footprint changes with larger viewing angles. These factors make it difficult to attribute small year-to-year differences in mapped canopy area solely to true canopy change without explicitly considering acquisition geometry and its interaction with canopy structure. The distortion of canopy area and placement resulting from these effects means that canopy products produced from NAIP imagery should not be used for pixel-to-pixel change comparisons. For that reason, we did not analyze small-scale (on each parcel, or by tree) change in urban forest canopy, as they could be the result of changing view angles in any given year. To illustrate the magnitude of this effect, we conducted a small sensitivity analysis by manually digitizing the same 11 tree crowns in NAIP imagery for each acquisition year (2016, 2018, 2020, 2022) in locations where view-angle artifacts were hand-selected to be visually apparent (Figure 2.8). Across years, both the apparent crown footprint and the apparent crown position shifted, producing between-year percent area differences that are larger than botanically possible from true tree growth over two-year intervals. While this experiment is not intended to quantify statewide bias, it demonstrates that acquisition geometry and orthorectification can generate canopy-change signals at small scales that are unrelated to tree growth.

Future work should estimate how frequently these distortions occur and evaluate their contribution to uncertainty in statewide canopy cover and change estimates. In the meantime, these results underscore that NAIP-derived canopy time series contain an inherent error that is unaccounted for in estimates. Policy or management applications that rely on detecting change should emphasize large-magnitude changes assessed over long time periods, rather than small year-to-year differences that may fall within imaging-related variability. Extending this time series beyond 2022 will further improve the ability to distinguish persistent canopy trends from short-term variability and acquisition artifacts.

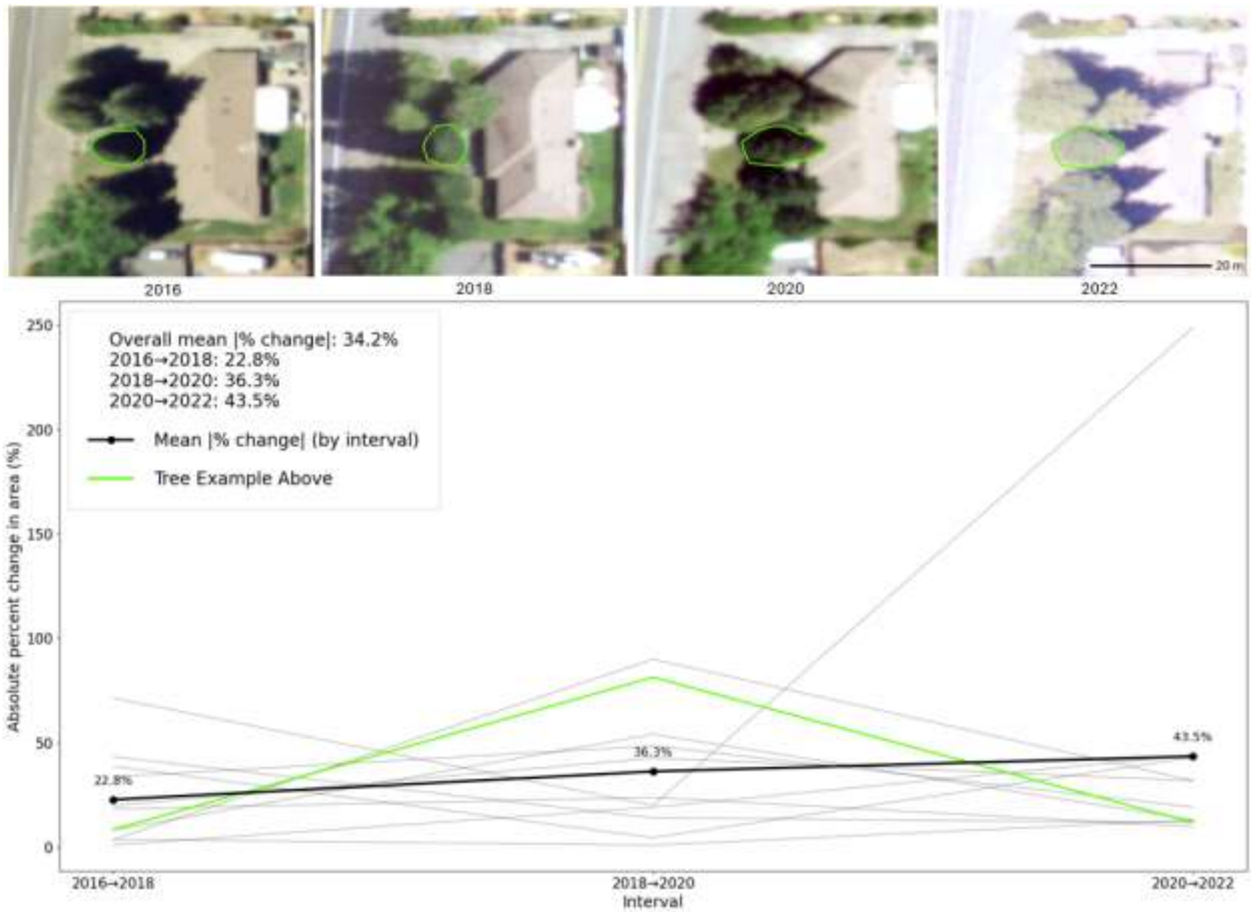

Figure 2.8 Absolute percent change in canopy area between successive years for 11 manually digitized conical tree crowns with clear view-angle effects. Each gray line shows one tree; the green line corresponds to the tree shown in the images above. Changes reflect year-to-year variability in mapped canopy area. Interval means are shown only to indicate the magnitude of variability and should not be interpreted as typical change.

2.5 Conclusions

We developed and evaluated a reproducible workflow for generating a multi-temporal, high-resolution canopy cover dataset across California census-designated places using NAIP imagery. The approach combines semi-automated LiDAR-derived training data, manual annotation, and error-adjusted area estimation to support consistent comparisons across years.

Statewide canopy cover declined modestly between 2016 and 2022, but the magnitude of change was small relative to total canopy extent. These findings suggest that short-term differences in NAIP-derived canopy cover should be interpreted cautiously, especially where image acquisition geometry and orthorectification can introduce apparent change at fine spatial scales. Continued monitoring over longer time periods will improve the ability to distinguish persistent structural trends from short-term variability.

Across most climate zones, canopy cover was relatively stable from 2016 to 2022, with the clearest decline occurring between 2018 and 2020 in the Inland Empire, Inland Valleys, and Southern California Coast. Canopy cover was generally higher in non-urban than urban portions of CDPs, except in the Southwest Desert, Southern California Coast, and Inland Empire. Most canopy within incorporated urban areas occurred on privately managed parcels, highlighting the importance of engaging private landowners in future canopy planning and protection efforts. Overall, this workflow provides a scalable framework for tracking canopy trends in future NAIP years and can be adapted for urban forest monitoring across other U.S. states.

2.6 Code and data access

Canopy cover data for all four years is open source. Canopy maps can be viewed at: https://experience.arcgis.com/experience/401c3c7a7b3742dcb548178251ed1c91.

Code for running and training the model as well as accuracy assessment points are accessible on GitHub at: https://github.com/camipawlak/canopy_cover. Raster data, training chips, and model checkpoints can be downloaded at DOI: 10.5061/dryad.rjdfn2zs9.

2.7 Appendices

Appendix 2A. Inputs and outputs for accuracy assessment and error-adjusted canopy area estimation. Available at https://github.com/camipawlak/canopy_cover.

Tables included are:

(A1) Statewide overall by year.

(A2) Urban and non-urban statewide by year.

(A3) Climate zones by year.

Columns report:

Column	**Description**
year	Analysis year
urban	Urban domain identifier
cz	Climate zone identifier
total_ref_points	Total number of sampled reference points
ref_tree_points	Number of reference canopy points (reference = 1)
ref_non_tree_points	Number of reference non-canopy points (reference = 0)
ref_na_points	Number of uncertain reference points (reference = NA)
OA	Overall accuracy
UA0	User's accuracy for non-canopy
UA1	User's accuracy for canopy
PA0	Producer's accuracy for non-canopy
PA1	Producer's accuracy for canopy
se_*	Standard errors for accuracy metrics

var_*	Variances for accuracy metrics
group_total_area_m2	Total statewide CDP area used as denominator for all proportions (m^2). For A2 and A3, this is the full state total, not the subgroup area.
group_total_area_km2	Same as above (km^2).
tree_area_m2	Mapped canopy area (m^2)
not_tree_area_m2	Mapped non-canopy area (m^2)
W_tree	Stratum weight for canopy
W_not_tree	Stratum weight for non-canopy
W_group_total	Fraction of total state CDP area occupied by this reporting group. Divide canopy_percent_adjusted by this value to get within-group canopy cover.
canopy_km2_mapped	Mapped canopy area (km^2)
canopy_percent_mapped	Mapped canopy as % of total state CDP area. Divide by W_group_total for within-group canopy cover.
canopy_km2_area_adjusted	Error-adjusted canopy area (km^2)
canopy_percent_adjusted	Error-adjusted canopy as % of total state CDP area. Divide by W_group_total for within-group canopy cover (values reported in manuscript).
canopy_km2_area_adjusted_se	Standard error of adjusted canopy area
canopy_percent_adjusted_se	Standard error of canopy_percent_adjusted (same denominator).
canopy_km2_area_adjusted_ci_lo	Lower 95% CI for adjusted canopy area
canopy_km2_area_adjusted_ci_hi	Upper 95% CI for adjusted canopy area
canopy_percent_adjusted_ci_lo	Lower 95% CI for canopy_percent_adjusted (same denominator).
canopy_percent_adjusted_ci_hi	Upper 95% CI for canopy_percent_adjusted (same denominator).

Appendix 2B: Inputs and outputs for accuracy assessment and error-adjusted canopy area estimation by year and parcel type (UF_Code). Columns are shared with Appendix A. Available at: https://github.com/camipawlak/canopy_cover.

Appendix 2C. Data sources and cities for LiDAR used to create automated training data.

Climate Zone	# of Tiles Created	City	Lidar Year	Dataset
Inland Empire	263	Azusa	2016	USGS_LPC_CA_LosAngeles_2016_LAS_2018
Inland Empire	391	Claremont	2018	USGS_LPC_CA_SoCal_Wildfires_B1_2018_LAS_2019
Inland Empire	1126	Redlands	2018	USGS_LPC_CA_SoCal_Wildfires_B1_2018_LAS_2019
Inland Empire	2699	Riverside	2018	USGS_LPC_CA_SoCal_Wildfires_B1_2018_LAS_2019
Inland Valleys	1002	Chico	2018	USGS_LPC_CA_NoCAL_Wildfires_B2_2018
Inland Valleys	471	Madera	2021	CA_SanJoaquin_2_2021
Inland Valleys	1318	Modesto	2021	CA_SanJoaquin_1_2021
Inland Valleys	3203	Sacramento	2018	USGS_LPC_CA_NoCAL_Wildfires_B5a_2018
Interior West	72	Crowley Lake	2017	USGS_LPC_CA_LongValleyCaldera_2017_LAS_2018
Interior West	19	Likely	2017	USGS_LPC_CA_FEMA_R9_Upper_Pit_2017_LAS_2019
Interior West	360	Mohawk Vista	2018	USGS_LPC_CA_NoCAL_Wildfires_PlumasNF_B2_2018
Interior West	82	Sunnyside-Tahoe City	2018	USGS_LPC_CA_NoCAL_Wildfires_B1_2018
Interior West	1073	Truckee	2018	USGS_LPC_CA_NoCAL_Wildfires_B1_2018
Northern California Coast	828	Novato	2018	USGS_LPC_CA_NoCal_Wildfires_B5b_QL1_2018

Northern California Coast	3668	San Francisco	2018	USGS LPC CA NoCAL Wildfires B5b 2018
Northern California Coast	387	San Luis Obispo	2018	CA_FEMA_Z4_B2_2018
Northern California Coast	648	San Rafael	2018	USGS_LPC_CA_NoCAL_Wildfires_B5b_2018, USGS_LPC_CA_NoCal_Wildfires_B5b_QL1_2018
Northern California Coast	469	Santa Cruz	2020	CA_SantaCruzCounty_2020
Southern California Coast	227	Inglewood	2016	USGS_LPC_CA_LosAngeles_2016_LAS_2018
Southern California Coast	2420	Long Beach	2016	USGS_LPC_CA_LosAngeles_2016_LAS_2018
Southern California Coast	1006	Oxnard	2018	USGS_LPC_CA_SoCal_Wildfires_B3_2018_LAS_2019
Southern California Coast	532	Santa Monica	2016	USGS_LPC_CA_LosAngeles_2016_LAS_2018
Southern California Coast	647	Torrance	2016	USGS_LPC_CA_LosAngeles_2016_LAS_2018
Southwest Desert	97	Calipatria	2021	CA_SaltonSea_EarthMRI_1_2021
Southwest Desert	3035	Lancaster	2016	USGS_LPC_CA_LosAngeles_2016_LAS_2018
Southwest Desert	1000	Needles	2021	CA_SanBern_EMRI_2_2021
Southwest Desert	3415	Palmdale	2016	USGS_LPC_CA_LosAngeles_2016_LAS_2018

Appendix 2D. Examples of relief displacement in NAIP imagery. A) NAIP imagery of trees on a slope, 2018. B) The same trees as A, but in 2020. C) The urban forest with a close-to-nadir view angle in 2018. D) The same trees as C, off-nadir in 2022.

2.8 Acknowledgements

This chapter is a submitted publication with the authors: Camille C. Pawlak, Jenn Yost, Jonathan Ventura, Griffen Guizan, Sara Arnold, Gregory Okin, Kyle Cavanaugh, G. Andrew Fricker, Matt Ritter, and Thomas W. Gillespie. It is available as a preprint at:

Pawlak, C. C., Yost, J., Ventura, J., Guizan, G., Arnold, S., Okin, G., Cavanaugh, K., Fricker, G. A., Ritter, M., & Gillespie, T. W. (2026). *Mapping California's Urban Forest at Scale: An Error-Adjusted Canopy Time Series for Monitoring Change*. Ecology. https://doi.org/10.64898/2026.05.04.722774

The authors would like to acknowledge the efforts of students who helped create training data for this work: Ryley Chase, Alexandra Crocker, Jessica Baiza, Katharine McDaniel and April Engelmeier. We would also like to acknowledge students who contributed to the LiDAR processing code: Nam Nguyen and Benjamin Hinchliff.

2.9 References

Akın, A., Çilek, A., & Middel, A. (2023). Modelling tree canopy cover and evaluating the driving factors based on remotely sensed data and machine learning. *Urban Forestry & Urban Greening*, *86*, 128035. https://doi.org/10.1016/j.ufug.2023.128035

Allred, B. W., McCord, S. E., & Morford, S. L. (2025). Canopy height model and NAIP imagery pairs across CONUS. *Scientific Data*, *12*(1), 322. https://doi.org/10.1038/s41597-025-04655-z

Bouffard, M., UVM Spatial Analysis Lab, Chesapeake Conservancy, USGS, & USFS. (2025, August). *Chesapeake Bay Tree Cover Status and Change*. Chesapeake Trees. https://chesapeaketrees.net/wp-content/uploads/2025/08/Chesapeake-Bay-TC-User-Guide_03-13-2023_Revised_2025_KMB_CIC2a_small.pdf

Bozinovski, S., & Fulgosi, A. (1976). The influence of pattern similarity and transfer learning on the base perceptron training. *Symposium Informatica 3-121-5*.

CalFire, USDA, USFS, & EarthDefine. (2025). *California's Urban Tree Canopy* [Dataset]. https://www.fs.usda.gov/r05/state-tribal-forestry/california-urban-canopy-data

California Department of Conservation, Division of Land Resource Protection. (2020). *California Farmland Conversion Report, 2016-2020*. Farmland Mapping and Monitoring Program. https://www.conservation.ca.gov/dlrp/fmmp/Documents/fmmp/pubs/2016-2018/FCR/FCR_1618_Report.pdf

Cavender-Bares, J. M., Nelson, E., Meireles, J. E., Lasky, J. R., Miteva, D. A., Nowak, D. J., Pearse, W. D., Helmus, M. R., Zanne, A. E., Fagan, W. F., Mihiar, C., Muller, N. Z., Kraft, N. J. B., & Polasky, S. (2022). The hidden value of trees: Quantifying the ecosystem services of tree lineages and their major threats across the contiguous US. *PLOS*

Sustainability and Transformation, *1*(4), e0000010. https://doi.org/10.1371/journal.pstr.0000010

Dewitz, J. (2021). *National Land Cover Database (NLCD) 2019 Products* [Dataset]. U.S. Geological Survey. https://doi.org/10.5066/P9KZCM54

Doick, K. J. (2021). *Selecting urban trees for ecosystem service provision*. Forest Research. https://www.forestresearch.gov.uk/research/quantification-and-valuation-of-benefits-provided-by-urban-trees/selecting-urban-trees-for-ecosystem-service-provision/

Erker, T., Wang, L., Lorentz, L., Stoltman, A., & Townsend, P. A. (2019). A statewide urban tree canopy mapping method. *Remote Sensing of Environment*, *229*, 148–158. https://doi.org/10.1016/j.rse.2019.03.037

Ethington, P. J., MacDonald, B., Stein, G., Deverell, W., & Longcore, T. (2020). *Historical Ecology of the Los Angeles River Watershed and Environs*. University of Southern California.

Giacinto, J. J., Fricker, G. A., Ritter, M., Yost, J., & Doremus, J. (2021). Urban forest biodiversity and cardiovascular disease: Potential health benefits from California's street trees. *PLOS ONE*, *16*(11), e0254973. https://doi.org/10.1371/journal.pone.0254973

Guo, J., Xu, Q., Zeng, Y., Liu, Z., & Zhu, X. X. (2023). Nationwide urban tree canopy mapping and coverage assessment in Brazil from high-resolution remote sensing images using deep learning. *ISPRS Journal of Photogrammetry and Remote Sensing*, *198*, 1–15. https://doi.org/10.1016/j.isprsjprs.2023.02.007

He, K., Zhang, X., Ren, S., & Sun, J. (2015). *Deep Residual Learning for Image Recognition* (Version 1). arXiv. https://doi.org/10.48550/ARXIV.1512.03385

Hulley, G. C., Dousset, B., & Kahn, B. H. (2020). Rising Trends in Heatwave Metrics Across Southern California. *Earth's Future*, *8*(7), e2020EF001480. https://doi.org/10.1029/2020EF001480

Hwang, B., Sou, H.-D., Oh, J.-H., & Park, C.-R. (2023). Cooling effect of urban forests on the urban heat island in Seoul, South Korea. *PLOS ONE*, *18*(7), e0288774. https://doi.org/10.1371/journal.pone.0288774

Kropp, H. (2024). Historical changes in tree and impervious surface cover following urban renewal in a small postindustrial city. *Environmental Management*, *73*(4), 814–825. https://doi.org/10.1007/s00267-023-01934-6

Le Roux, D. S., Ikin, K., Lindenmayer, D. B., Manning, A. D., & Gibbons, P. (2014). The Future of Large Old Trees in Urban Landscapes. *PLoS ONE*, *9*(6), e99403. https://doi.org/10.1371/journal.pone.0099403

Lehrbass, B., & Wang, J. (2012). Urban Tree Cover Mapping with Relief-corrected Aerial Imagery and Lidar. *Photogrammetric Engineering & Remote Sensing*, *78*(5), 473–484. https://doi.org/10.14358/PERS.78.5.473

Liang, D., & Huang, G. (2023). Influence of Urban Tree Traits on Their Ecosystem Services: A Literature Review. *Land*, *12*(9), 1699. https://doi.org/10.3390/land12091699

Lillesand, T. M., Kiefer, R. W., & Chipman, J. W. (2015). *Remote sensing and image interpretation* (7. ed). Wiley.

Livesley, S. J., McPherson, E. G., & Calfapietra, C. (2016). The Urban Forest and Ecosystem Services: Impacts on Urban Water, Heat, and Pollution Cycles at the Tree, Street, and City Scale. *Journal of Environmental Quality*, *45*(1), 119–124. https://doi.org/10.2134/jeq2015.11.0567

Loshchilov, I., & Hutter, F. (2017). *Decoupled Weight Decay Regularization* (Version 3). arXiv. https://doi.org/10.48550/ARXIV.1711.05101

MacFaden, S. W., O'Neil-Dunne, J. P. M., Royar, A. R., Lu, J. W. T., & Rundle, A. G. (2012). High-resolution tree canopy mapping for New York City using LIDAR and object-based image analysis. *Journal of Applied Remote Sensing*, *6*(1), 063567–1. https://doi.org/10.1117/1.JRS.6.063567

Martins, J. A. C., Nogueira, K., Osco, L. P., Gomes, F. D. G., Furuya, D. E. G., Gonçalves, W. N., Sant'Ana, D. A., Ramos, A. P. M., Liesenberg, V., Dos Santos, J. A., De Oliveira, P. T. S., & Junior, J. M. (2021). Semantic Segmentation of Tree-Canopy in Urban Environment with Pixel-Wise Deep Learning. *Remote Sensing*, *13*(16), 3054. https://doi.org/10.3390/rs13163054

McDonald, R. I., Biswas, T., Sachar, C., Housman, I., Boucher, T. M., Balk, D., Nowak, D., Spotswood, E., Stanley, C. K., & Leyk, S. (2021). The tree cover and temperature disparity in US urbanized areas: Quantifying the association with income across 5,723 communities. *PLOS ONE*, *16*(4), e0249715. https://doi.org/10.1371/journal.pone.0249715

McPherson, E. G., Xiao, Q., Van Doorn, N. S., De Goede, J., Bjorkman, J., Hollander, A., Boynton, R. M., Quinn, J. F., & Thorne, J. H. (2017). The structure, function and value of urban forests in California communities. *Urban Forestry & Urban Greening*, *28*, 43–53. https://doi.org/10.1016/j.ufug.2017.09.013

Mincey, S. K., Schmitt-Harsh, M., & Thurau, R. (2013). Zoning, land use, and urban tree canopy cover: The importance of scale. *Urban Forestry & Urban Greening*, *12*(2), 191–199. https://doi.org/10.1016/j.ufug.2012.12.005

Morgenroth, J., Doick, K., Hauer, R., Locke, D. H., Barona, C. O., Roman, L. A., Conway, T. M., Dobbs, C., Duinker, P., Gulsrud, N. M., Jim, C. Y., Koeser, A. K., Landry, S., Livesley, S., Nesbitt, L., Shackleton, C. M., Tan, P. Y., & Yang, J. (2025). Urban tree cover targets: The good, the bad and the SMART. *Urban Forestry & Urban Greening*, *112*, 128979. https://doi.org/10.1016/j.ufug.2025.128979

Olofsson, P., Foody, G. M., Herold, M., Stehman, S. V., Woodcock, C. E., & Wulder, M. A. (2014). Good practices for estimating area and assessing accuracy of land change. *Remote Sensing of Environment*, *148*, 42–57. https://doi.org/10.1016/j.rse.2014.02.015

Pawlak, C. C., Love, N. L. R., Yost, J. M., Fricker, G. A., Doremus, J. M., & Ritter, M. K. (2023). California's native trees and their use in the urban forest. *Urban Forestry & Urban Greening*, *89*, 128125. https://doi.org/10.1016/j.ufug.2023.128125

Richardson, J. J., & Moskal, L. M. (2014). Uncertainty in urban forest canopy assessment: Lessons from Seattle, WA, USA. *Urban Forestry & Urban Greening*, *13*(1), 152–157. https://doi.org/10.1016/j.ufug.2013.07.003

Ronneberger, O., Fischer, P., & Brox, T. (2015). *U-Net: Convolutional Networks for Biomedical Image Segmentation*. https://doi.org/10.48550/ARXIV.1505.04597

Summers, J. K., Lamper, A., McMillion, C., & Harwell, L. C. (2022). Observed Changes in the Frequency, Intensity, and Spatial Patterns of Nine Natural Hazards in the United States from 2000 to 2019. *Sustainability*, *14*(7), 4158. https://doi.org/10.3390/su14074158

Timilsina, S., Aryal, J., & Kirkpatrick, J. B. (2020). Mapping Urban Tree Cover Changes Using Object-Based Convolution Neural Network (OB-CNN). *Remote Sensing*, *12*(18), 3017. https://doi.org/10.3390/rs12183017

U.S. Census Bureau. (2016). *Census Defined Places* [Dataset]. https://www.census.gov/cgi-bin/geo/shapefiles/index.php?year=2016&layergroup=Places

U.S. Census Bureau. (2018). *Census Defined Places* [Dataset]. https://www.census.gov/cgi-bin/geo/shapefiles/index.php?year=2018&layergroup=Places

U.S. Census Bureau. (2020a). *Census Defined Places* [Dataset]. https://www.census.gov/cgi-bin/geo/shapefiles/index.php?year=2020&layergroup=Places

U.S. Census Bureau. (2020b). *Population, 2020, Dicennial Census* [Computer software].

U.S. Census Bureau. (2022). *Census Defined Places* [Dataset]. https://www.census.gov/cgi-bin/geo/shapefiles/index.php?year=2022&layergroup=Places

Velasquez-Camacho, L., Etxegarai, M., & de-Miguel, S. (2023). Implementing Deep Learning algorithms for urban tree detection and geolocation with high-resolution aerial, satellite, and ground-level images. *Computers, Environment and Urban Systems*, *105*, 102025. https://doi.org/10.1016/j.compenvurbsys.2023.102025

Velasquez-Camacho, L., Van Doorn, N., Preisler, H., Etxegarai, M., Alas, O., Gonzalez Castro, J. M., & de-Miguel, S. (2025). Monitoring temporal changes in large urban street trees using remote sensing and deep learning. *PLOS One*, *20*(6), e0326562. https://doi.org/10.1371/journal.pone.0326562

Wang, Z., Fan, C., & Xian, M. (2021). Application and Evaluation of a Deep Learning Architecture to Urban Tree Canopy Mapping. *Remote Sensing*, *13*(9), 1749. https://doi.org/10.3390/rs13091749

Weinstein, B. G., Marconi, S., Bohlman, S., Zare, A., & White, E. (2019). Individual Tree-Crown Detection in RGB Imagery Using Semi-Supervised Deep Learning Neural Networks. *Remote Sensing*, *11*(11), 1309. https://doi.org/10.3390/rs11111309

Williams, A. P., Cook, B. I., & Smerdon, J. E. (2022). Rapid intensification of the emerging southwestern North American megadrought in 2020–2021. *Nature Climate Change*, *12*(3), 232–234. https://doi.org/10.1038/s41558-022-01290-z

Zhang, Y., Chen, G., Myint, S. W., Zhou, Y., Hay, G. J., Vukomanovic, J., & Meentemeyer, R. K. (2022). UrbanWatch: A 1-meter resolution land cover and land use database for 22 major cities in the United States. *Remote Sensing of Environment*, *278*, 113106. https://doi.org/10.1016/j.rse.2022.113106

Chapter 3. Tracking Urban Forest Condition and Removals

Abstract

Understanding tree types, loss, and decline is essential for proper management of urban forests and for calculating urban forest benefits. With the majority of urban canopy on private property, field surveys cannot fully capture where and when canopy is removed. This research combines biannual high-resolution canopy maps with high-spatial- and high-temporal-resolution PlanetScope data to assess urban tree foliage types, identify individual tree removals, and estimate the month of removal. Foliage type was correctly predicted using linear discriminant analysis of PlanetScope time series for 84% of trees across two California cities. Removals were correctly predicted with 91.7% accuracy using NAIP-derived canopy change and with 81.0% accuracy using a PlanetScope-based time-series linear discriminant analysis. Tree removal timing was predicted within independently validated removal windows for 36 of 49 examined trees (73.5%). NAIP can identify canopy loss between two image dates, but PlanetScope time series provide a way to estimate when that loss occurred within that interval. For urban forest management, monthly removal estimates could help cities identify where and when canopy loss is occurring and better plan to achieve urban canopy goals.

3.1 Introduction

Urban forests are dynamic systems where trees are planted, maintained, decline, and are removed. Understanding where and when tree removals occur is important because canopy benefits depend not only on how much canopy exists, but also on how quickly canopy is lost and replaced. Urban trees are under increasing pressure from drought, pests, disease, physical damage, extreme weather, and other stressors, which can lead to canopy loss with ecological, social, and financial consequences (Hilbert et al., 2019; Tabassum et al., 2021). Tree removal and tree decline are related but not identical. In cities, trees may be removed because they are dead or declining, but also because of development, risk management, infrastructure conflicts, storm damage, or landowner preference. For these reasons, detecting removals is a separate monitoring task from diagnosing the cause of decline. Cities invest heavily in managing and maintaining their urban forests (Song et al., 2018), and tree removals reduce the benefits urban forests provide, including heat mitigation, carbon sequestration, noise reduction, stormwater regulation, improved air quality, and recreational space (Allen et al., 2021; Kraemer & Kabisch, 2022; Livesley et al., 2016; Rey-Gozalo et al., 2023).

Despite the importance of urban forest monitoring, few remote sensing studies have developed methods to track individual urban tree removals through time. Many cities also lack the resources for frequent and comprehensive in-situ monitoring. Field surveys, typically conducted by trained experts, can be time-consuming and require specialized municipal resources (Roman et al., 2020; Van Doorn et al., 2020). For example, the U.S. Forest Service recommends a rotating five-year inspection cycle, in which approximately one-fifth of a municipality's trees are inspected each year (Van Doorn et al., 2020). Privately managed trees, which account for 80% of California's urban forest (Love et al., [In Press]), are not tracked. These limitations make it difficult to detect tree loss soon after it occurs or to evaluate whether planting programs are keeping pace with removals. Remote sensing offers a scalable alternative to field-based surveys (Morales-Gallegos et al., 2023; Nazeer et al., 2024; Plowright et al., 2016), and in natural forests, remotely sensed data are already widely used to monitor tree health and mortality (Lausch et al., 2016; Orusa &

Mondino, 2021). However, most remote sensing approaches either map canopy change between image dates or assess canopy condition, rather than dating and identifying individual tree removals.

Applying remote sensing approaches in urban settings presents unique challenges. Urban forests are highly heterogeneous, both biologically and physically. Tree species vary widely from natural spaces (Love et al., 2022; Pawlak & Love et al., 2023), and spectral responses to stress can differ significantly across species (Chi et al., 2020; Xiao & McPherson, 2005). Foliage type is one important source of this variation because evergreen, deciduous, and partly deciduous trees have different seasonal vegetation patterns. These differences matter for removal and decline detection because a seasonal drop in vegetation index may reflect normal phenology for one tree type but abnormal canopy loss for another. In addition to this biological variation, urban environments also introduce background noise from buildings, pavement, vehicles, and other infrastructure, which complicates the interpretation of remotely sensed signals (Leisenheimer et al., 2024; Minarik et al., 2020). As a result of both biological variation and background noise, methodologies developed for natural or rural forests do not always translate well to urban contexts.

Satellite time series with high spatial and temporal resolution provide an opportunity to address some of these limitations. Many existing urban forest assessments rely on single time points or multi-year image comparisons, which can identify canopy change but provide limited information about when removals occurred. PlanetScope imagery, with 3-m pixel resolution and daily repeat observations, has the potential to track individual or near-individual tree canopy signals at a cadence that is more useful for urban forest management than canopy losses observed between widely spaced aerial imagery dates (Planet Team, 2025). Integrating frequent satellite observations with high-resolution canopy maps and existing tree records may allow urban tree losses to be identified and dated more precisely than is possible using periodic imagery or field inventories alone.

3.2 Objectives

This study combines biannual NAIP-derived canopy maps, monthly 3-m PlanetScope imagery, and arborist records to evaluate whether individual urban tree removals can be detected and dated more precisely between aerial imagery acquisitions. It also examines whether seasonal vegetation patterns can be distinguished among foliage types and whether signs of canopy decline are visible before removal. This research addresses three primary questions:

1. Can urban tree phenological and functional types (evergreen, semi-deciduous, deciduous) be distinguished using high-resolution satellite imagery (PlanetScope)?
2. How well can urban tree removals be detected using remote sensing, and can removals first identified in NAIP imagery at a multi-year (~2-year) time scale be more precisely dated using higher-frequency PlanetScope imagery?
3. Can signs of canopy decline or dieback be observed in high-resolution satellite imagery (PlanetScope) for trees with known health issues before they are removed?

These questions evaluate the potential of high-temporal-frequency satellite imagery to move urban forest monitoring beyond canopy change over time towards dated records of individual tree loss. More precise information on where and when individual trees are lost could help cities update inventories, evaluate whether planting is keeping pace with removals, and target management resources.

3.3 Methods

I used the PlanetScope, NAIP, CUFI, and arborist datasets to address three related questions (Figure 3.1). First, I used monthly PlanetScope NDVI time series to characterize seasonal patterns and classify foliage type. Second, I used NAIP-derived canopy maps to identify likely tree removals between 2022 and 2024, then used PlanetScope CIre time series to classify removals and estimate when they occurred within that interval. Third, I used arborist records to identify a small set of trees with documented health issues and tested whether spectral decline was visible before removal.

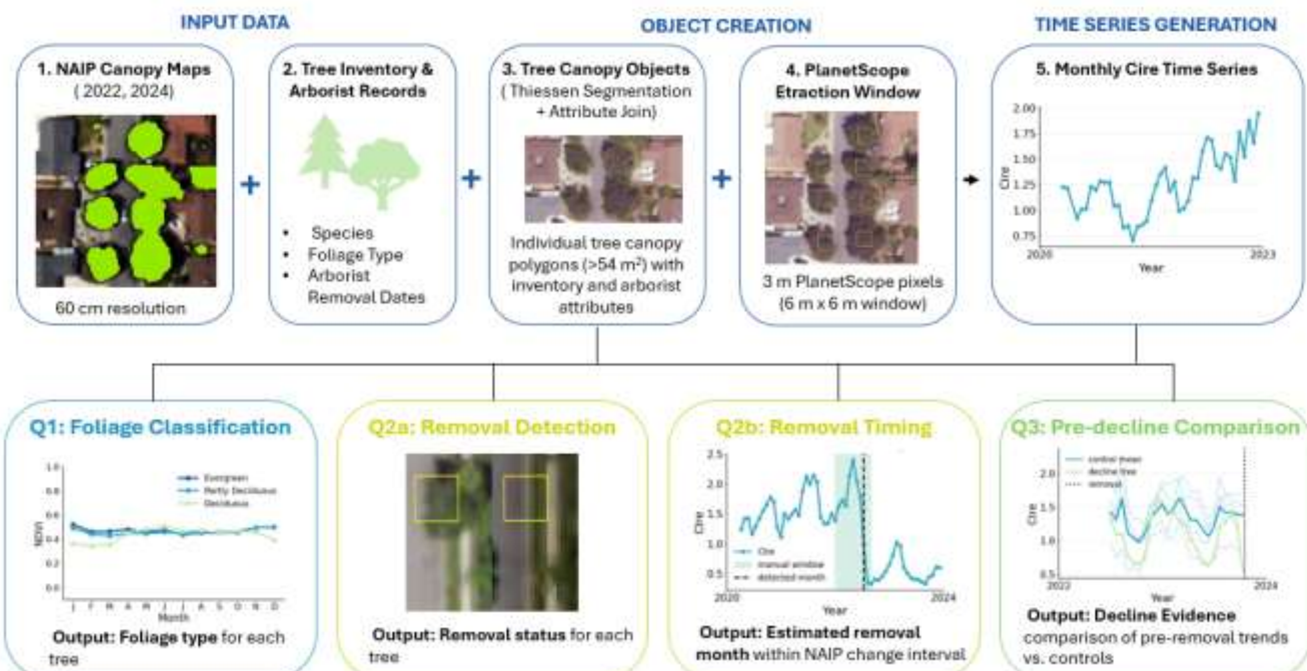

Figure 3.1 A workflow diagram. First, I combined canopy maps, segmented them, and added species, foliage type, and removal data. Then, using extraction windows, I created time series for each tree, which I used to classify foliage type, detect removals and their timing, and compare the time series of removed trees with known health issues to those of control trees.

3.3.1 Study Area

This research was conducted in two California cities: Claremont and Burlingame (Figure 3.2). Cities were selected to represent the state's diverse climates and to have removal records for large trees, as well as robust street tree inventories. Claremont is in Southern California, inland from the coast at the foot of the San Gabriel Mountains, and is characterized by hotter, drier conditions, while Burlingame is located along the northern California coast, which has a cooler, more maritime climate.

Figure 3.2 A map of the two study sites as well as windows used to extract canopy data on top of NAIP imagery (upper, 2020) and PlanetScope imagery (lower, 2020) (Planet Team, 2026).

3.3.2 Tree-Level Dataset Creation

I created the tree-level dataset by segmenting remotely sensed canopy into individual-tree objects and linking those objects to tree inventory and arborist records. Tree canopy objects were extracted from the raster canopy layers produced in Chapter 2. For each city, canopy layers were clipped to the same urban boundary used by Ventura et al. (2024) to ensure dataset consistency between canopy and tree points (Land IQ, 2017). I converted the predicted canopy from rasters to polygons. To associate canopy area with individual trees, I used a point-based tree detection dataset from Ventura et al. (2024) to generate Thiessen polygons, which divided the study area into polygons with boundaries defined by distance to tree points. These polygons were then clipped to the canopy polygon boundaries, resulting in segmented tree canopies (Figure 3.2). I retained canopy objects with at least 54 m^2 of assigned canopy area in 2022. This threshold corresponds to approximately six PlanetScope pixels and reduces the influence of small canopy fragments, co-registration errors, and mixed pixels during time-series extraction. This was also chosen to ensure that the planet extraction window size (two-by-two pixels, Appendix 3A) was smaller than the canopy itself.

I then joined the segmented canopy dataset to the tree attribute data. Species information and foliage type were assigned by spatially joining canopy objects to the California Urban Forest Inventory (CUFI), and removal and maintenance information were joined using the dataset of health inspections and removals from a private arborist company, retaining only cases with a single spatial match to reduce errors.

The California Urban Forest Inventory is a collection of nearly 8 million urban tree records, including species and locations in California (Love et al., 2022). Tree records were collected by professional arborists during tree inventory assessments and compiled into a statewide dataset. Data typically includes species, collection date, location, and DBH. This dataset mostly represents street and park trees, with occasional records for trees cared for by inventory companies on private property. A private tree care company shared arborist records of tree maintenance and removal across California, including species identification and tree health assessments. Records used in this study are first assessed by an arborist for a known health issue, then later removed. Maintenance events are classified into categories such as Disease, Plant Health Care, Removals, and Maintenance, with additional details on treatment type.

After all segmentation and joins were completed, the final tree-level dataset linked segmented canopy polygons with available species, foliage type, maintenance, and removal information. This tree-level dataset was used in the subsequent PlanetScope analyses.

3.3.3 PlanetScope Imagery and Time-Series Extraction

PlanetScope imagery comes from a constellation of CubeSat satellites and requires preprocessing to ensure data quality. Following Dixon et al. (2023), imagery was filtered to include only scenes with less than 10% cloud cover, and the Planet Usable Data Mask 2 was be applied to select clear-sky pixels. To control for any remaining variation across platforms, I compiled monthly means into a time series for each tree, which is what I used for analysis. I tested the influence of individual scenes by recalculating monthly means after dropping one scene at a time; mean absolute change was very small overall, averaging a maximum difference of 0.007 units of Normalized Difference Vegetation Index (NDVI). Data were downloaded for each city from 2020 to 2024. In this study, only PSB.SD (2019-present): PlanetScope sensors were used.

For each tree, the segmented canopy was converted to a standardized PlanetScope extraction window. The centroid of each segmented canopy polygon was used to create a 6-m x 6-m square window, corresponding to a 2 x 2 PlanetScope pixels at 3-m resolution (Figure 3.1- 3.2). The window size was selected based on preliminary testing using known tree removals from the private arborist company dataset. The 2 x 2 window size captured clear differences in vegetation indices before and after documented removals while including multiple PlanetScope pixels, which reduced sensitivity to noise from individual pixels, geolocation mismatch, and mixed-pixel effects (Appendix 3A).

For each tree canopy window on each date, I calculated the mean value of all pixels in the window. Vegetation indices were calculated from the date-specific means of each band (Table 3.1). To detect removals, Chlorophyll Index Red Edge (Cire) and NDVI were used. To identify tree decline prior to removal, four vegetation indices were tested (Table 3.1).

Table 3.1 Vegetation indices used in previous urban tree health research. Citation refers to the first or an early citation of the use of the index.

Vegetation Index	Equation	Citation	Uses in urban forest research
Chlorophyll Index Red Edge	*(NIR / RedEdge) − 1*	Gitelson et al., 2003	Traffic induced stress, leaf level chlorophyll, LAI, urban induced stress (Carlan et al., 2020; Degerickx et al., 2018; Miller et al., 2020)
Normalized Difference Red Edge Index	*(NIR − RedEdge) / (NIR + RedEdge)*	Barnes et al., 2000	Discoloration, pests, canopy level chlorophyll (Chi et al., 2020; Degerickx et al., 2018; Minarik et al., 2020)
Normalized Difference Vegetation Index	*(NIR − Red) / (NIR + Red)*	Rouse et al., 1973	General tree health, canopy condition, drought severity, LAI, pest disturbance stages (Carlan et al., 2020b; Fang et al., 2020; Minarik et al., 2020; Miller et al., 2020, 2022; Morales-Gallegos et al., 2023)
Green Yellow Ratio	*Green / Yellow*	Karlson et al., 2016	General tree health (Fang et al., 2020)

3.3.4 Data Analysis

3.3.3.1 Phenological Classification

To test whether foliage groups show statistically distinguishable seasonal vegetation index signals, I first fit a mixed-effects model using all valid tree-level NDVI observations as the response variable, with foliage type, month, and their interaction included as fixed effects, and a unique identifier included as a random intercept to account for repeated observations. The model was fit using restricted maximum likelihood (REML) with statsmodels MixedLM in Python on 932,041 observations across 6,321 trees. I then used the fitted model to test pairwise differences in estimated mean NDVI among foliage types within each month. For each month, I compared deciduous with evergreen, deciduous with partly deciduous, and evergreen with partly deciduous trees. For each comparison, I recorded the estimated difference in mean NDVI, its 95% confidence interval, and the corresponding test statistic. I adjusted p-values across the monthly pairwise comparisons using the Holm correction.

After testing for differences between foliage types across months, I trained a classifier to predict foliage type for trees without labels. I created five features from each tree's monthly NDVI values: seasonal amplitude (peak minus low monthly mean), the calendar month of peak NDVI, mean winter low (December-February), mean summer peak (June-August), and a seasonality ratio (summer peak divided by winter low). Because the number of usable trees differed between cities (Burlingame: 1,179, Claremont: 5,142), I created an equal-city sample for the linear discriminant analysis (LDA) experiments for training and testing. I randomly subsampled Claremont to 1,179 trees, matching the Burlingame sample size.

I then used linear discriminant analysis to classify trees into foliage type. I conducted three experiments to find the best model and test for transferability of the model using an 80/20 held-out split for each experiment, stratified by both city and foliage type: first, a Claremont-trained model tested on a held-out Claremont sample and applied to Burlingame; second, a Burlingame-trained model tested on a held-out Burlingame sample and applied to Claremont; and third, a combined-city model trained on both cities. Using held-out data, I compared the number of incorrect foliage-type assignments across canopy sizes. Model performance was summarized using precision, recall, F1-score, overall accuracy, and confusion matrices. I applied the best model to the trees in the dataset that lacked foliage-type labels from the California Urban Forest Inventory (CUFI).

3.3.3.2 Tree Removals

NAIP-Based Removal Detection

To identify removed trees, I first used an object-based analysis using canopy polygons derived from NAIP imagery for 2022 and 2024. Because tree polygons derived from aerial imagery may shift year to year, I assigned polygons to years based on their Thiessen polygons. I classified trees as removed if they had a canopy area in 2022 (and area > 54 m^2) and had zero canopy area in the Thiessen tree polygon in 2024. These removal statuses were used to help stratify the manual validation dataset. For a tree to be included in the initial 2022 dataset, it had to be identified as living; to do this, I used NDVI values from hand-annotated targets in California and applied a threshold of NDVI > 0.2 (Appendix 3B).

Validation Dataset

I assessed the accuracy of NAIP-detected removals using a manually created validation dataset of stable and removed trees in Claremont and Burlingame. To stratify my sample, I used NAIP-predicted removed and not-removed tree classes (50 across each city per class, 200 total). If it was unclear which tree was being referred to due to differences in imagery over the years, I assigned a status of NA. I reviewed each tree in Google Earth Pro using historical imagery. For removed trees, I recorded the date of the last image in which the tree was present and the date of the first image in which it was absent. These dates defined the manually validated removal window for each tree.

PlanetScope Removal Features

To test whether removals could be identified using PlanetScope imagery alone, I created CIre time series for each tree polygon from PlanetScope PSB.SD imagery (Table 3.2). A baseline pre-period was defined as all observations before 2022-06-01 to assess each tree's usual patterns, and the post-period (when a tree may have potentially been removed) was defined as from 2022-06-01 through 2024-12-31. Summer was defined as May through September. Winter was defined as December through February. Trees were only assessed for removal if they had a summer NDVI of 0.2 in 2022. To train an LDA to assign removal status, I used CIre index values to create predictor features for the pre/baseline and post/potential removal periods (Table 3.2).

Table 3.2 Features created for LDA predicting tree removal status. Features are made from CIre values. A total of 16 features were calculated from each tree's CIre time series.

Group	Features calculated	Months used	Equation/definition
Seasonal mean	Pre-summer mean, post-summer mean, pre-winter mean, post-winter mean	Summer: May-September; winter: December-February	Mean CIre within each season and period
Seasonal maximum	Pre-summer maximum, post-summer maximum	Summer: May-September	Maximum CIre within each period
Seasonal change	Summer mean drop, summer maximum drop, winter change	Summer: May-September; winter: December-February	Post-period value minus pre-period value
Seasonal amplitude	Pre-period amplitude, post-period amplitude, amplitude ratio	Summer: May-September; winter: December-February	Amplitude = summer mean − winter mean; amplitude ratio = post-period amplitude / pre-period amplitude
Overall signal	Pre-period mean, post-period mean, mean drop, minimum drop	All months	Mean drop = post-period mean − pre-period mean; minimum drop = post-period minimum − pre-period median

I then tested those features for pairwise correlations, then defined a series of reduced LDA models using hand-selected combinations of decline metrics without high correlations, including summer drop, minimum drop, mean post-period, and post amplitude. These candidate models were evaluated on a 70/30 train-test split using overall accuracy, precision, recall, F1 score, and receiver operating characteristic area under the curve (ROC AUC), and the final reduced feature set was selected based on performance and model simplicity. The final reduced Planet-based feature set consisted of four predictors: summer drop, mean post-period, post amplitude, and minimum drop. The resulting LDA trained on those features was my base model for comparison.

To create a more conservative Planet-based removal classifier, I applied an additional threshold to the LDA output using mean drop. Trees were retained as removed only if they were classified as removed by the LDA and also had a mean drop <= 0. Using held-out data, I compared the number of incorrect removal assignments by canopy size and season.

I also evaluated foliage-aware versions of the reduced Planet model by adding categorical foliage-type indicators to the same four-feature LDA. Foliage type was represented using dummy variables for deciduous, evergreen, and partly deciduous classes. These foliage-aware models were tested both with and without the additional mean drop threshold. All methods were validated against the manually created validation dataset and compared using confusion matrices, precision, recall, F1 score, and overall accuracy.

Removal Timing

To estimate the month of removal, I applied a mean-shift breakpoint detector to each removed tree's CIre time series. Timing was evaluated only for trees classified as removed by the Planet-based classifier. Within the detection period from January 1, 2022, through December 31, 2024, the algorithm compared the mean CIre of the six-monthly observations before each candidate breakpoint with the mean of the six-monthly observations after it. The removal date was assigned to the point with the largest decline in CIre if the decline was less than -0.20. Timing accuracy was evaluated using manually validated removal windows. A detected removal was counted as correct if the predicted month fell within the manually validated removal interval. For detections outside the correct months, I calculated the number of months early or late.

Pre-Decline Detection

To explore whether trees with known health issues could be detected in PlanetScope data before removal, I used WCA records as a proxy for documented pest or decline symptoms. I selected trees with active pest, disease, or decline-related work history before removal, including records for diseased or declining evaluations, ISHB, insecticide treatments, Merit injections, trunk injections, or soil injections. Because some inventory coordinates were offset from the actual tree, I manually reviewed and corrected locations in QGIS, then joined the points to the 2022 canopy polygons and associated PlanetScope time series.

Before the pre-decline analysis, I selected several vegetation indices that have been used in previous urban tree health research and compared their ability to capture pre-removal change (Table 3.1). For each confirmed pest-related removal, I extracted monthly time series of CIre, NDVI, NDRE, and Green-Yellow Ratio from PlanetScope imagery. I fit a linear trend over the two years before removal. I compared the pre-removal slopes across indices, and CIre showed the strongest negative trend, so I used it for the remaining analysis.

To test whether CIre declined significantly before removal, I compared each pest tree to up to five nearby same-species control trees from the 2022 canopy dataset, excluding trees with known health issues from arborist records. For each month, I calculated the difference between the pest tree's CIre and the mean CIre of its controls, creating a seasonally adjusted deviation time series. This removed the shared species-level seasonal signal and isolated whether the pest tree was diverging from nearby healthy trees.

For each pest tree, I tested whether monthly deviations were consistently negative using a one-sided Wilcoxon signed-rank test and estimated a linear trend through the deviation series. I also calculated the same anomaly slope for each control tree and z-scored the pest tree's slope against the control distribution. Time to divergence was defined as the first month when the pest tree fell more than one control standard deviation below the control mean, and lead time was calculated as the number of months between that date and confirmed removal. Given the small sample size, results are reported descriptively, with p-values and slope z-scores used as supporting evidence rather than confirmatory inference.

3.4 Results

3.4.1 Phenology

The mixed-effects model showed significant differences in seasonal NDVI trajectories among foliage types for most pairwise comparisons across the year (n = 932,041 observations, 6,321 tree-city records). After Holm correction, deciduous and evergreen trees were different in 11 of 12 months, deciduous and partly deciduous trees in 10 of 12 months, and evergreen and partly deciduous trees in 8 of 12 months. Non-significant comparisons were primarily in late summer and autumn: evergreen vs. partly deciduous was not significant from July through October, deciduous vs. partly deciduous was not significant in April or October, and deciduous vs. evergreen was not significant in October (Figure 3.3).

Effect sizes varied by pair and season (Figure 3.4). The deciduous vs. evergreen contrast was largest in winter, with deciduous trees lower than evergreen trees in January by 0.13 NDVI units (Cohen's $d = -2.29$), and weakest in autumn. The deciduous vs. partly deciduous contrast followed the same seasonal pattern but with smaller differences. The evergreen vs. partly deciduous contrast was the smallest of the three pairs and peaked in January (Cohen’s d = 0.97).

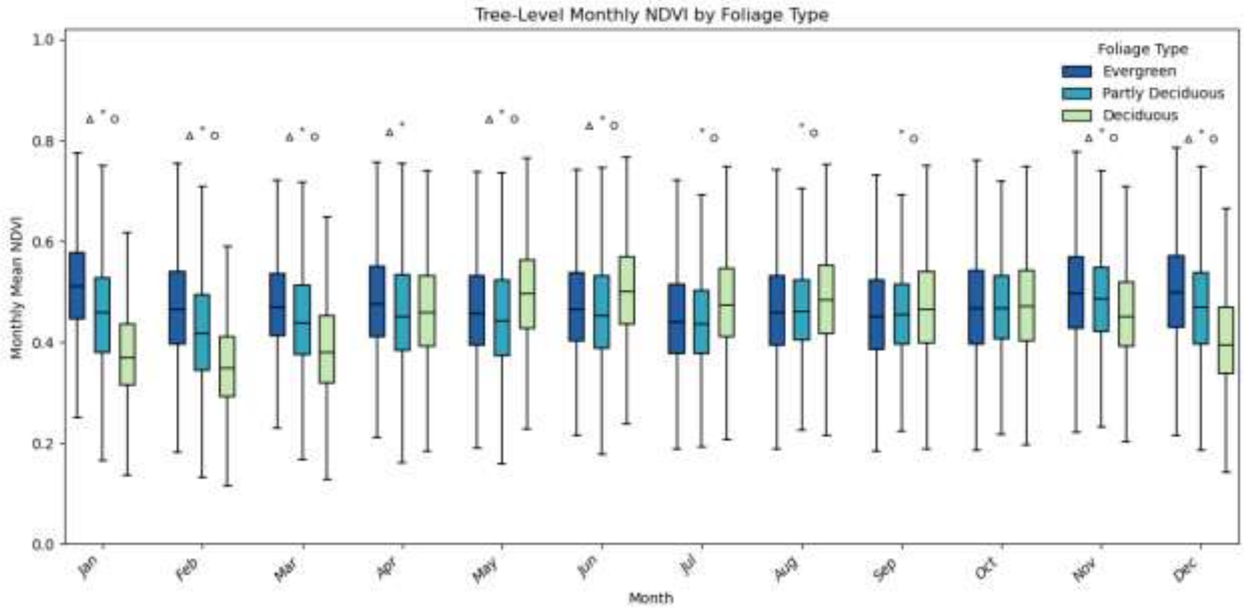

Figure 3.3 Tree-level mean NDVI by foliage type and month. Boxes show the interquartile range; whiskers extend to 1.5× IQR; outliers are omitted. Significance symbols indicate pairwise comparisons that were significant with Holm correction within each month: * = deciduous vs. evergreen; ○ = deciduous vs. partly deciduous; △ = evergreen vs. partly deciduous.*

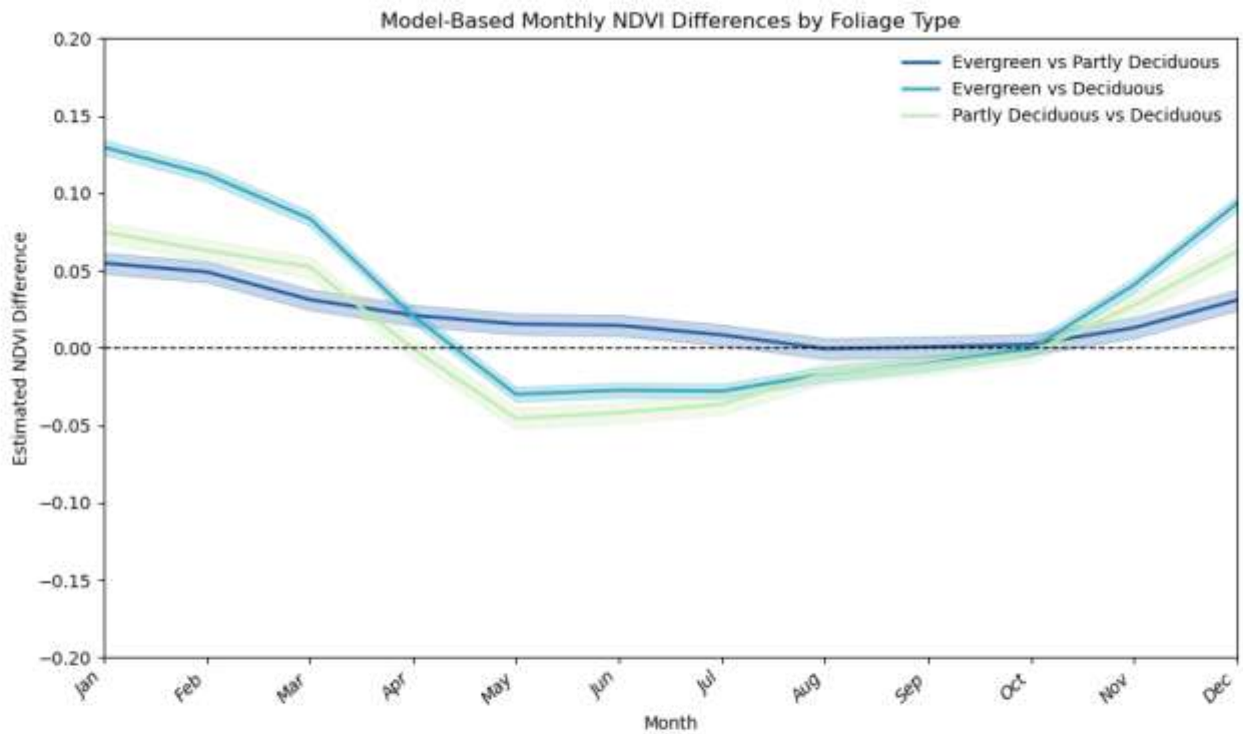

Figure 3.4 Model-estimated monthly NDVI differences between foliage type pairs with 95% confidence intervals. The dashed line indicates zero difference.

LDA classification from the five seasonal NDVI features performed consistently for evergreen and deciduous trees, but partly deciduous trees were poorly recovered across experiments (Table 3.3). Across the single-city training and transfer tests, overall accuracy ranged from 69% when the Burlingame-trained model was applied to Claremont to 88% when the Claremont-trained model was applied to Burlingame. Evergreen and deciduous trees were classified reliably across experiments, while partly deciduous recall remained low, reaching a maximum of 18% and dropping to zero in both transfer tests. The combined-city model was trained on the equal-sample pool using an 80/20 stratified split (train = 1,886; test = 472) and achieved 84% overall accuracy, with 80% accuracy for the Claremont test subset and 89% for Burlingame.

Table 3.3 LDA classification performance by experiment and foliage type. Precision, recall, and F1 reported per class; overall accuracy reported per experiment.

		Applied								
		Claremont			*Burlingame*			*Both*		
Trained	**Foliage Type**	**P**	**R**	**F1**	**P**	**R**	**F1**	**P**	**R**	**F1**
Claremont trained	**D**	0.83	0.73	0.78	0.94	0.91	0.92	-	-	-
	E	0.73	0.96	0.83	0.79	0.87	0.83	-	-	-
	PD	0.64	0.18	0.29	0	0	0	-	-	-
		Accuracy = 75%			*Accuracy = 88%*					
Burlingame trained	**D**	0.63	0.85	0.72	0.91	0.92	0.92	-	-	-
	E	0.74	0.81	0.77	0.81	0.86	0.83	-	-	-
	PD	0	0	0	0	0	0	-	-	-
		Accuracy = 69%			*Accuracy = 88%*					
Combined model	**D**	0.85	0.85	0.85	0.94	0.91	0.92	0.91	0.89	0.9
	E	0.77	0.97	0.86	0.79	0.89	0.84	0.78	0.94	0.85
	PD	0.88	0.18	0.3	0	0	0	0.78	0.16	0.27
		Accuracy = 80%			*Accuracy = 89%*			*Accuracy = 84%*		

Figure 3.5 shows how well the seasonal NDVI features separate foliage types. Deciduous and evergreen trees form more distinct groups, while partly deciduous trees overlap with both. The LD1 distributions confirm this pattern: partly deciduous trees do not form a clearly separate group, which helps explain their lower classification accuracy.

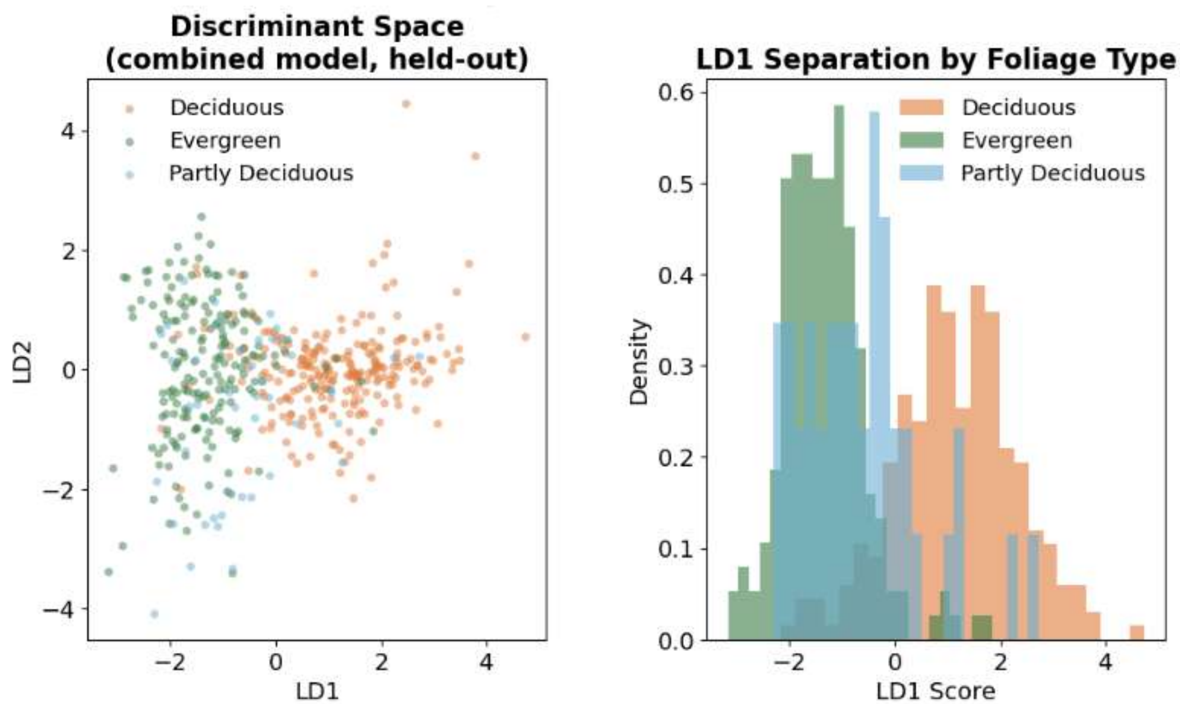

Figure 3.5 Linear discriminant analysis of PlanetScope-derived phenology metrics for the held-out test set in the combined-city foliage-type model. Points in discriminant space separate deciduous trees primarily along LD1, while evergreen and partly deciduous trees show greater overlap. The LD1 density plot highlights the strongest class separation: deciduous trees are shifted toward higher LD1 scores, evergreens toward lower LD1 scores, and partly deciduous trees occupy an intermediate, overlapping range.

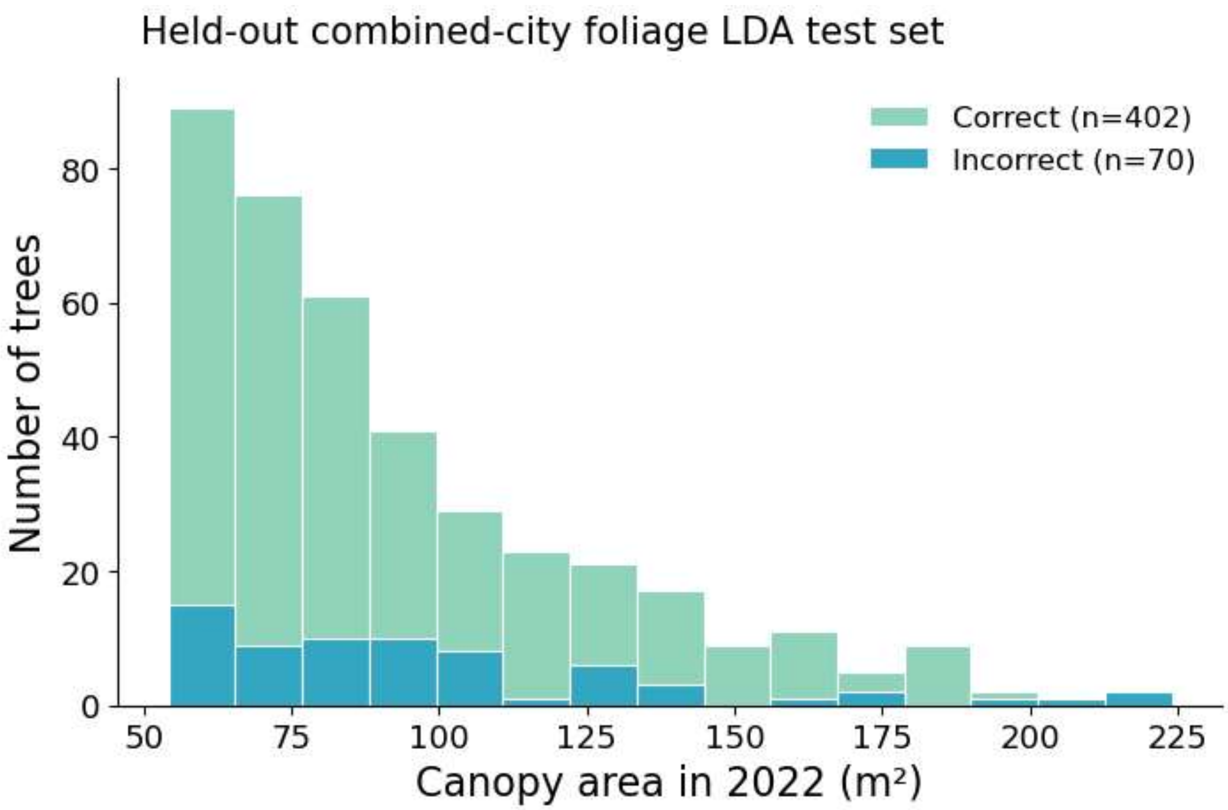

Figure 3.6 Foliage type accuracy by size. The histogram shows the 2022 canopy area for trees correctly and incorrectly classified by the combined-city foliage-type model. Correctly classified trees are shown in light green-blue and incorrectly classified trees in blue. Most classification errors are spread across canopy sizes, suggesting canopy size alone did not explain foliage-type misclassification for trees larger than 54 m^2.

3.4.2 Tree Removals

NAIP-Based Detection

Evaluated against the manually validated labels (Table 3.4), the NAIP-based removal assessment achieved an overall accuracy of 91.7%, with a precision of 0.862, recall of 0.964, and F1 score of 0.910 for predicting removal status across the two-year image period for NAIP.

Performance was similar across cities, with an accuracy of 91.8% in Claremont and 91.7% in Burlingame.

Table 3.4 Confusion matrix for NAIP-based removal detection evaluated against hand-validated labels.

	Predicted: Not Removed	**Predicted: Removed**	**Total**
Actual: Not Removed	96	13	109
Actual: Removed	3	81	84
Total	99	94	193

LDA and Combined Classifier

In the final base LDA, the largest coefficients were for summer drop (-12.130), post-period amplitude (-2.878), minimum drop (-2.730), and mean post-period (-0.843) (Figure 3.7). To compare methods on the same held-out trees, I evaluated the NAIP label, the reduced Planet LDA, the reduced Planet LDA + drop rule, and foliage-aware models on the same test subset (n = 58; 33 stable and 25 removed, including 27 trees from Claremont and 31 from Burlingame). Using the manually validated dataset, the base LDA classifier had an overall accuracy of 81.0% on the held-out test set, with a precision of 0.889, recall of 0.640, F1 score of 0.744, and ROC AUC of 0.834 for the removed class. The otherwise identical foliage-aware version of the same base model produced the same test-set performance.

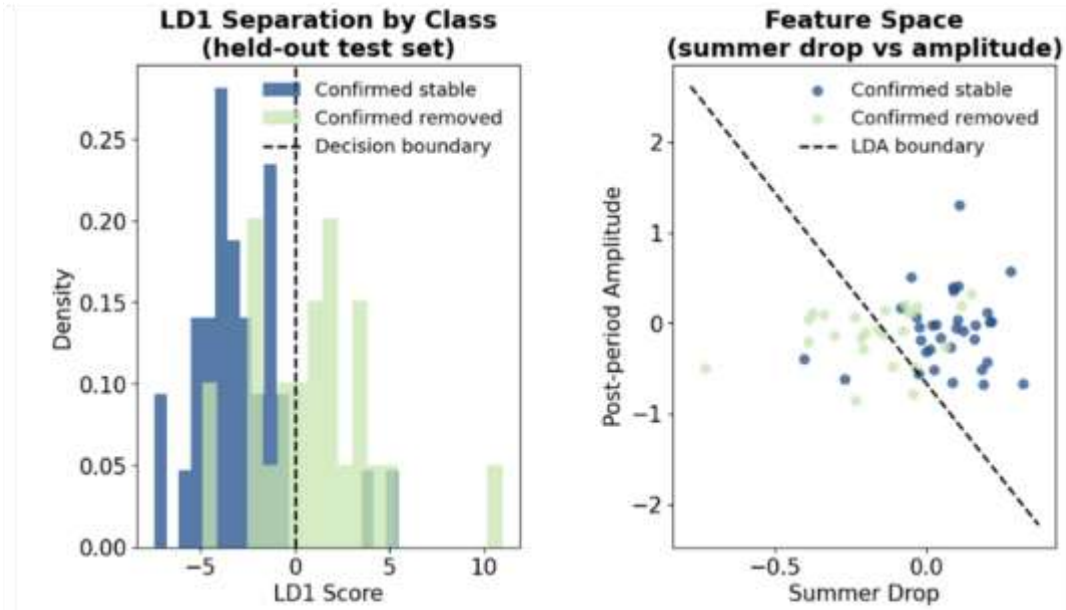

Figure 3.7 Linear discriminant analysis of validated stable and removed trees in the held-out test set. The LD1 density plot shows partial separation between confirmed stable and confirmed removed trees, with removed trees generally shifted toward higher LD1 scores. The dashed line marks the LDA decision boundary. The feature-space plot shows the same classification using summer drop and post-period amplitude, illustrating that removed trees tend to occupy a different region of feature space, although overlap between classes remains.

Adding the mean drop <= 0 threshold to create the combined classifier reduced overall accuracy on the held-out test set to 79.3%, with a precision of 0.882, recall of 0.600, and F1 score of 0.714 for the removed class (Table 3.5). The foliage-aware thresholder model also produced the same test-set performance.

Table 3.5 Precision, recall, F1, and overall accuracy for the NAIP label, reduced Planet LDA, reduced Planet LDA + drop rule, and foliage-aware variants evaluated on the same held-out test set (n = 58).

Metric	NAIP label	Base LDA	Base LDA + Drop Rule	Base LDA + Foliage	Base LDA + Foliage + Drop
Precision (removed class)	0.962	0.889	0.882	0.889	0.882
Recall (removed class)	1.000	0.640	0.600	0.640	0.600
F1 score (removed class)	0.980	0.744	0.714	0.744	0.714
Overall accuracy	0.983	0.810	0.793	0.810	0.793

The accuracy was consistent across tree class sizes for the NAIP removal detection. For the planet-based LDA, removal was less accurate for small trees. (Figure 3.8).

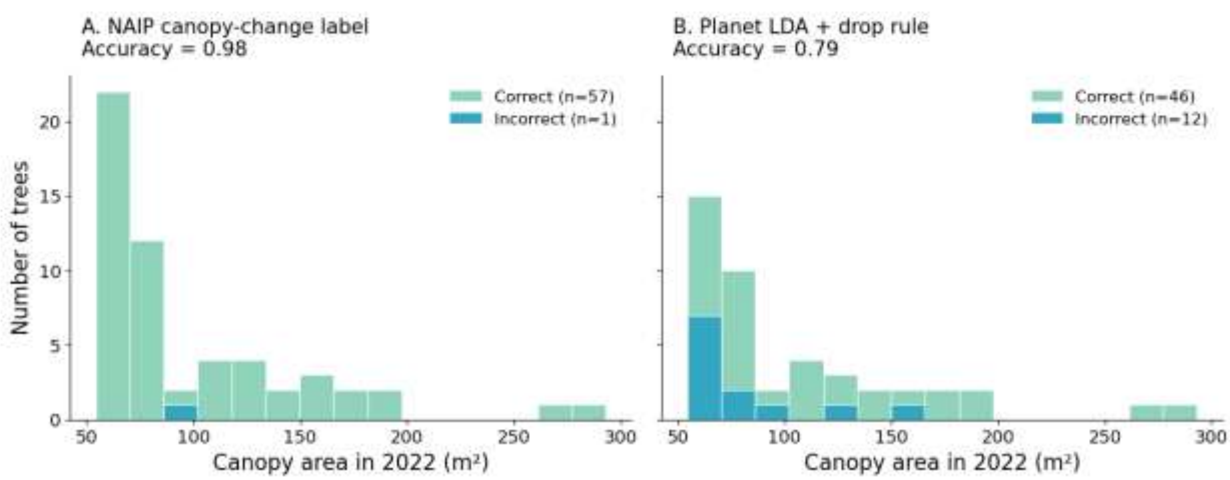

Figure 3.8 Removal detection accuracy by size. The histogram shows the 2022 canopy area for trees correctly and incorrectly classified by the NAIP canopy-change label and the Planet LDA + drop rule. Correctly classified trees are shown in light green-blue and incorrectly classified trees

in blue. The NAIP classifier had one error, while Planet LDA + drop errors were more frequent and concentrated among smaller canopy objects. Canopy size may influence Planet-based removal detection for trees larger than 54 m^2, with smaller tree removals being harder to detect.

Removal Timing

Using the Planet LDA + drop rule classifier, 1,112 polygons were classified as removed, including 855 in Claremont and 257 in Burlingame. Of these, the mean-shift breakpoint detector estimated a removal date for 1,055 polygons (799 in Claremont and 256 in Burlingame; Figure 3.9).

Of the validation dataset, 84 trees were removed; of those, 49 had both a detected Planet removal date and a manually validated removal window, so timing accuracy was evaluated on those 49 trees. Across all validated trees with timing estimates, 36 of 49 trees, or 73.5%, were detected within the manual date range. The median timing offset was 0 months, and the mean timing offset was -0.27 months. Figure 3.10 shows an example monthly CIre time series for correctly timed removals, with Maxar timing windows and the estimated removal dates overlaid.

By city, 24 Claremont trees and 25 Burlingame trees had both a timing estimate and a usable Maxar window. In Claremont, 21 of 24 trees, or 87.5%, were detected within the Maxar month window, with a median offset of 0 months and a mean offset of -0.50 months. In Burlingame, 15 of 25 trees, or 60.0%, were detected within the Maxar month window, with a median offset of 0 months and a mean offset of -0.04 months.

Table 3.6 Removal timing validation against Maxar ground truth windows.

City	Trees with timing estimate (n)	Within Maxar window	Within-window rate	Median month offset	Mean month offset
Claremont	24	21	0.875	0.0	-0.50
Burlingame	25	15	0.600	0.0	-0.04
Overall	49	36	0.735	0.0	-0.27

Of the trees where timing was not estimated correctly within the removal window, ten occurred during winter (Figure 3.9).

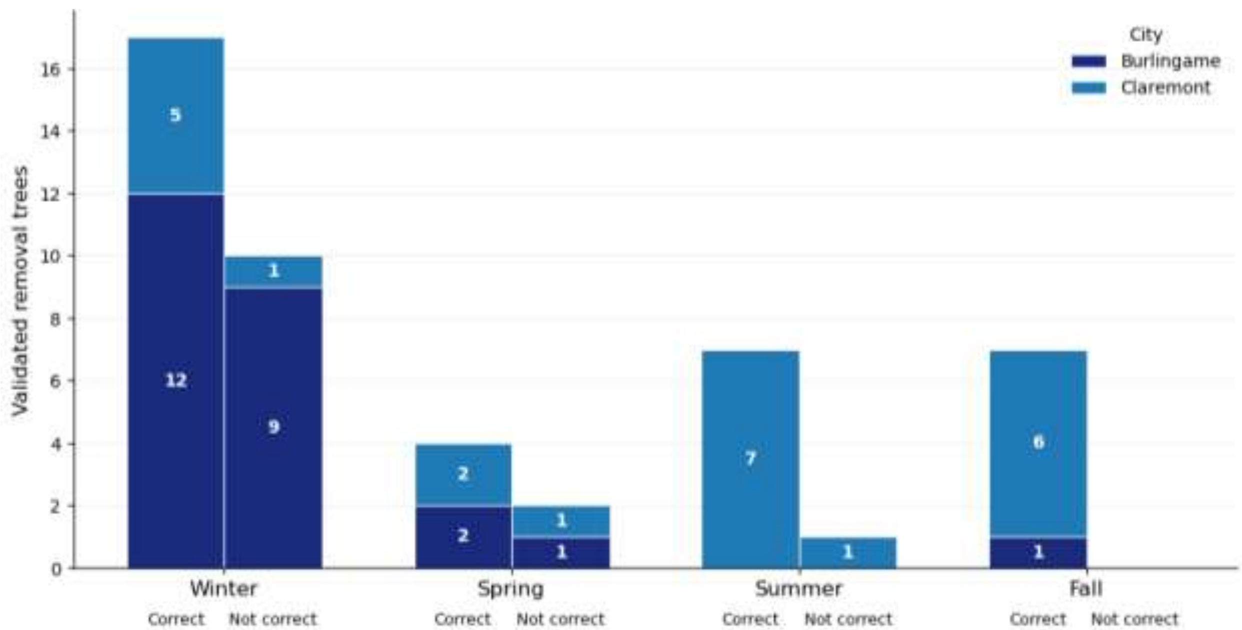

Figure 3.9 Validated removal-timing accuracy by season and city. Winter removals were most common in the validation sample, but winter also contained the largest number of incorrectly timed detections.

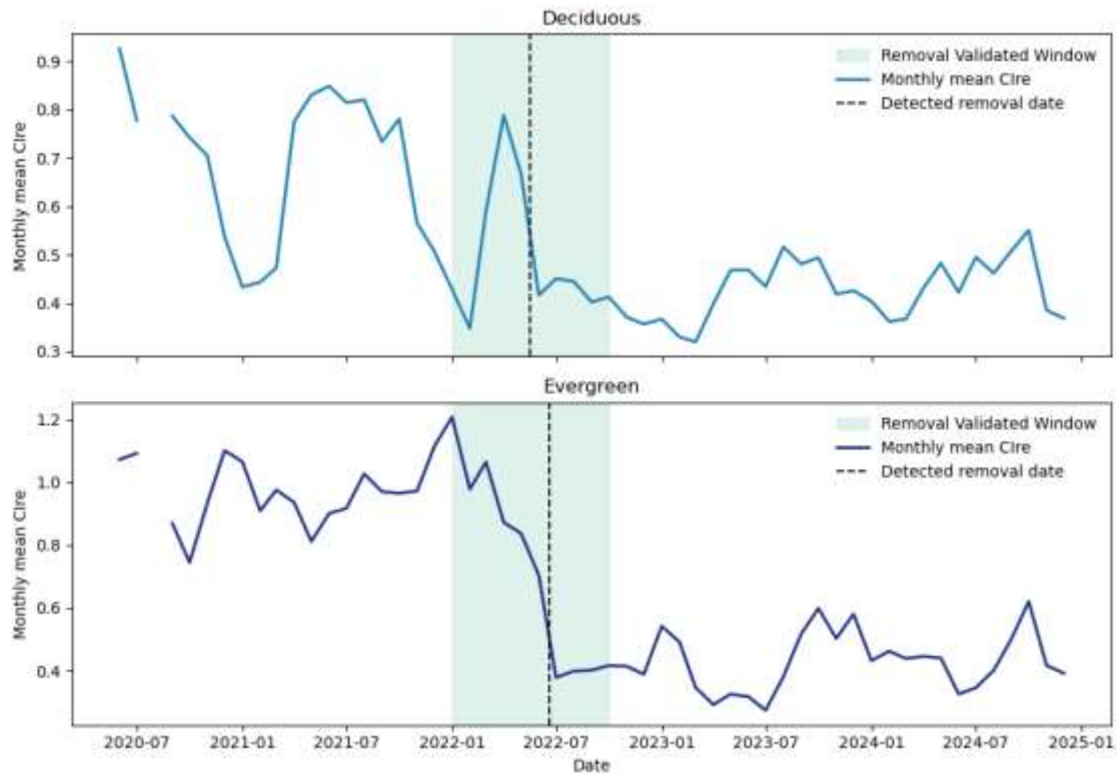
Deciduous
Removal Validated Window
Monthly mean CIre
Detected removal date
Monthly mean CIre
Evergreen
Removal Validated Window
Monthly mean CIre
Detected removal date
Monthly mean CIre
2020-07
2021-01
2021-07
2022-01
2022-07
2023-01
2023-07
2024-01
2024-07
2025-01
Date


8 m
08/2022
01/2022
09/2022
Tree Present- Deciduous
15 m
Imagery ©2026 Google
01/2022
09/2022
03/2023

Figure 3.10 Example monthly Clre timeseries for two trees (Upper a deciduous tree, lower an evergreen tree) with correctly predicted removal dates. The light green region indicates the window or removal determined from Google Earth Pro historical imagery. The dashed line is the detected removal date. Below, the same trees (upper deciduous and lower evergreen) in high-resolution imagery from Google across the removal dates.

3.4.3 Pre-Decline Detection

Across the four vegetation indices evaluated, CIre produced the steepest mean pre-removal slope (-0.0009 CIre/month), with 12 of 18 tree records showing a negative trend in the two years before removal. NDVI, NDRE, and the Green-Yellow ratio showed shallower and less consistent slopes across the same trees. CIre was used for all subsequent analysis.

Of the 12 unique pest/disease trees with sufficient Planet data (3 Claremont, 9 Burlingame), five showed CIre values below those of same-species controls across the two-year pre-removal window (Wilcoxon $p < 0.05$). Two of these had anomaly slopes more than one standard deviation below the control distribution ($z = -1.58$ and $z = -3.76$). The remaining seven trees showed no consistent deviation from the controls, and several were consistently above the controls. Among trees that diverged below -1 standard deviation of the control spread at least once during the pre-removal window, lead times ranged from 17 to 23 months prior to removal (median 19 months).

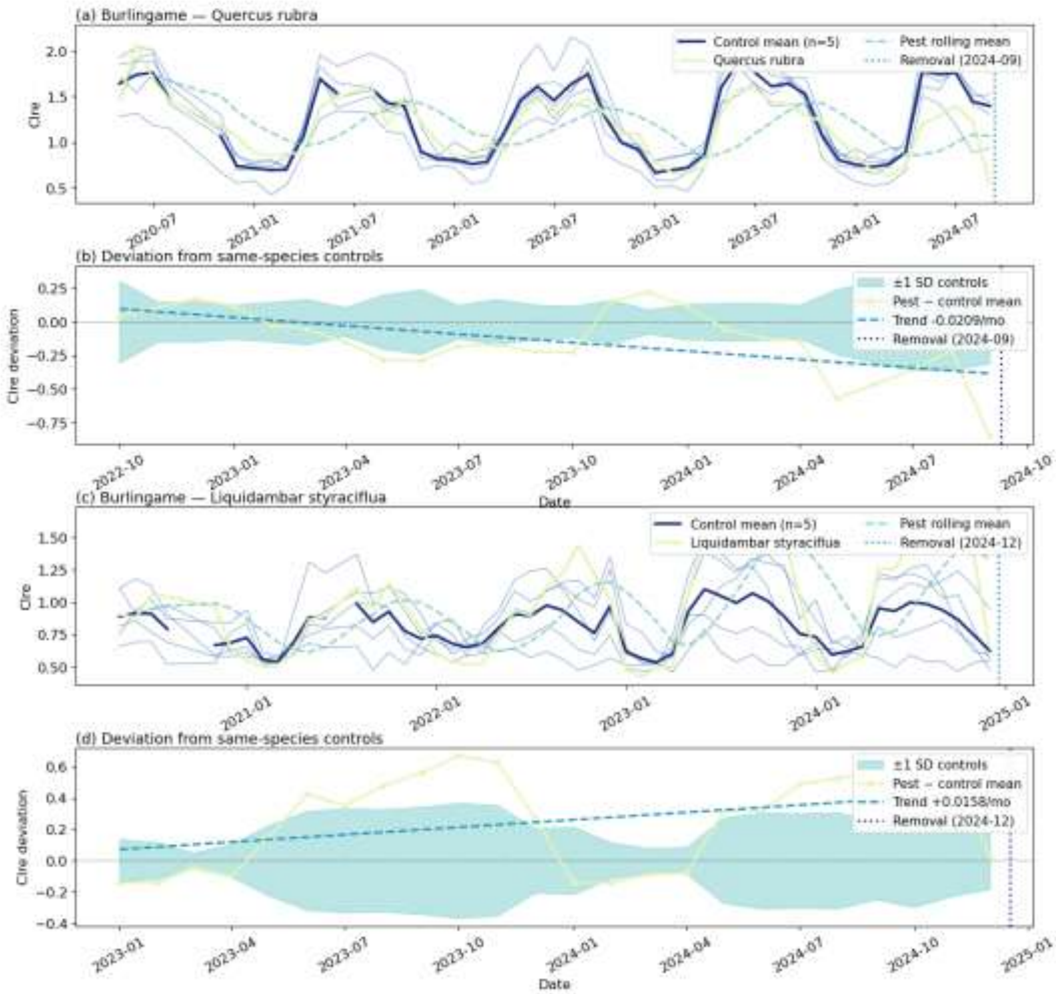

Figure 3.11 Monthly CIre trajectories for two pest/disease trees relative to same-species controls prior to removal. (a, b) Quercus rubra (Burlingame, poly_id 2272), a case in which pre-removal spectral decline was detectable. (c, d) Liquidambar styraciflua (Burlingame, poly_id 2684), a case in which no decline was apparent. Top panels (a, c) show raw monthly CIre for the pest tree (yellow) and its five nearest same-species controls (light blue), with the control mean in dark blue and the pest tree rolling mean as a dashed line. Bottom panels (b, d) show the monthly deviation of the pest tree from the control mean, with the green shaded band indicating ±1 standard deviation of the control spread and the dashed green line showing the linear trend fitted to the deviation series. The removal date is marked with a dotted vertical line.

3.5 Discussion

This study shows that PlanetScope 3-m imagery, combined biannual canopy cover maps and inventory records, can be used to monitor and date individual tree loss. PlanetScope data can be used reliably to narrow NAIP-detected canopy losses to monthly removal windows. The monitoring methods created in this research can be used on any urban forest with access to NAIP data or other high-resolution aerial imagery and the purchase of PlanetScope data for removals, and in any city globally for phenology predictions. This method allows cities to go beyond tracking public trees on the ground and provides a scalable way to monitor where and when trees are being lost across both the public and private urban forest.

3.5.1 Phenology

This study builds on Dixon et al. (2025), who demonstrated that PlanetScope can capture urban tree phenology in a Mediterranean city by extending detection of differences to predict foliage type for trees where it was not previously known. Using CUFI species labels as ground truth, I show that seasonal NDVI signals contain enough consistent information to train a transferable classifier across climatically different cities. The combined-city model classified foliage type with 84% overall accuracy, with higher performance for evergreen and deciduous trees than for partly deciduous trees. This classification step is useful because foliage type shapes both seasonal canopy behavior and how trees respond to climate. Dixon et al. (2025) showed that PlanetScope can detect precipitation- and temperature-linked shifts in urban tree phenology, and predicting foliage type in additional cities could enable broader evaluation of those patterns, even where species-level inventories are incomplete.

The difference in accuracy between Claremont and Burlingame is likely explained by the higher number of partly deciduous trees in Claremont, which the LDA had trouble classifying. This is likely because the group is unclear; partly deciduous is a less distinct functional group than evergreen or deciduous. Misclassified foliage types were spread across canopy sizes rather than concentrated only among the smallest crowns. This suggests that, above the 54-m^2 threshold used here, foliage-type misclassification was driven more by overlap among foliage groups than by canopy size alone.

Although not formally evaluated in this work, species-level phenological differences were also visible in the time series (Appendix 3C). Although this study grouped trees by foliage type, these profiles suggest that additional within-class variation is present, consistent with Wang et al. (2024), who found that PlanetScope NDVI time series could distinguish phenological patterns among common urban street tree genera. Future work could extend the foliage-type classifier toward species- or genus-level phenology models where sufficient labeled inventory data are available.

3.5.2 Removal Detection and Timing

Removal of trees is a unique problem in the urban forest because trees are often removed for reasons unrelated to their health (Clark et al., 2020; Morgenroth et al., 2017). In forests, tree mortality is tracked using remote sensing at both broader and finer spatial scales and can often be linked to environmental causes (Schiefer et al., 2025; Young et al., 2023; Zhou et al., 2026). Trees in the urban forest get removed for a variety of reasons that are difficult to understand retroactively, including development, pest or storm damage, simply landowner preference, or requirements for maintaining defensible space (Croeser et al., 2020; Marchin et al., 2022; Morgenroth et al., 2017). Understanding where trees are removed at broader scales, such as citywide, as demonstrated here, can help clarify where, when, and potentially why trees are being removed. The NAIP canopy-based removal detection performed well, with 91.7% accuracy and near-perfect recall, showing that two-date aerial canopy maps can reliably identify many removals over a multi-year interval. NAIP alone cannot determine when, within that interval, a removal occurred. The Planet-based LDA addressed a different problem by using CIre time series to detect removals within that multi-year window. The base Planet model had lower accuracy than the NAIP label. However, it identified removals from PlanetScope time series alone with 81.0% accuracy and high precision on the held-out test set. This shows that PlanetScope can provide removal information at a finer temporal scale than biannual aerial imagery can, even if the classifier does not detect every removal. NAIP is better for confirming canopy loss, but combining it with PlanetScope time series data is useful because it adds temporal resolution.

The size analysis helps explain the difference between the two approaches. NAIP-based errors were not strongly patterned by canopy size, while Planet LDA + drop errors were more frequent among smaller canopy objects. This is consistent with the spatial resolution of PlanetScope: smaller crowns are more likely to contain mixed pixels from nearby trees, turf, pavement, or buildings, making a removal signal harder to isolate. This does not weaken the Planet result so much as define where it works best. For larger canopy trees, the signal is clearer; for trees closer to the 54-m^2 threshold, detection is more error-prone. Adding foliage type to the Planet removal model did not improve performance. The most likely explanation is that the reduced CIre feature set already captured the relevant seasonal information. Summer drop and post-period amplitude reflect the same seasonal behavior as foliage type, so the explicit label is redundant.

The timing analysis shows why adding PlanetScope to NAIP-based canopy change is useful. NAIP can identify that canopy loss occurred between two image dates, but the PlanetScope time series provides a way to estimate when that loss happened within the interval. This matters for urban forest management because canopy goals depend on both gains and losses. California has set legislative targets to increase urban canopy cover (California AB 2251), but tracking progress is difficult because removals are only detected years after the fact. Monthly removal dates allow cities to calculate net canopy change at finer intervals and evaluate whether planting programs are keeping pace with losses. The timing results also indicate where the method remains limited. Early detections likely reflect trees that had already lost canopy function before they were physically removed. Late or missed detections may reflect gradual removals, partial canopy loss, or months with sparse usable PlanetScope observations.

3.5.3 Pre-Decline Detection

The pre-decline analysis showed mixed results, which reflects both the complexity of the problem and real data limitations. Detecting decline before removal requires three things to align: a documented health issue, a correctly matched canopy object, and sufficient satellite observations prior to removal. In practice, those conditions were rare. Arborist records are collected for operational purposes, not for remote sensing validation, and removal causes are often mixed or incomplete. Many pest- or disease-flagged trees were also removed before the PlanetScope PSB.SD record began, limiting the number of usable cases.

Within the available sample, results were promising for some trees and not others. CIre showed a steeper decline in trees with known issues than NDVI and NDRE, consistent with red-edge chlorophyll indices being more sensitive to early physiological stress before structural decline appears (Chi et al., 2020; Degerickx et al., 2018; Gitelson et al., 2003). The clearest evidence that this kind of detection is achievable comes from Falanga et al. (2024), who used PlanetScope at the same 3-m resolution to detect pine tortoise scale infestation in Italian stone pines in Rome, achieving 99% accuracy using a summer RDVI drop relative to healthy reference trees. That study had a large, well-matched dataset of confirmed pest-infested trees observed concurrently with the satellite data. The results here suggest that with better-matched ground truth records, a similar approach could work for the species and pest types present in California urban forests.

3.5.4 Limitations

In addition to the limitations mentioned in the specific sections above, canopy segmentation with Thiessen polygons approximates individual tree crowns rather than providing a true crown delineation. This means that some polygons likely include mixed pixels from nearby trees, grass, pavement, or buildings, especially near polygon edges and for smaller trees close to the 54-m² area threshold. The approach also cannot fully separate overlapping canopies in dense plantings.

The 54-m² minimum area threshold helped reduce mixed-pixel noise, but it also excluded many smaller urban trees. As a result, this analysis is focused on larger canopy trees and may not fully represent smaller street trees, newly planted trees, or trees with narrow crowns.

3.5.5 Future Directions

The next step is to move from testing this approach on past removals toward using it as an ongoing monitoring tool. A version that cities could use would require, at minimum, a city tree inventory and access to PlanetScope imagery, both of which are increasingly available across cities globally (Ossola, 2020). In California, the CUFI dataset covers much of the state, PlanetScope provides near-daily global coverage, and Chapter 2 produced canopy maps for every city in the state using NAIP imagery. These methods could therefore be applied across California and in other cities meeting these criteria. In cities without tree inventories, PlanetScope data could still be used to identify potential removals and evaluate where canopy is changing.

Applying the removal dataset across multiple cities would also make it possible to investigate the activities associated with tree loss. Future work could compare removals across public and private land and among major parcel types. On private property, removal locations could be linked with U.S. Department of Housing and Urban Development data, building permits, demolition records, and redevelopment indicators to assess how often tree loss coincides with development or other changes to the built environment.

The phenology classifier could also support broader climate-phenology analyses. Dixon et al. (2025) showed that urban tree phenology can respond to precipitation and temperature, but applying that type of analysis across many cities requires foliage or species information that is often incomplete. A transferable foliage-type classifier could extend climate-sensitivity analyses to cities without complete inventory attributes, allowing future work to compare how urban tree phenology shifts across coastal, inland, and arid climate zones. Future analyses could also test classification approaches that are more robust to correlated phenological predictors and overlapping seasonal signatures. These models may improve winter performance, when distinctions among foliage types were weakest, and improve identification of partly deciduous trees. Species-specific models are the next step for both phenology classification and removal detection.

Additional pest, disease, pruning, and tree-condition records that overlap with satellite observations would strengthen the pre-decline component of this work. A larger sample drawn from more cities could test whether repeated satellite observations consistently identify canopy decline before removal and distinguish biological decline from seasonal variation, pruning, or other management-related changes.

The most significant near-term improvement may come from using data from Planet's forthcoming Owl constellation, which is designed to provide near-daily imagery at approximately 1-m resolution. At 1-m resolution, individual crowns could be delineated more precisely, annual canopy masks could be produced directly from Planet data using the model developed in Chapter 2, and the minimum detectable tree size could be reduced. This would address current limitations related to crown delineation, temporal alignment, and size exclusion and could allow the full methodology to rely on a single imagery source.

3.5 References

Allen, M. A., Roberts, D. A., & McFadden, J. P. (2021). Reduced urban green cover and daytime cooling capacity during the 2012–2016 California drought. *Urban Climate*, *36*, 100768. https://doi.org/10.1016/j.uclim.2020.100768

Chi, D., Degerickx, J., Yu, K., & Somers, B. (2020). Urban Tree Health Classification Across Tree Species by Combining Airborne Laser Scanning and Imaging Spectroscopy. *Remote Sensing*, *12*(15), 2435. https://doi.org/10.3390/rs12152435

Clark, C., Ordóñez, C., & Livesley, S. J. (2020). Private tree removal, public loss: Valuing and enforcing existing tree protection mechanisms is the key to retaining urban trees on private land. *Landscape and Urban Planning*, *203*, 103899. https://doi.org/10.1016/j.landurbplan.2020.103899

Croeser, T., Ordóñez, C., Threlfall, C., Kendal, D., Van Der Ree, R., Callow, D., & Livesley, S. J. (2020). Patterns of tree removal and canopy change on public and private land in the City of Melbourne. *Sustainable Cities and Society*, *56*, 102096. https://doi.org/10.1016/j.scs.2020.102096

Dixon, A. K., Alonzo, M., Roberts, D. A., & McFadden, J. P. (2025). Sensitivity of urban tree leaf phenology to precipitation and temperature in a Mediterranean climate city. *Urban Forestry & Urban Greening*, *113*, 129022. https://doi.org/10.1016/j.ufug.2025.129022

Dixon, D. J., Zhu, Y., Brown, C. F., & Jin, Y. (2023). Satellite detection of canopy-scale tree mortality and survival from California wildfires with spatio-temporal deep learning. *Remote Sensing of Environment*, *298*, 113842. https://doi.org/10.1016/j.rse.2023.113842

Falanga, V., Francini, S., Parisi, F., Cavalli, A., De Fioravante, P., Cucca, B., D'Amico, G., Chirici, G., Lasserre, B., Ottaviano, M., Munafò, M., & Marchetti, M. (2024). Near-Real-

Time Detection of Insect Outbreaks in Urban Trees Using a PlanetScope Time Series. *Forests*, *15*(12), 2261. https://doi.org/10.3390/f15122261

Hilbert, D., Roman, L., Koeser, A., Vogt, J., & Van Doorn, N. (2019). Urban Tree Mortality: A Literature Review. *Arboriculture & Urban Forestry*, *45*(5). https://doi.org/10.48044/jauf.2019.015

Kraemer, R., & Kabisch, N. (2022). Parks Under Stress: Air Temperature Regulation of Urban Green Spaces Under Conditions of Drought and Summer Heat. *Frontiers in Environmental Science*, *10*, 849965. https://doi.org/10.3389/fenvs.2022.849965

Land IQ. (2017). *Land Use—2014—Land IQ [ds2677]* [Dataset]. https://map.dfg.ca.gov/metadata/ds2677.html

Lausch, A., Erasmi, S., King, D., Magdon, P., & Heurich, M. (2016). Understanding Forest Health with Remote Sensing -Part I—A Review of Spectral Traits, Processes and Remote-Sensing Characteristics. *Remote Sensing*, *8*(12), 1029. https://doi.org/10.3390/rs8121029

Leisenheimer, L., Wellmann, T., Jänicke, C., & Haase, D. (2024). Monitoring drought impacts on street trees using remote sensing—Disentangling temporal and species-specific response patterns with Sentinel-2 imagery. *Ecological Informatics*, *82*, 102659. https://doi.org/10.1016/j.ecoinf.2024.102659

Livesley, S. J., McPherson, E. G., & Calfapietra, C. (2016). The Urban Forest and Ecosystem Services: Impacts on Urban Water, Heat, and Pollution Cycles at the Tree, Street, and City Scale. *Journal of Environmental Quality*, *45*(1), 119–124. https://doi.org/10.2134/jeq2015.11.0567

Love, N. L. R., Grady, E., Pawlak, C., Ventura, J., Fricker, G. A., Doremus, J., Ritter, M. K., & Yost, J. M. (In Submission). *Most urban trees occur on private land in California: A statewide mapping assessment [In Submission]*.

Love, N. L. R., Nguyen, V., Pawlak, C., Pineda, A., Reimer, J. L., Yost, J. M., Fricker, G. A., Ventura, J. D., Doremus, J. M., Crow, T., & Ritter, M. K. (2022). Diversity and structure in California's urban forest: What over six million data points tell us about one of the world's largest urban forests. *Urban Forestry & Urban Greening*, *74*, 127679. https://doi.org/10.1016/j.ufug.2022.127679

Marchin, R. M., Esperon-Rodriguez, M., Tjoelker, M. G., & Ellsworth, D. S. (2022). Crown dieback and mortality of urban trees linked to heatwaves during extreme drought. *Science of The Total Environment*, *850*, 157915. https://doi.org/10.1016/j.scitotenv.2022.157915

Minařík, R., Langhammer, J., & Lendzioch, T. (2020). Automatic Tree Crown Extraction from UAS Multispectral Imagery for the Detection of Bark Beetle Disturbance in Mixed Forests. *Remote Sensing*, *12*(24), 4081. https://doi.org/10.3390/rs12244081

Morales-Gallegos, L. M., Martínez-Trinidad, T., Hernández-de La Rosa, P., Gómez-Guerrero, A., Alvarado-Rosales, D., & Saavedra-Romero, L. D. L. (2023). Tree Health Condition in Urban Green Areas Assessed through Crown Indicators and Vegetation Indices. *Forests*, *14*(8), 1673. https://doi.org/10.3390/f14081673

Morgenroth, J., O'Neil-Dunne, J., & Apiolaza, L. A. (2017). Redevelopment and the urban forest: A study of tree removal and retention during demolition activities. *Applied Geography*, *82*, 1–10. https://doi.org/10.1016/j.apgeog.2017.02.011

Nazeer, M., Wong, M. S., Yu, X., Kwok, C. Y. T., Peng, Q., & Dai, Y. (2024). Urban tree health assessment using multifaceted remote sensing datasets: A case study in Hong Kong. *Remote*

Sensing Applications: Society and Environment, *36*, 101347. https://doi.org/10.1016/j.rsase.2024.101347

Orusa, T., & Mondino, E. (2021). Exploring Short-Term Climate Change Effects on Rangelands and Broad-Leaved Forests by Free Satellite Data in Aosta Valley (Northwest Italy). *Climate*, *9*(3), 47. https://doi.org/10.3390/cli9030047

Ossola, A., Hoeppner, M. J., Burley, H. M., Gallagher, R. V., Beaumont, L. J., & Leishman, M. R. (2020). The Global Urban Tree Inventory: A database of the diverse tree flora that inhabits the world's cities. *Global Ecology and Biogeography*, *29*(11), 1907–1914. https://doi.org/10.1111/geb.13169

Pawlak, C. C., Love, N. L. R., Yost, J. M., Fricker, G. A., Doremus, J. M., & Ritter, M. K. (2023). California's native trees and their use in the urban forest. *Urban Forestry & Urban Greening*, *89*, 128125. https://doi.org/10.1016/j.ufug.2023.128125

Planet Team. (2026). *Planet Application Program Interface: In Space for Life on Earth* [Dataset]. https://api.planet.com

Plowright, A. A., Coops, N. C., Eskelson, B. N. I., Sheppard, S. R. J., & Aven, N. W. (2016). Assessing urban tree condition using airborne light detection and ranging. *Urban Forestry & Urban Greening*, *19*, 140–150. https://doi.org/10.1016/j.ufug.2016.06.026

Rey-Gozalo, G., Barrigón Morillas, J. M., Montes González, D., & Vílchez-Gómez, R. (2023). Influence of Green Areas on the Urban Sound Environment. *Current Pollution Reports*, *9*(4), 746–759. https://doi.org/10.1007/s40726-023-00284-5

Roman, L. A., Battles, J. J., & McBride, J. R. (2014). The balance of planting and mortality in a street tree population. *Urban Ecosystems*, *17*(2), 387–404. https://doi.org/10.1007/s11252-013-0320-5

Schiefer, F., Schmidtlein, S., Hartmann, H., Schnabel, F., & Kattenborn, T. (2025). Large-scale remote sensing reveals that tree mortality in Germany appears to be greater than previously expected. *Forestry: An International Journal of Forest Research*, *98*(4), 535–549. https://doi.org/10.1093/forestry/cpae062

Song, X. P., Tan, P. Y., Edwards, P., & Richards, D. (2018). The economic benefits and costs of trees in urban forest stewardship: A systematic review. *Urban Forestry & Urban Greening*, *29*, 162–170. https://doi.org/10.1016/j.ufug.2017.11.017

Tabassum, S., Manea, A., Ossola, A., Thomy, B., Blackham, D., & Leishman, M. R. (2021). The angriest summer on record: Assessing canopy damage and economic costs of an extreme climatic event. *Urban Forestry & Urban Greening*, *63*, 127221. https://doi.org/10.1016/j.ufug.2021.127221

Van Doorn, N. S., Roman, L. A., McPherson, E. G., Scharenbroch, B. C., Henning, J. G., Östberg, J. P. A., Mueller, L. S., Koeser, A. K., Mills, J. R., Hallet, R. A., Sanders, J. E., Battles, J., Boyer, D. J., Fristensky, J. P., Mincey, S. K., Peper, P. J., & Vogt, J. M. (2020). *Urban tree monitoring: A resource guide* (PSW-GTR-266; p. PSW-GTR-266). U.S. Department of Agriculture, Forest Service, Pacific Southwest Research Station. https://doi.org/10.2737/PSW-GTR-266

Wang, H., & Gong, F.-Y. (2024). Quantifying City- and Street-Scale Urban Tree Phenology from Landsat-8, Sentinel-2, and PlanetScope Images: A Case Study in Downtown Beijing. *Remote Sensing*, *16*(13), 2351. https://doi.org/10.3390/rs16132351

Xiao, Q., & McPherson, E. G. (2005). Tree health mapping with multispectral remote sensing data at UC Davis, California. *Urban Ecosystems*, *8*(3–4), 349–361. https://doi.org/10.1007/s11252-005-4867-7

Young, D. J. N., Slaton, M. R., & Koltunov, A. (2023). Temperature is positively associated with tree mortality in California subalpine forests containing whitebark pine. *Ecosphere*, *14*(2), e4400. https://doi.org/10.1002/ecs2.4400

Zhou, X., Guindon, L., Perbet, P., Reisi Gahrouei, O., Côté, J.-F., Waldron, K., Kneeshaw, D., & Béland, M. (2026). Mapping the extent and severity of tree mortality and defoliation caused by spruce budworm using landsat time series. *International Journal of Remote Sensing*, *47*(6), 2447–2475. https://doi.org/10.1080/01431161.2026.2617734

3.6 Appendix

Appendix 3A: Window size experiment on a removed vs. stable tree. NDVI values before and after removal, and across the same time period for the stable tree. Each tree was visually inspected. Some trees did not show change; this was due to being already dead in the removal period, for example, Tree 7.

Appendix 3B: Known polygons were digitized in Claremont, CA of know targets of trees, buildings, roads and grass.

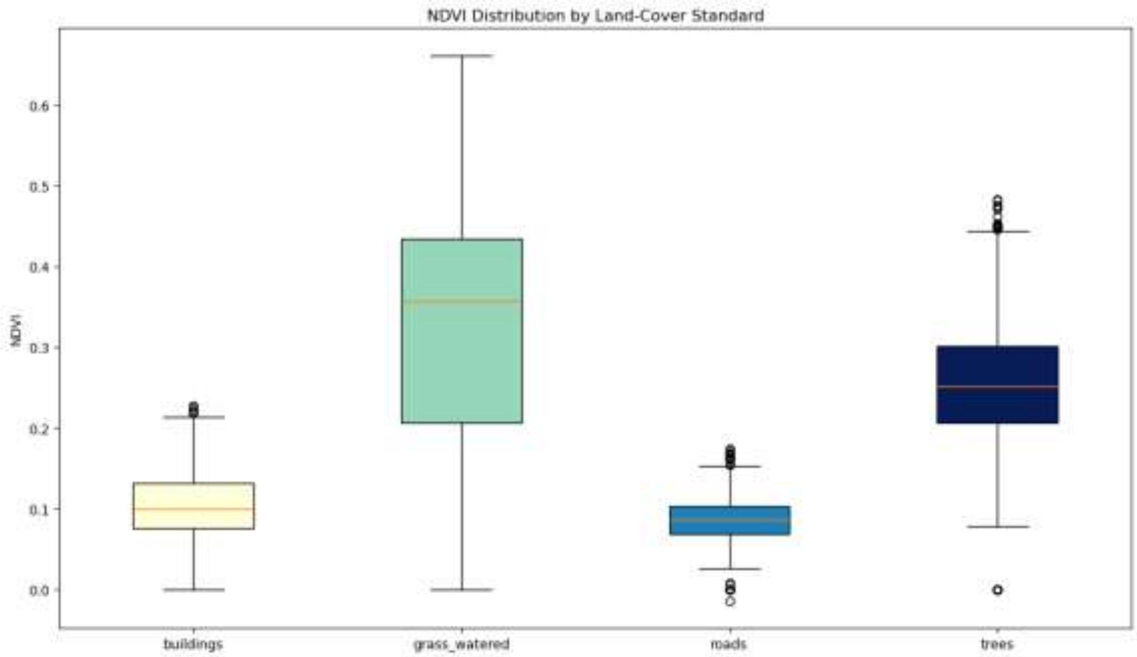

Appendix 3C: Monthly NDVI from selected tree species showing seasonality varying by species.

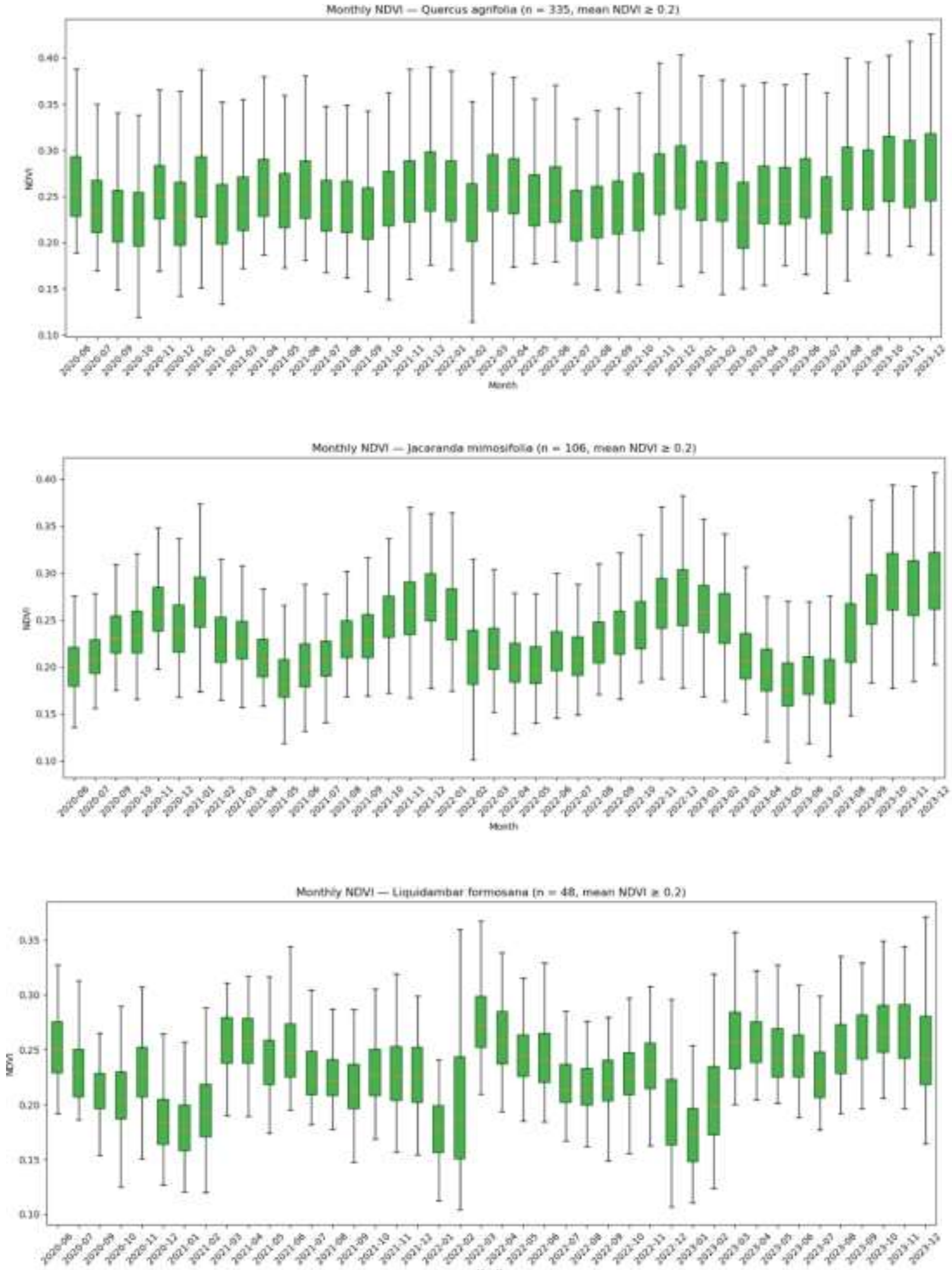

Chapter 4. Urban Canopy Post-Fire: Using remote sensing to measure urban tree recovery

Abstract

In January 2025, major fires burned in urban areas of Los Angeles County, California, destroying homes, infrastructure, and trees. Vegetation response to severe fire disturbance is well studied in forestry literature, but how urban trees respond to and recover from fire remains relatively unexplored. Here, I use high-spatial- and high-temporal-resolution PlanetScope imagery, pre-fire canopy maps, and tree inventory data to examine individual tree canopy condition relative to pre-fire baselines following the Palisades and Eaton fires. Approximately three months after the fires, in April 2025, 26.7% of large fire-affected urban trees fell within their own pre-fire ±2 standard deviation range of NDVI values. By April 2026, this increased to 38.5%, although the mean canopy condition in both cities remained below the recovery threshold. Burn severity was the most consistent predictor of how far trees fell below their pre-fire baseline across all recovery outcomes after accounting for spatial autocorrelation, property type, foliage type, and city. Recovery also varied by foliage type, species, property type, and city, although these associations were less consistent than the effect of burn severity. Post-fire urban forest recovery, as measured here, should be interpreted as an early snapshot of canopy condition in Altadena and Pacific Palisades shaped by fire damage, biological factors, and human intervention together. Continued monitoring can show which trees continue to recover, which remain persistently below their pre-fire condition, and where canopy loss occurs as rebuilding continues.

4.1 Introduction

In January 2025, two major urban areas within Los Angeles County, California, USA, (Altadena and the Pacific Palisades) experienced massive urban wildfires that led to human fatalities and the near-total destruction of large swaths of urban areas. In the year and a half following the fires, the clearing and rebuilding of urban infrastructure have taken place, including the urban forest. Urban trees provide urban residents with measurable benefits, such as cooling (Ettinger et al., 2024; Ziter et al., 2019), but also perceived benefits such as a sense of place and home. After a major fire, urban trees become part of the reconstruction process: they must be assessed, retained, removed, or replaced.

How trees respond to and recover from fire in wildlands is well studied (Pena-Molina et al., 2024; Rodrigues et al., 2024; Ryu et al., 2018), but little is known about how urban forests respond to and recover from fire. Unlike many natural forests, urban forests are composed largely of non-native tree species (Love et al., 2022; Pawlak et al., 2023), often selected for aesthetics or performance under urban stressors. Responses to stress can differ significantly across species (Chi et al., 2020; Xiao & McPherson, 2005). Previous research has shown that urban canopy cover recovery post-fire can vary by city, with differences in recovery trajectories influenced by local biome, elevation, and socio-ecological context (Escobedo et al., 2024), but variation in recovery by species within urban areas is largely unexplored and needs to be better understood so that cities can better plan for and respond to future devastating fires.

Even without fire, cities are high-stress environments for trees, with pressures such as soil compaction, limited space, drought, pollution, pests, and vandalism (Hilbert et al., 2019). Following wildfire, surviving urban trees may be exposed to additional compounding stress from construction, root damage, or changes in soil hydrology. While some trees may recover over time, others may appear structurally sound yet suffer from internal decline that leads to delayed mortality. In natural systems, some tree species are known to recover even after severe damage (Bar, 2019), but it remains unclear how these dynamics play out in the species-diverse, human-modified landscapes of cities.

Remote sensing can be used to monitor recovery after fire in natural forests (Goetz et al., 2006; Mitri & Gitas, 2013). Trees' response to stress can cause spectral trait variations that can be measured using remote sensing (Lausch et al., 2016). Urban forests are challenging environments for remote sensing due to species heterogeneity and complex built environments. Urban environments have background noise from buildings, pavement, vehicles, and other infrastructure, which complicates the interpretation of remotely sensed signals and makes it difficult to obtain standard values across a species or group of interest (Leisenheimer et al., 2024; Minarik et al., 2020). Higher spatial and temporal resolution can reduce some of these limitations. PlanetScope satellites provide daily imagery of the globe with relatively high resolution (3 meters). Previous studies have used PlanetScope to accurately identify stressed trees in an urban environment (Falanga et al., 2024). Building on Chapter 2, which demonstrated the use of PlanetScope time series for individual urban trees, this study evaluates post-fire canopy condition and recovery trajectories relative to each tree's own pre-fire baseline.

4.1.1 Objectives

This research examines how urban trees persist, recover, or are lost following wildfire in Altadena and Pacific Palisades. Using PlanetScope time series imagery, pre-fire canopy maps, and tree inventory data, I track individual tree canopies from pre-fire baselines (2022-2024) through one year post-fire (2025) and spring of 2026 (April) to answer two primary research questions:

1. What patterns of recovery or removal are present across burnt urban trees in the Pacific Palisades and Altadena on public and private land?
2. Is there variation across tree species/foliage types in their recovery after the major urban fire events?

By measuring post-fire canopy condition relative to each tree's own pre-fire baseline, this study provides a method for monitoring post-fire urban forest outcomes and documents early recovery patterns in the urban forests of Altadena and Pacific Palisades.

4.2 Methods

4.2.1 Study Area

The Pacific Palisades (part of the City of Los Angeles) and Altadena (an unincorporated community) both occur in Los Angeles County, California at the wildland-urban interface (Figure 4.1). Altadena had a population of 43,037, and is located in the foothills of the San Gabriel Mountains, part of the Transverse Ranges (U.S. Census Bureau, 2020). The Pacific Palisades (Zip-Code 90272) had a population of 22,849 and is located in the Santa Monica Mountains, also part of the Transverse Ranges (U.S. Census Bureau, 2020). The region experiences a Mediterranean climate, with hot, dry summers and mild, wet winters.

Altadena's urban forest includes an estimated 60,867 trees (excluding wildland areas), based on the 2020 California TreeDetector dataset (Ventura et al., 2024). Of these, 27,786 have canopy areas over 54 m^2, and of those, 2,246 trees have associated species data from the

California Urban Forest Inventory (CUFI), representing 141 unique species (Love et al., 2022). The Eaton Fire burned through portions of Altadena and surrounding wildlands, ultimately covering 5,674 hectares before being fully contained (Figure 4.1).

The Pacific Palisades urban forest includes an estimated 48,954 trees (excluding wildland areas), based on the 2020 California TreeDetector dataset (Ventura et al., 2024). Of these, 21,223 have canopy areas over 54 m^2, and of those 2,103 trees have associated species data from the California Urban Forest Inventory (CUFI), representing 134 unique species (Love et al., 2022). The Palisades Fire burned 23,448 acres before being fully contained (Figure 4.1). Both fires ignited on January 7th, 2025. Prior to the fires, October 2024 through January 7th 2025 was Southern California's second driest period on record, following two wet winters in 2022 and 2023 (Guirguis et al., 2025).

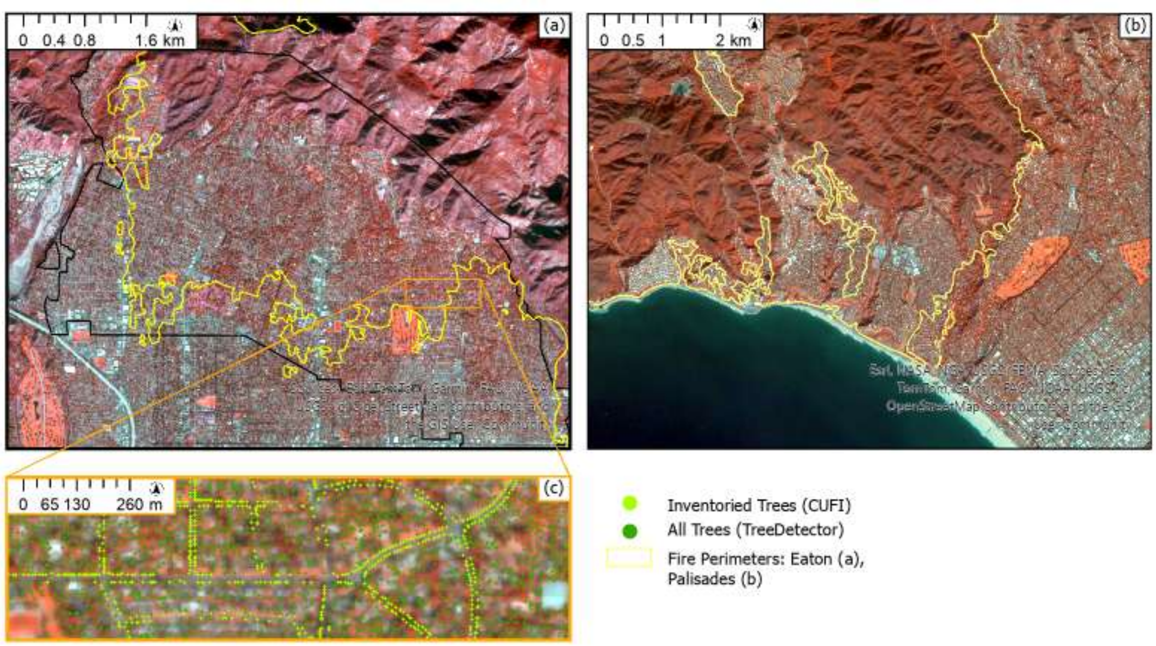

Figure 4.1 Fire perimeters for the Eaton (a) and Palisades (b) fires in urban areas. (c) An example of inventoried and detected trees used in analysis.

4.2.2 Dataset compilation

Building on methods in the first two chapters of this dissertation, I created a dataset of large trees (six PlanetScope pixels, >54 m^2) for Pacific Palisades and Altadena. First, I created a dataset of Thiessen polygons based on 2020 TreeDetector points (Ventura et al., 2024). I then cropped these polygons using canopy rasters I created using my Chapter 2 canopy classification workflow, run on 2024 NAIP imagery. Then, I filtered the resulting tree-associated canopy segments to retain only polygons greater than or equal to 54 m^2, approximately equivalent to six PlanetScope pixels.

I added species information using the California Urban Forest Inventory (Love et al., 2022) by spatially joining tree points with species identified to the segmented canopy polygons. To avoid ambiguous species assignments, I only assigned species identity when exactly one CUFI point intersected a given canopy polygon. Polygons with zero CUFI matches or more than one CUFI match were retained in the dataset but left without a species assignment. Based on tree species, each tree was assigned to a foliage type (deciduous, evergreen, or partially deciduous) (SelecTree, 2025). Each canopy was then assigned to a property type based on the majority overlap with parcel data, except for trees within the right-of-way. Because many areas of Altadena lack sidewalks and view-angle distortion can make it difficult to determine which parcel a tree belongs to, any tree canopy that overlapped a transportation parcel was classified as transportation, representing trees along roadways. Parcel data containing property type is from 2013 (McPherson et al., 2017). Property types included (Residential (Muti-family, MF), Residential (Single Family, SF), Commercial/Industrial/Institutional (CII), Open Space, Transportation Corridors, Water, and Unclassified). Each tree was defined as within the fire perimeter or outside of it based on Los Angeles County's final published perimeter maps (Los

Angeles County, 2025). Burn severity was calculated using the differenced Normalized Burn Ratio (dNBR) derived from cloud-free Landsat 8 and 9 Collection 2 Level-2 surface reflectance imagery. NBR was calculated as (NIR -SWIR2) / (NIR + SWIR2) using Band 5 (NIR) and Band 7 (SWIR2). Pre-fire imagery was acquired January 6th, 2025, and cloud-free post-fire imagery from January 14th, 2025. dNBR was computed as the difference between the pre-fire and post-fire NBR composites and scaled by a factor of 1000 (Key and Benson, 2006). All processing was performed in Google Earth Engine. I grouped inside-perimeter dNBR values into five study-specific quintiles: lowest severity (<192), low severity (192-275), moderate-low severity (275-337), moderate-high severity (337-401), and high severity (>401) (Appendix 4A). dNBR often does not transfer from region to region (Cansler & McKenzie, 2012), and for this dataset, following the standard Key and Benson thresholds resulted in most trees in a low severity category, which does not reflect the conditions of the Palisades and Eaton fires. I compared three dNBR metrics extracted at each tree location: the single Landsat pixel containing the tree centroid, the mean dNBR within a 3×3 Landsat pixel window, and the mean dNBR within a 6×6 Landsat pixel window. For each metric, I tested how strongly the quintile classes separated post-fire recovery outcomes using Kruskal-Wallis tests on April 2025 and April 2026 anomaly z-scores. The 3×3 mean dNBR metric was selected because it had the strongest separation among recovery classes (Appendix 4B).

4.2.3 PlanetScope time series and recovery metrics

To construct a spectral time series for each tree, I used canopy centroid points to define 2 × 2 PlanetScope pixel sampling windows (6 m × 6 m). I used PlanetScope SuperDove surface reflectance imagery from PSB.SD sensors only, limiting the time series to the SuperDove period from January 2022 onward (Planet Team, 2026). Images were initially filtered at download to include only scenes with 10% reported cloud cover and standard image quality, then manually inspected to remove scenes with remaining local cloud, haze, smoke, shadow, or other image artifacts over the study areas. For each accepted image, NDVI was calculated as (NIR - Red) / (NIR + Red), and the mean NDVI of all pixels within each 6-m × 6-m window was assigned to that tree on that date. Monthly mean NDVI values were then calculated by averaging across all accepted images in a given month, typically about three images per month. The time series spans January 2022 through December 2025, with April 2026 included as an additional post-fire date.

In wildland recovery studies, spectral recovery of vegetation is defined as the return to a pre-disturbance baseline. How that baseline is defined and set varies. Some studies compare against a site's own baseline by looking at historical values and using either a range or average of those values (Bousquet et al., 2022; Joao et al., 2018). Others compare burnt vegetation to nearby unburnt vegetation (Rodrigues et al., 2024; Ryu et al., 2018). In this study I tested both approaches. I defined control trees as those within the same city but outside of the fire perimeter. Before using trees outside of the perimeter as controls for comparison, I tested whether inside- and outside-fire-perimeter trees were statistically equivalent during 2022-2024 using mean monthly NDVI values. I used a permutation test that compared group means against a null distribution of 999 permuted differences, with Cohen's d to calculate effect size. Inside- and outside-perimeter trees differed during the pre-fire period in both cities. In Altadena, pre-fire NDVI values were higher inside the perimeter than outside across all months (d up to 0.24). In the Pacific Palisades, the trees inside the perimeter showed lower greenness in summer and autumn (d up to -0.44).

Because the two groups differed before the fires, recovery was assessed through each tree's individual baseline in the same calendar month. This method is similar to other non-urban forest recovery literature, where recovery of plants is defined as relative to each pixel's individual pre-disturbance range (Bousquet et al., 2022; Joao et al., 2018). For each tree and calendar month, a pre-fire mean and standard deviation were calculated from all selected PlanetScope observations in that same month across 2022-2024, approximately three image dates per month per year. A tree was considered as within its own pre-fire range in a post-fire month if its NDVI fell within +-2 standard deviations of its own range.

Prior to comparison, each tree's NDVI value was adjusted to make it more comparable to previous years. Across all outside-perimeter control trees in both cities, mean NDVI was lower in every month of 2025 than the historical monthly baseline (mean decline = 0.048, range = 0.011-0.095). This could be due to sensor variation or climate. To accommodate this, the mean NDVI difference for that month between the baseline status of trees outside the fire perimeter and the 2025 conditions of those same trees was added to the NDVI of trees within the fire perimeter. Comparing each tree with its own historical values controls for differences in species, phenology, canopy structure, and local background conditions. It does not account for citywide year-to-year shifts in NDVI caused by climate, sensor conditions, or other non-fire factors. I used outside-perimeter trees to estimate those monthly shifts and adjust inside-perimeter NDVI values before calculating recovery metrics to partially account for those differences.

I applied the recovery classification from February through December 2025 and again in April 2026. Key windows reported are April 2025 (early growing season, approximately three months post-fire), the average of June through August 2025 (peak growing season), and April 2026 (one full year into the growing season following the fire). In addition to the binary classification, a continuous recovery metric was computed for each tree and month as a de-seasonalized anomaly z-score: the difference between the tree's adjusted post-fire NDVI and its own calendar-month pre-fire mean, divided by its pre-fire standard deviation for that same calendar month. A z-score ranging from ±2 indicates the tree is performing similarly to its own historical average for that time of year; negative values indicate below-baseline greenness, and positive values indicate above-baseline greenness. The anomaly z-score was used as the primary continuous outcome in subsequent analyses because it is directly comparable across trees with different baseline NDVI levels, different species, and different months. A recovery trajectory metric (RTI, Joao et al., 2018) was also computed for each tree as the Theil-Sen slope across monthly anomaly z-scores for 2025, capturing whether the recovery trend across the post-fire year was positive or negative, independent of the absolute recovery level at any single timepoint.

4.2.4. Initial burn impact and analysis sample

Fire exposure within a perimeter is not spatially uniform. Trees may remain relatively unaffected because of local variation in fire behavior, suppression activity, site conditions, or tree traits associated with lower damage. A deciduous tree in January, when foliage is naturally absent or reduced, may appear spectrally similar to a burned tree regardless of fire exposure.

We calculated each tree's change in adjusted NDVI from its January pre-fire mean to January 2025. A tree was classified as "did not burn" within the fire perimeter if two conditions were met: its adjusted January 2025 NDVI falls within ± 1 SD of its own January pre-fire mean, and it was located in either of the two lowest dNBR quintiles. These criteria excluded trees within the fire perimeter that were in broader patches with little burn damage (dNBR measured within a 90-m × 90-m window) and had little evidence of damage. dNBR was included to ensure that deciduous trees, which may have a similarly low greenness in winter before and after the fire, remained included in the analysis. Trees that met both conditions (n = 4,193) were excluded from all subsequent recovery analyses.

4.2.5. Statistical Analysis

I first summarized post-fire recovery patterns descriptively by foliage type, property type, and dNBR severity class. I then fit spatial error models to evaluate the joint effects of burn severity, property type, foliage type, and city while accounting for spatial autocorrelation among nearby trees. The five continuous recovery outcomes were April 2025 anomaly z-score, mean summer 2025 anomaly z-score, April 2026 anomaly z-score, change in anomaly z-score from April 2025 to April 2026, and 2025 recovery trajectory index (RTI). I first fit models to the full burned-tree analysis sample using continuous 3 × 3 mean dNBR, property type, and city as predictors. These models included all fire-affected trees with complete recovery, dNBR, property type, and spatial-coordinate data. I then fit a second set of models to the CUFI-labeled subset to evaluate foliage-type differences while controlling for dNBR, property type, and city. Finally, I fit species-level models for species represented by at least 30 trees. Deciduous trees, multifamily residential properties, and Altadena were used as reference categories.

Spatial error models were used because recovery outcomes were spatially clustered among nearby trees. I evaluated spatial-weight sensitivity across k-nearest-neighbor definitions from k = 4 to k = 16 by comparing the estimated 3 × 3 dNBR coefficient and 95% confidence interval, along with Moran's I for filtered model residuals (Appendix 4C). dNBR coefficients were stable across k values. I selected an 8-nearest-neighbor weights matrix because filtered residual Moran's I values were near zero and nonsignificant across all five outcomes, ranging from -0.005 to -0.013. Because the data showed mild heteroscedasticity, I fit models using the generalized method-of-moments spatial error estimator with heteroskedasticity (spreg.GM_Error_Het; PySAL Developers, 2018). For each model, I reported coefficient estimates, standard errors, 95% confidence intervals, z statistics, and p-values. I used joint Wald tests to assess the overall contribution of each predictor.

For species-level models, foliage type was replaced with species while retaining the same recovery outcomes and spatial error framework. Pairwise contrasts among species property types were calculated from adjusted model estimates for each recovery outcome. I adjusted p-values for multiple comparisons using the Holm correction and considered Holm-adjusted $p < 0.05$ statistically significant.

4.2.6 Validation

Validation combined field observations with visual assessment of high-resolution imagery. A stratified sample of 200 trees was selected from the post-fire dataset, with 25 trees sampled from each of four analysis strata in each fire area. Strata were defined from the April 2025 NDVI condition metrics used in the analysis and included trees classified as did not burn, trees with April NDVI near their historical baseline (±2 SD), trees with very low April NDVI (<0.2), and trees with April NDVI below baseline but above the low-NDVI threshold. This design represented the range of observed post-fire canopy conditions. The did-not-burn exclusion criterion was evaluated separately using January high-resolution imagery in Google Earth Pro. Trees with a January canopy score of 5, indicating a fully intact canopy, were treated as visually consistent with the did-not-burn class, while trees with lower scores were treated as not fully intact. This reference was compared with the satellite did-not-burn classification used to exclude trees from later analyses.

A separate opportunistic field sample was collected in Altadena on May 29, 2025. Thirty-five trees encountered across accessible burned neighborhoods during a one-day driving survey were assessed for canopy condition and percent green canopy. Field observations were compared with April 2025 anomaly z-scores and adjusted NDVI to assess whether the satellite metrics reflected observed variation in canopy condition.

4.3 Results

4.3.1 Tree samples and recovery statuses

Of 32,808 large trees identified within the combined fire perimeters, 4,193 (12.8%) were classified as did-not-burn and were excluded from subsequent analyses, leaving 28,615 analysis trees. Of the 28,615 analysis trees, 2,270 had foliage type assignments from the CUFI and were used in foliage-stratified and species-stratified analyses; of these, 1,556 (68.1%) were evergreen, 401 (17.7%) partly deciduous, and 323 (14.2%) deciduous. Individual recovery trajectories varied. Some trees returned or were progressively returning toward their own pre-fire seasonal range. Others remained well below baseline after mortality or removal (Figure 4.2).

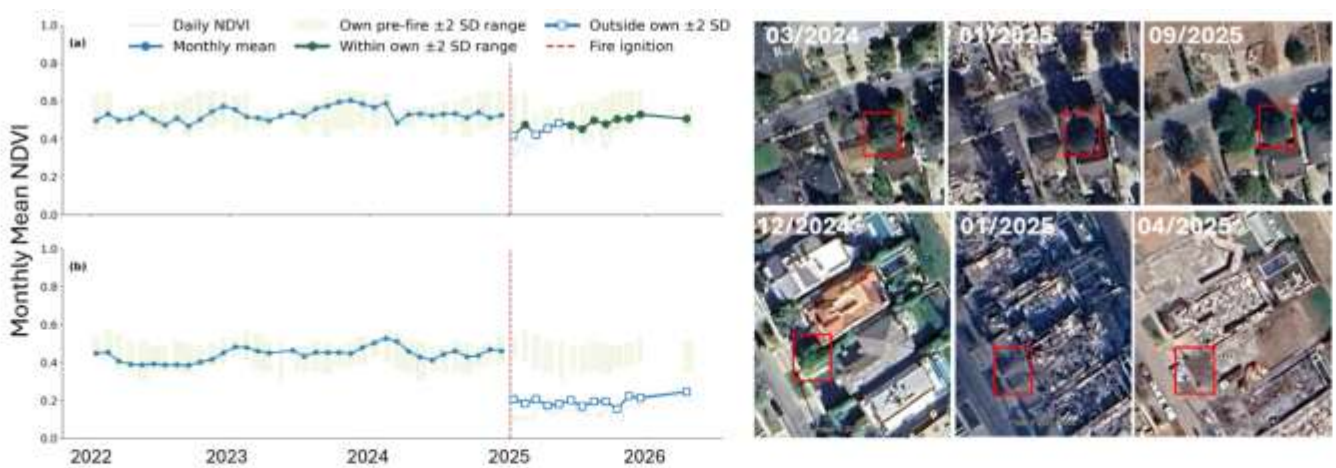

Figure 4.2 Post-fire NDVI trajectories for two example trees representing a recovered tree (A), and a tree with relatively low NDVIs that was removed (B). Lines show daily NDVI observations across the pre-fire (2022-2024) and post-fire (2025) periods. Monthly means are

shown as dots: filled circles indicate the monthly value fell within the tree's own pre-fire ±2 SD range for that calendar month; open squares indicate it fell outside. Green shading shows the pre-fire ±2 SD range per calendar month. Dashed red line marks fire ignition (January 7, 2025). Red boxes correspond to the tree in the time series next to it.

4.3.2 Recovery rates and trajectories

Recovery increased throughout the post-fire year but remained incomplete. In April 2025, approximately three months after the fires, 26.7% of analysis trees fell within their own pre-fire ±2 standard deviation range for that calendar month. Recovery rates increased throughout the 2025 growing season, reaching 38.5% by April 2026 (Figure 4.3).

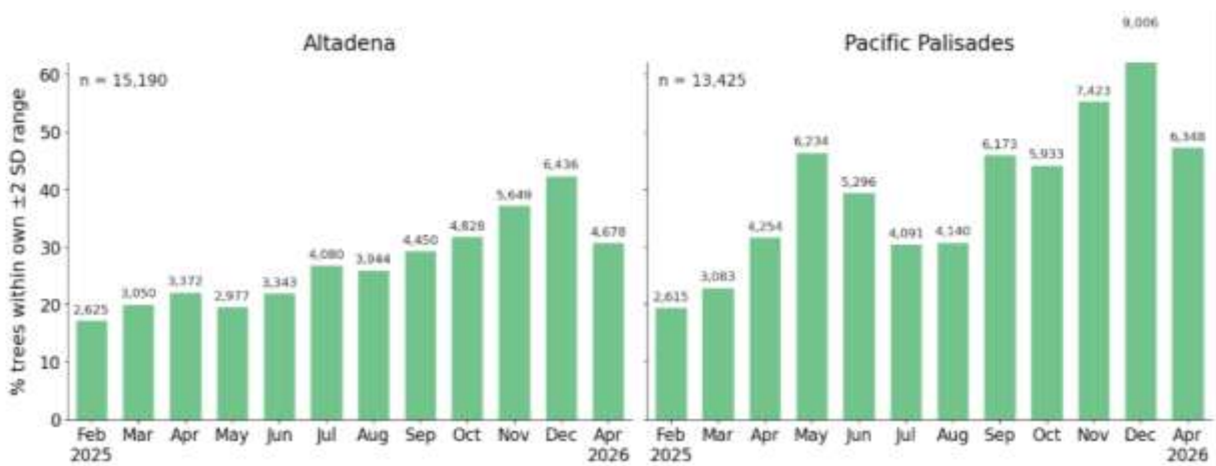

Figure 4.3 Monthly canopy recovery rates for fire-affected trees in Altadena and Pacific Palisades, February 2025-April 2026. Bars show the percentage of trees whose NDVI fell within ±2 standard deviations of their own pre-fire baseline; numbers above bars indicate the count of recovered trees that month.

Despite this improvement, the mean anomaly z-score across all analysis trees remained well below the recovery threshold at all timepoints: -5.07 in Altadena and -3.90 in Pacific

Palisades in April 2025, and -3.81 in Altadena and -2.53 in Pacific Palisades by April 2026 (Figure 4.4). Descriptively, Pacific Palisades trees had higher mean anomaly z-scores than Altadena trees at both April timepoints.

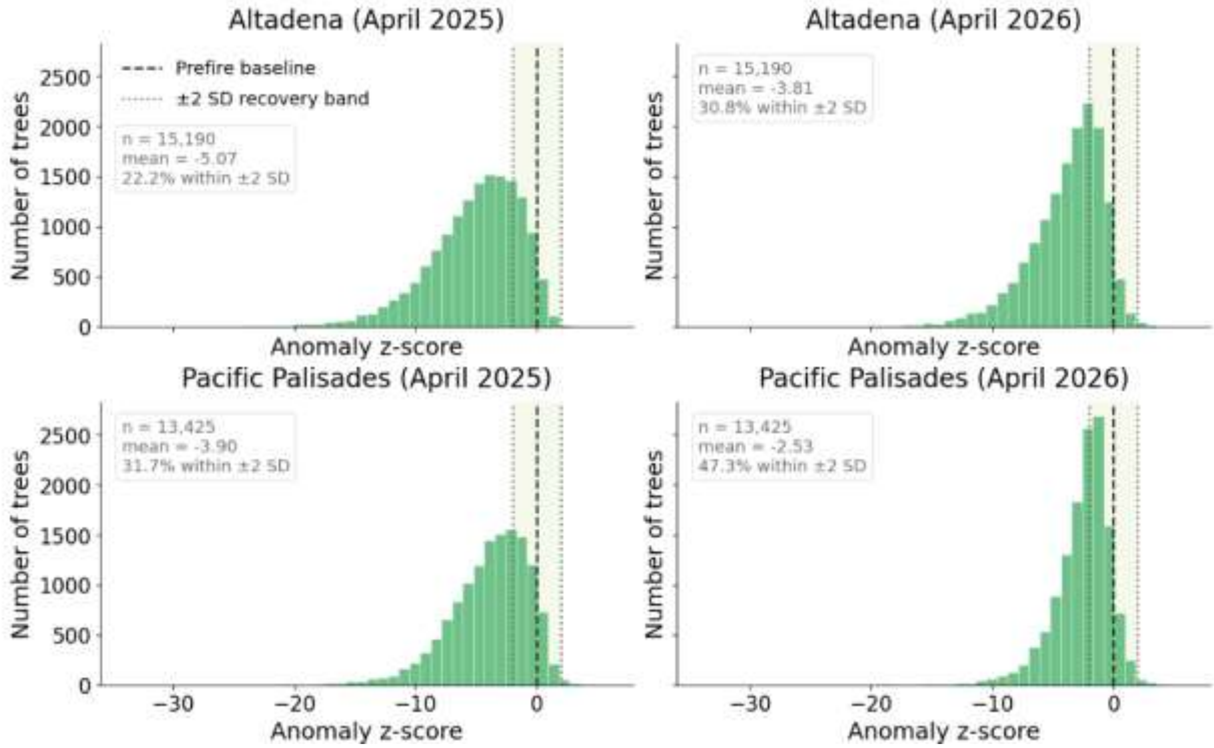

Figure 4.4 Distribution of de-seasonalized NDVI anomaly z-scores for inside-perimeter burned trees in April 2025 and April 2026, shown separately for Altadena and Pacific Palisades. A z-score of 0 indicates that a tree is performing at its own historical April baseline. The shaded band marks the ±2 standard deviation range around the baseline, with dotted lines at z = -2 and z = 2.

4.3.3 Spatial error models of recovery

Spatial error models were used to evaluate the effects of burn severity, property type, and city while accounting for spatial autocorrelation among nearby trees. The burned-tree analytical dataset contained 28,615 trees. Full-sample spatial error models were estimated for 28,350 trees with complete recovery, dNBR, property-type, city, and coordinate data. Across all five recovery outcomes, 3×3 mean dNBR was the strongest and most consistent predictor of recovery. Higher dNBR was associated with lower anomaly z-scores in April 2025, summer 2025, and April 2026. At $k = 8$, the dNBR coefficient was -12.97 for April 2025 condition, −9.11 for summer 2025 condition, and -7.23 for April 2026 condition (Table 4.1). The dNBR coefficient was positive for April-to-April change (5.62) and RTI (0.83), indicating greater improvement over time among trees with higher burn severity, although these trees also had lower anomaly z-scores at the main recovery timepoints. Joint Wald tests confirmed that dNBR was significant across all five recovery outcomes ($\chi^2 = 586.94\text{-}1814.31$, all $p < 0.001$). Property type was also significant across all five outcomes ($\chi^2 = 94.27\text{-}254.45$, all $p < 0.001$). City was significant across all five outcomes as well, although its association with April-to-April change was comparatively weak ($\chi^2 = 5.16$, $p = 0.023$) relative to the condition outcomes and RTI ($\chi^2 = 23.16\text{–}204.72$, all $p < 0.001$).

Table 4.1 Recovery outcomes from full-sample spatial error model coefficients with 95% confidence intervals for post-fire recovery outcomes (n = 28,350). All models include 3 × 3 mean dNBR, property type, and city and account for spatial autocorrelation using an 8-nearest-neighbor spatial weights matrix. Reference categories are multifamily residential land use and Altadena. dNBR coefficients represent the expected change in recovery outcome per 1,000-unit increase in dNBR. * $p < 0.05$; ** $p < 0.01$; *** $p < 0.001$.

	Recovery Outcome				
Predictor	**25-Apr**	**Summer 2025**	**26-Apr**	**Slope 25–26**	**RTI 2025**
3×3 dNBR	-12.97 [-13.56, -12.37]***	-9.11 [-9.55, -8.67]***	-7.23 [-7.70, -6.76]***	5.62 [5.17, 6.08]***	0.83 [0.78, 0.88]***
Unclassified	-1.59 [-2.60, -0.58]**	-1.76 [-2.70, -0.81]***	-1.45 [-2.39, -0.50]**	0.10 [-0.63, 0.83]	0.07 [-0.02, 0.16]
SF residential	-0.14 [-0.36, 0.07]	-0.22 [-0.37, -0.08]**	-0.17 [-0.34, -0.00]*	-0.05 [-0.19, 0.10]	0.00 [-0.01, 0.02]
Comm/Inst/Ind	0.42 [0.13, 0.71]**	0.26 [0.06, 0.47]*	0.20 [-0.03, 0.43]	-0.24 [-0.45, -0.04]*	-0.00 [-0.03, 0.02]
Open space	0.44 [0.16, 0.72]**	0.36 [0.17, 0.55]***	0.25 [0.05, 0.46]*	-0.16 [-0.37, 0.05]	0.10 [0.07, 0.12]***
Transportation	0.58 [0.35, 0.80]***	0.25 [0.10, 0.40]**	0.24 [0.06, 0.42]**	-0.36 [-0.51, -0.21]***	-0.04 [-0.06, -0.02]***
Palisades	0.94 [0.76, 1.13]***	0.56 [0.40, 0.73]***	1.11 [0.96, 1.26]***	0.17 [0.02, 0.31]*	0.04 [0.02, 0.06]***

The unadjusted dNBR trajectories show the same severity gradient visually: trees in the highest-severity class remained farthest below baseline throughout the post-fire period, while the gap between severity classes narrowed between April 2025 and April 2026 (Figure 4.5).

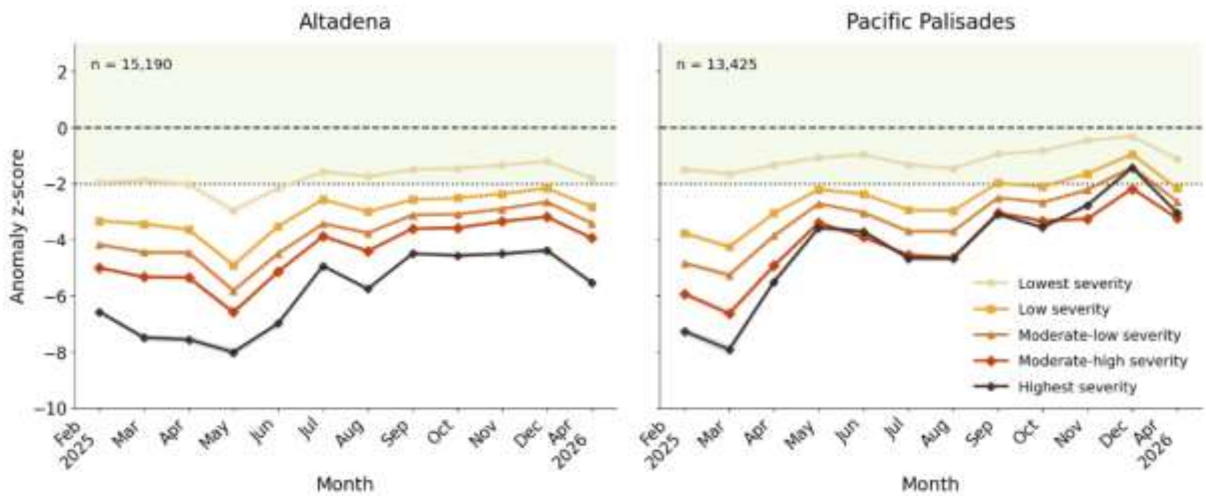

Figure 4.5 Monthly recovery trajectories by 3×3 dNBR severity class for inside-perimeter burned trees in Altadena and Pacific Palisades. Severity classes were defined as study-specific quintiles of the 3×3 dNBR distribution among all inside-perimeter trees before exclusion of trees classified as did not burn. Classes shown here represent relative severity categories within the retained burned-tree analysis sample. Lines show mean de-seasonalized NDVI anomaly z-score and ribbons show ±2 standard errors.

Property-type effects were less consistent than the burn-severity gradient, but property type was a significant overall predictor block for every recovery outcome in the full-sample models (Table 4.1; Figure 4.6). Relative to multifamily residential trees, property type differences varied across timepoints and recovery metrics rather than forming a single, stable ordering (Figure 4.6). In the model excluding foliage type and species, pairwise comparisons showed that single-family residential trees had lower adjusted condition than trees in transportation, open-space, and commercial, institutional, and industrial parcels at all three condition timepoints. In contrast, both single- and multifamily residential trees improved more from April 2025 to April 2026 than transportation trees, while open-space trees had the highest RTI relative to the other major property types.

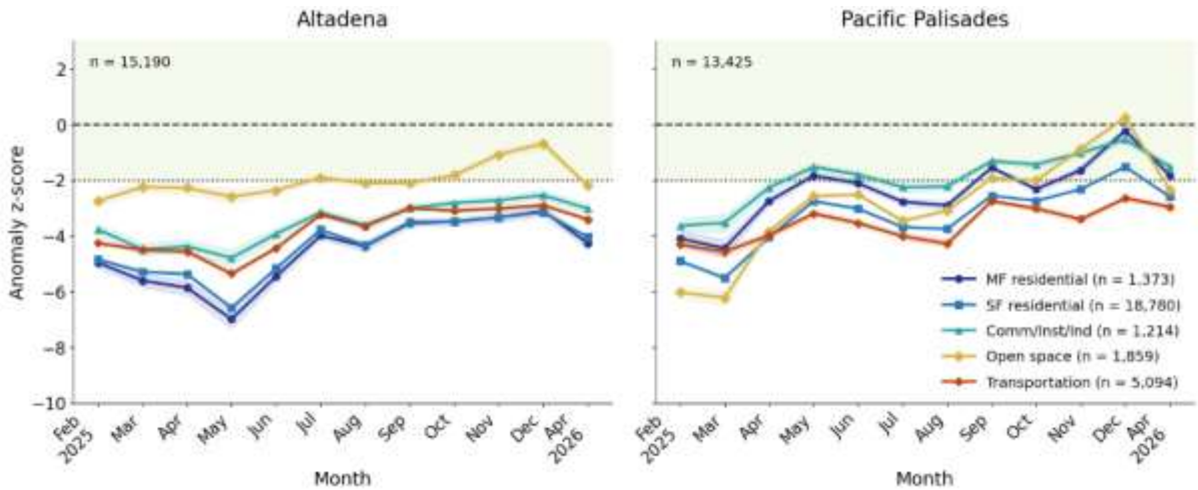

Figure 4.6 Monthly recovery trajectories by land-use class for burned inside-perimeter trees in Altadena and Pacific Palisades. Lines show mean de-seasonalized NDVI anomaly z-score and ribbons show ±2 standard errors.

Foliage type was also associated with recovery condition after accounting for dNBR, land-use class, city, and spatial autocorrelation. Compared with deciduous trees, evergreen trees had lower adjusted recovery condition at the main post-fire timepoints, while partly deciduous trees were generally intermediate. These foliage-type effects were smaller than the dNBR effect (Table 4.2). Property type and city coefficients from the CUFI-labeled subset are presented as adjustment variables for foliage-type estimates. They are not interpreted as primary land-use or city effects because the CUFI subset is substantially smaller and unevenly distributed across property classes and cities.

Table 4.2 Values are spatial error model coefficients with 95% confidence intervals for the CUFI-labeled complete-case subset of trees (n = 2,263). All models include 3×3 dNBR, foliage type, property type, and city. Reference categories are deciduous foliage, MF residential land use, and Altadena. * p < 0.05; ** p < 0.01; *** p < 0.001.

	Recovery Outcome				
Predictor	**Apr-25**	**Summer 2025**	**Apr-26**	**Slope 25–26**	**RTI 2025**
3×3 dNBR	-16.15 [-17.88, -14.42]***	-12.80 [-14.08, -11.53]***	-11.08 [-12.62, -9.53]***	4.92 [3.87, 5.97]***	0.63 [0.50, 0.76]***
Evergreen	-0.80 [-1.15, -0.44]***	-0.10 [-0.37, 0.18]	-0.81 [-1.12, -0.49]***	-0.06 [-0.30, 0.17]	0.02 [-0.01, 0.05]
Partly deciduous	0.01 [-0.43, 0.44]	0.04 [-0.30, 0.38]	-0.03 [-0.41, 0.34]	-0.08 [-0.37, 0.21]	-0.06 [-0.10, -0.02]**
SF residential	0.22 [-1.59, 2.03]	-0.63 [-1.59, 0.33]	-0.55 [-1.77, 0.66]	-0.79 [-1.89, 0.31]	0.08 [0.00, 0.16]*
Comm/Inst/Ind	0.94 [-1.21, 3.10]	-0.13 [-1.54, 1.27]	0.17 [-1.55, 1.90]	-0.80 [-2.10, 0.51]	-0.01 [-0.14, 0.11]
Open space	2.30 [0.43, 4.17]*	0.89 [-0.08, 1.87]	0.67 [-0.58, 1.92]	-1.61 [-2.77, -0.44]**	0.18 [0.09, 0.27]***
Transportation	0.72 [-1.06, 2.50]	-0.42 [-1.35, 0.51]	-0.35 [-1.54, 0.84]	-1.10 [-2.19, -0.02]*	0.02 [-0.05, 0.10]
Palisades	0.29 [-0.15, 0.72]	-0.55 [-0.96, -0.14]**	0.18 [-0.25, 0.61]	-0.11 [-0.37, 0.16]	-0.06 [-0.09, -0.02]**

In the unadjusted foliage trajectories, deciduous trees had higher mean anomaly z-scores than partly deciduous and evergreen trees across much of the post-fire period (Figure 4.7).

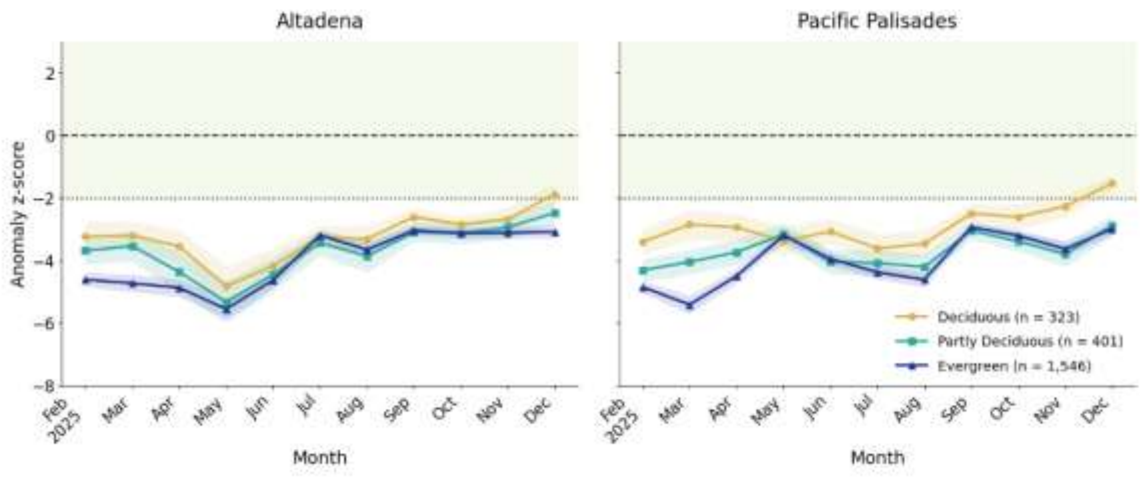

Figure 4.7 Monthly recovery trajectories by foliage type for CUFI-labeled burned trees in Altadena and Pacific Palisades. Lines show mean de-seasonalized NDVI anomaly z-score, and ribbons show ±2 standard errors.

4.3.4 Species level recovery

Recovery by species varied (Figure 4.8). The three best-recovering species by model-adjusted April 2026 mean were *Platanus racemosa* (z = -1.37, n = 117), *Eucalyptus sideroxylon* (z= -2.02, n=45), and *Jacaranda mimosifolia* (z = -2.16, n=129). The two worst-recovering were *Cinnamomum camphora* (z = -4.79, n = 108) and *Fraxinus uhdei* (z = -4.54, n=47). Pairwise species comparisons showed that the strongest-performing species were statistically distinct from several of the lowest-performing species, although not all adjacent ranks differed from one another (Appendix 4D).

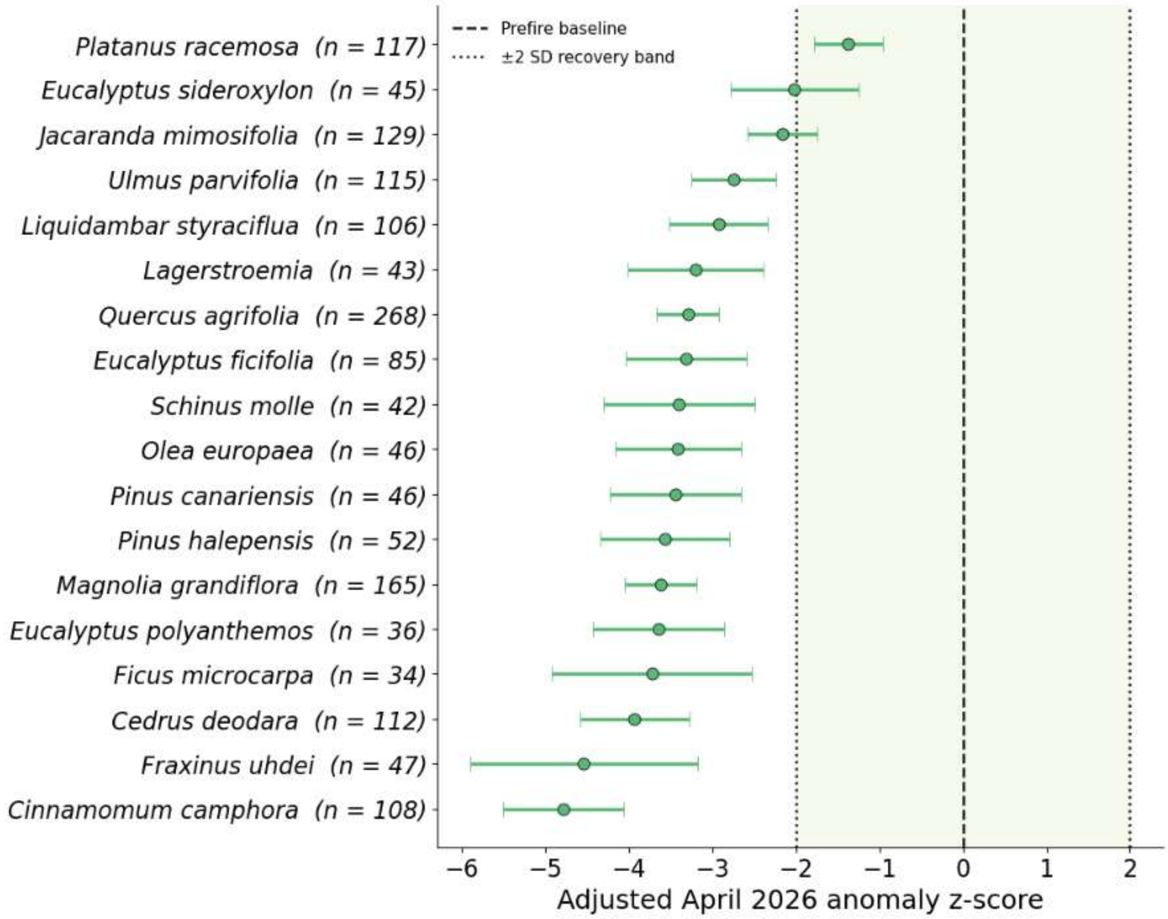

Figure 4.8 Adjusted April 2026 species condition from the spatial species model. Points show adjusted marginal means and horizontal bars show 95% confidence intervals. Models adjust for 3×3 dNBR, property type, city, and spatial autocorrelation. A z-score of 0 indicates each tree's own pre-fire April baseline, while z = -2 marks the recovery threshold. Species are sorted by adjusted April 2026 anomaly z-score.

Species-level spatial error models showed that species rankings differed across recovery outcomes. Species with the highest April 2026 condition were not always the same species with the greatest April-to-April improvement or highest RTI (Figure 4.9). Some species had low initial anomaly z-scores but large positive change, while others maintained higher absolute condition throughout the post-fire period (Figure 4.9).

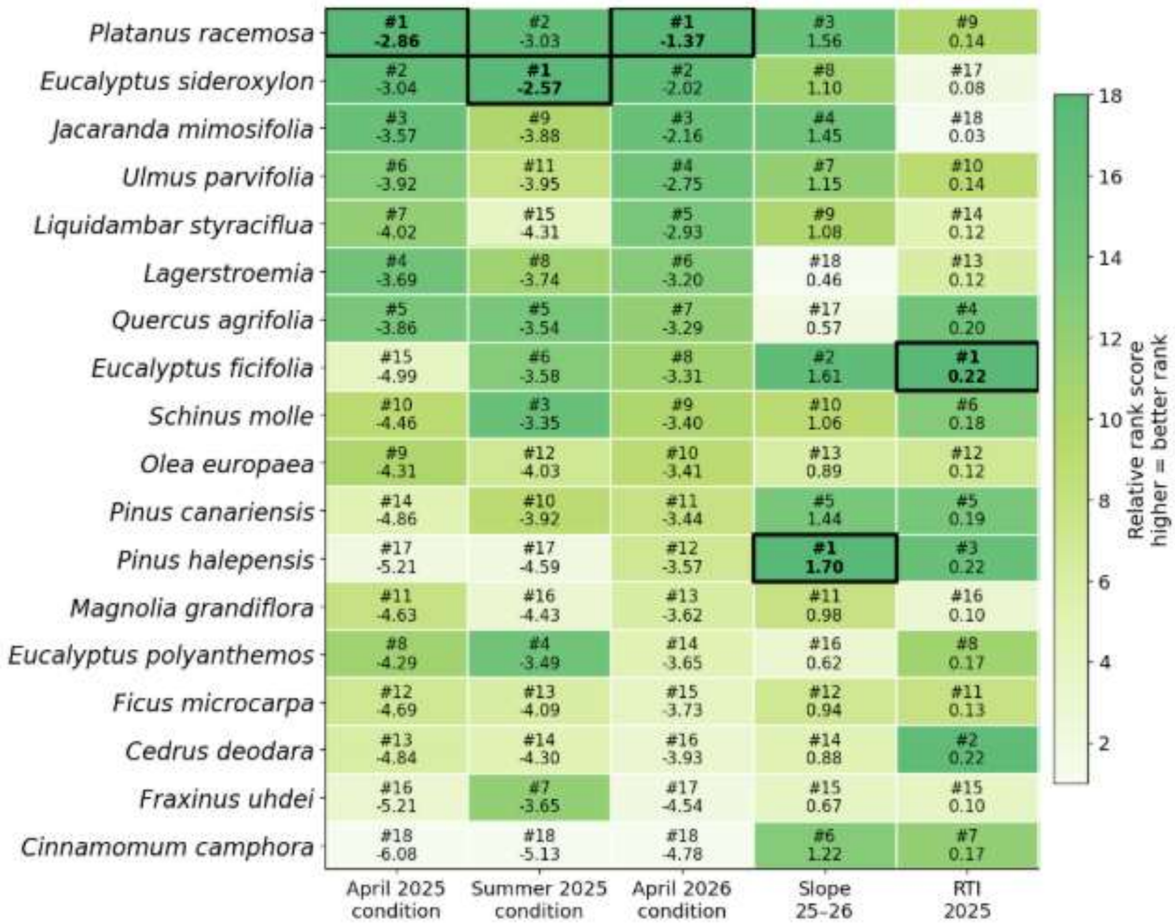

Figure 4.9 Multi-outcome species recovery summary from adjusted spatial species models. Rows show species and columns show recovery outcomes. Cell color represents relative rank score, where darker green indicates a better adjusted rank within that outcome. Cell text shows the species rank and adjusted mean estimate. Black outlines indicate the highest-ranked species for each outcome. Higher values are interpreted as better relative recovery for all outcomes shown: less negative condition anomaly z-scores, more positive April-to-April slope, and higher RTI.

4.3.5 Validation

Of the 200 validation trees, two were classified as NA due to unclear imagery (shadows and blur present), one of which was a tree classified as did-not-burn. Of 49 remaining trees classified as did-not-burn in the visual validation sample, 100% received a January greenness score of 5 (full green canopy) from independent visual assessment of high-resolution imagery on Google Earth. High-resolution greenness and January 2025 anomaly z-score and April 2025 anomaly z-score were related, with a rho of 0.72 and 0.79, respectively (Figure 4.10). A field survey of 35 Altadena trees on May 29, 2025, found a positive correlation between field-estimated percent green canopy and the May satellite z-score. Together, these comparisons support the z-score as a valid indicator of individual tree canopy condition in the post-fire period (Figure 4.11). Visual review also identified a potential source of error in a small number of cases: green ground vegetation beneath severely damaged or dead canopies could increase the NDVI measured within the 6-m × 6-m sampling window and appear as partial canopy recovery. This pattern was observed in 5 of the 200 visually assessed trees. Although uncommon in the validation sample, understory or ground-cover greening may cause canopy condition to be overestimated for some heavily damaged trees.

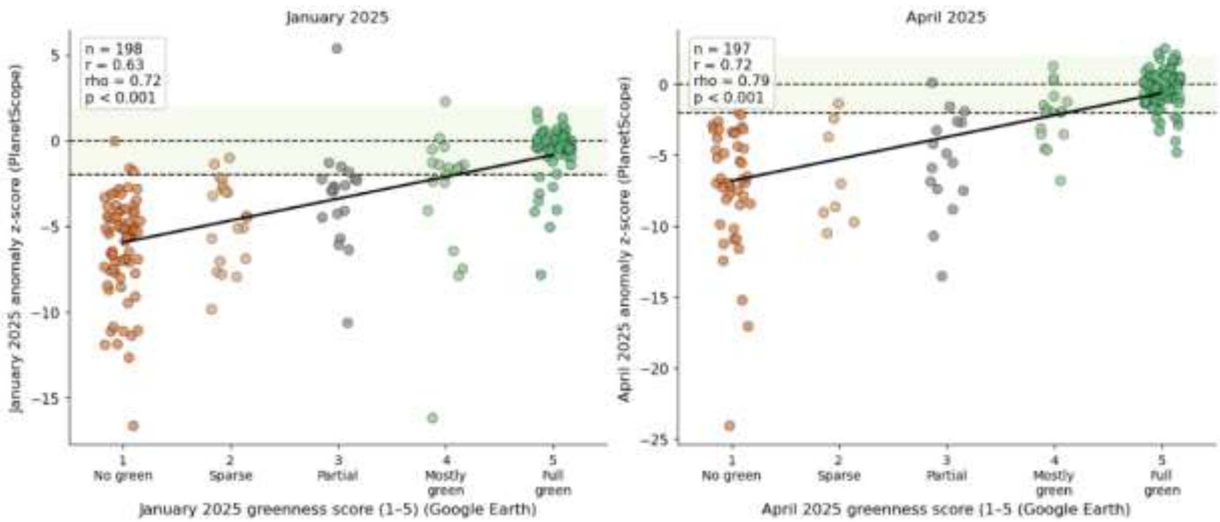

Figure 4.10 PlanetScope z-score versus high-resolution visual greenness score for 200 sampled trees in January and April 2025. Each point is one tree. The dashed lines mark the recovery threshold (z = -2) and pre-fire baselines.

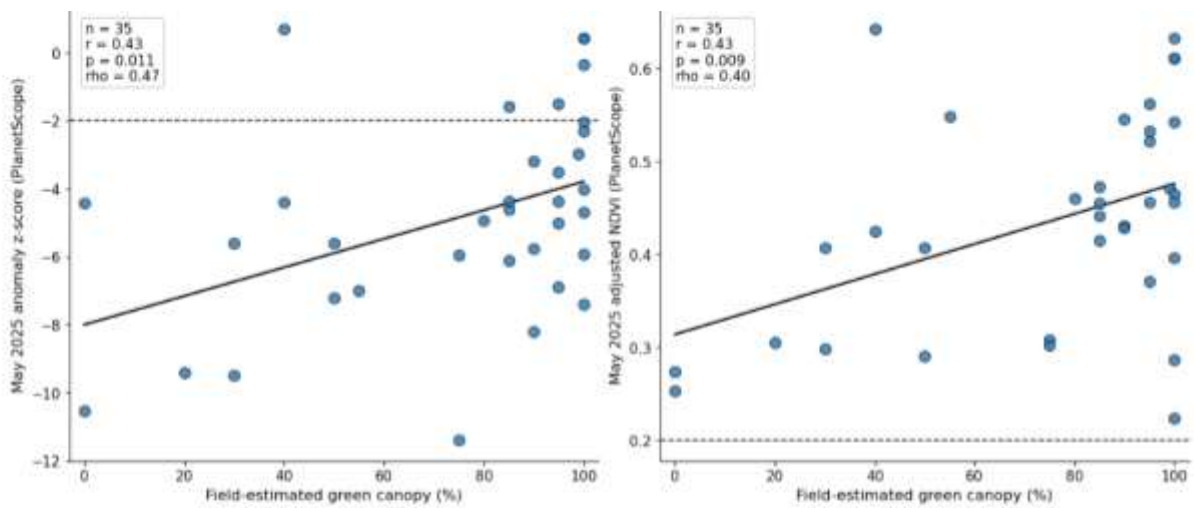

Figure 4.11 Field-estimated percent green canopy versus satellite May 2025 anomaly z-score for 35 trees surveyed in Altadena on May 29, 2025. Each point is one tree assessed during a driving survey of accessible burned neighborhoods. The positive correlation indicates that the satellite metric reflects canopy greenness conditions visible on the ground during the early post-fire growing season.

4.4 Discussion

4.4.1 One year after the fire, urban tree recovery remained incomplete

This study provides an early snapshot of individual urban tree canopy condition after the Eaton and Palisades fires. Recovery from urban wildfire was ongoing through the first post-fire year, but remained incomplete across much of the burned urban forest. Of the 28,615 analysis trees, 26.7% had returned to within their own pre-fire seasonal range by April 2025, approximately three months after the fires. By April 2026, this increased to 38.5%, indicating substantial improvement across the first year of recovery. However, the majority of trees still remained outside their own historical range one year after the fires. Continuous anomaly z-scores showed the same pattern. Although recovery rates increased over time, mean anomaly z-scores remained below baseline in both cities. In April 2025, mean anomaly z-scores were -5.07 in Altadena and -3.90 in Pacific Palisades. By April 2026, these values had improved to -3.81 in Altadena and -2.53 in Pacific Palisades, but both cities remained below the $z = -2$ recovery threshold on average. Positive April-to-April slopes and RTI values show that many trees were becoming greener over time even when they remained below their historical range, indicating a short-term recovery towards their historic baselines that is incomplete. Although NDVI can indicate recovery, a tree that returns to its historical NDVI range may have only recovered spectrally, but still might have physiological or structural damage that could result in later mortality.

Recovery timing is difficult to compare directly with wildland studies because recovery depends on the metric being measured. Recovery following wildfire is typically assessed at the stand or community scale in wildland ecosystems, rather than at the individual tree scale. Reported recovery times range from approximately 3-5 years in rapidly recovering

Mediterranean vegetation, as measured using spectral indices (Bastos et al., 2011; Gouveia et al., 2010), to over a decade to multiple decades when recovery is assessed using structural metrics (Tanase et al., 2011). Recent work has further emphasized that recovery estimates are influenced by how recovery is defined, with assessments based on vegetation greenness often indicating recovery much earlier than evaluations based on forest structure, biomass, or community composition (Rodrigues et al., 2024). These differences reflect not only ecological variation among systems, but also differences in how recovery is defined and measured. Whereas most wildland studies evaluate recovery of vegetation communities or forest structure, this study tracks recovery of individual urban tree canopies relative to their own pre-fire baseline. Spectral recovery does not indicate full physiological recovery in a tree. Structural damage can show spectral signs much later in the time series (Rodrigues et al., 2024). The results here provide a progress report on recovery of the urban forest, but a longer time series might reveal other patterns such as delayed decline from the damage, or differing species coming back the strongest.

4.4.2 Burn severity was the strongest predictor of how far trees fell from baseline and how much they improved

Burn severity was the clearest pattern in post-fire recovery. Across the spatial error models, dNBR was significant for every recovery outcome, and the descriptive trajectories showed the same gradient: trees in lower-severity areas were consistently closer to their own pre-fire baselines, while trees in higher-severity areas remained much farther below baseline through April 2026. This pattern was visible soon after the fires and persisted across the first post-fire year. The severity result also helps explain why recovery condition and recovery trajectory need to be interpreted together. The April 2025, summer 2025, and April 2026 anomaly z-scores describe how far trees were from their own historical seasonal range at specific points in time. For these outcomes, higher dNBR was associated with a lower recovery condition, meaning that trees in more severely burned areas remained farther below baseline. In the descriptive severity classes, the lowest-severity trees were near the recovery threshold by April 2026, while the highest-severity trees were still far below their pre-fire range. The slope and RTI outcomes capture a different part of the recovery process: whether trees were moving upward through time. For these trajectory metrics, higher dNBR was associated with greater improvement. This does not mean that high-severity trees were healthier or more recovered. Rather, many of the most severely affected trees began the post-fire period at very low anomaly z-scores, so they had more room to increase. By April 2026, they had improved, but they still remained farther from baseline than trees in lower-severity areas.

The importance of burn severity is consistent with post-fire forest studies that identify severity as a major control on vegetation recovery and resilience (Rodrigues et al., 2024). Because dNBR is derived from NIR and SWIR2 reflectance, wavelengths sensitive to vegetation condition, water content, ash, and char, some relationship with subsequent NDVI recovery is expected. However, the burn-severity metric was intentionally measured at a broader scale than the individual PlanetScope tree windows. The 3×3 Landsat-pixel dNBR metric captured local burn context around each tree rather than simply repeating the same tree-level greenness signal. The persistence of the severity gradient through April 2026 indicates that the broader burn context continued to structure individual canopy conditions beyond the first post-fire year. While there is a correlation between total canopy cover and dNBR (Appendix 4E), this relationship is modest ($r \approx 0.14$-0.21), and the number of large trees within the same windows shows no meaningful relationship with dNBR ($r \approx -0.03$ to -0.04), suggesting that burn severity as measured here is not simply a proxy for pre-fire tree density.

4.4.3 Species and foliage type shape recovery trajectories, but within the broader effect of burn severity

Species and foliage type were associated with post-fire recovery, but their effects were less consistent than those of burn severity. In the spatial error models, evergreen trees had lower recovery condition than deciduous trees at the main April timepoints after accounting for dNBR, land-use class, city, and spatial autocorrelation. Evergreen trees were 0.80 anomaly z-score units lower than deciduous trees in April 2025 and 0.81 units lower in April 2026. Partly deciduous trees were generally closer to deciduous trees in the condition models, although they had lower RTI in 2025. The unadjusted foliage trajectories followed the same general pattern: deciduous trees had higher April 2026 anomaly z-scores than partly deciduous and evergreen trees, but the magnitude of the foliage effect was much smaller than the severity gradient.

The relatively stronger recovery of deciduous trees may be partly related to the timing of the fires. Both fires occurred in January, when many deciduous trees were dormant or had reduced leaf area. In this specific event, being deciduous during a winter fire may have reduced direct foliage loss or made it easier for trees to leaf out again during the following growing season. This should not be interpreted as evidence that deciduous trees are generally more fire-resilient than evergreen trees. Rather, it indicates that phenology and fire timing likely shaped the recovery patterns observed in this study. A fire during a different season could produce different relationships among foliage types.

Species-level results showed additional variation within broad foliage groups. Adjusted species models showed that some common species (*e.g. Platanus racemosa, Eucalyptus sideroxylon,* and *Jacaranda mimosifolia)* had much higher April 2026 condition than others after accounting for burn severity, property type, city, and spatial autocorrelation. Pairwise comparisons showed that the strongest-performing species were statistically distinct from several of the lowest-performing species (e.g. *Platanus racemosa* vs. *Schinus molle* and *Eucalyptus sideroxlyon* vs. *Magnolia grandiflora*), although not every adjacent rank differed (Appendix 4D).

These species and foliage patterns shown here should be interpreted as observed post-fire recovery trajectories, not as fixed rankings of fire tolerance. Species were not randomly distributed across the burned landscape, and species identity is tied to other urban factors such as planting location, irrigation, maintenance, property type, neighborhood context, and pre-fire condition. The CUFI-labeled trees also represent a subset of all analysis trees, mostly those close to rights-of-way or in open space. For these reasons, the species results are best understood as evidence that species and phenology contributed to recovery differences within this specific winter urban fire event, while burn severity remained the dominant constraint on recovery.

4.4.4 Property type was associated with recovery, but had less consistent effects than burn severity

Property type was associated with recovery across all five outcomes, indicating that property context contributed to post-fire canopy condition after accounting for dNBR and city. However, property type effects did not form a single, stable recovery gradient. Some property classes had higher adjusted condition than multifamily residential trees at particular timepoints, whereas single-family residential trees had lower condition by April 2026. Trajectory metrics showed a similarly mixed pattern: open-space trees had higher RTI, while transportation and commercial/institutional/industrial trees showed little or slightly less April-to-April improvement than the multifamily residential reference class.

Property type likely captures both differences in fire exposure and differences in what happens to trees after the fire. For example, Kenny et al. (2026) found that buildings closer together were more likely to burn. Property classes may reflect some of these built-environment patterns, such as denser residential development, roadside corridors, or open areas with different surrounding fuels and structure density. They may also reflect who manages the trees after the fire. Trees on private residential lots are managed by homeowners and may be removed during debris clearance or rebuilding, whereas trees along transportation corridors are under city or county management and may be cleared, but under different mechanisms than full-lot clearing. These differences could affect whether a damaged tree is retained long enough to recover, pruned, or removed entirely. Property type helps describe the urban setting in which recovery occurs, but these associations do not demonstrate that property type itself caused recovery differences or that lower spectral condition necessarily represents removal. Burn severity remained the clearest and most consistent predictor of recovery across the full analysis sample.

4.4.5 Urban forest recovery reflects both biological recovery and human removal

Post-fire outcomes for urban trees reflect both their biological response to fire and the management decisions made during reconstruction. Many trees remained below their pre-fire spectral baselines one year after the fires. Some may continue to recover, while others may have sustained irreversible damage or been removed during cleanup and rebuilding before their longer-term recovery potential could be observed.

The full-sample spatial models suggest that these urban processes may contribute to differences among property types. By April 2026, trees along transportation corridors had higher adjusted condition than the multifamily residential reference class, whereas trees on single-family residential properties had lower adjusted condition. This pattern is consistent with imagery and field observations showing extensive clearing during residential rebuilding, while some trees along transportation corridors remained in place. The time series cannot determine whether these differences reflect variation in initial fire damage, removal decisions, maintenance practices, or other unmeasured features of the built environment.

Recovery in this study was defined relative to each tree's own pre-fire spectral baseline, which differs from ecological measures of survival or long-term structural recovery. Survival and recovery are not synonymous. Trees can persist after severe fire injury through epicormic or basal resprouting, partial canopy recovery, and other regenerative responses despite substantial canopy loss (Burrows, 2002; Clarke et al., 2013). Greenness may also recover before forest structure or biomass, which can take decades to return (Tanase et al., 2011; Rodrigues et al., 2024). In urban settings, a low or declining NDVI trajectory may reflect mortality, persistent stress, pruning, or removal. Green ground vegetation beneath damaged or dead canopies can also increase the sampled NDVI and make a small number of trees appear greener than their canopy condition alone would suggest; this occurred in five of the 200 visually assessed trees. Post-fire urban forest recovery, as measured here, should therefore be interpreted as an early indicator of canopy condition shaped by fire damage, biological resilience, and human intervention together.

4.4.6 Future Work

Continued monitoring is needed to determine whether the improvements observed through April 2026 represent sustained recovery, temporary increases in canopy greenness, or the early stages of delayed mortality. As reconstruction and neighborhood recovery continue, the condition and survival of individual trees may change through delayed decline, removal, altered site conditions, or renewed maintenance. Tracking these changes will be important for identifying where canopy is being retained or lost and where replanting and long-term urban forest investment are most needed.

Future work could compare the spatial error models used here with spatial lag models. Spatial lag models estimate how strongly each tree's outcome is associated with outcomes among nearby trees and could be used to test whether explicitly modeling this local dependence improves estimates of post-fire recovery.

Applying the same analysis in other fire-affected communities, such as Paradise, California, would help determine which recovery patterns are consistent across urban wildfires and which are specific to the Eaton and Palisades fires, their vegetation, development patterns, and post-fire management conditions. As wildfires increasingly affect populated areas, longer-term and comparative monitoring will be important for identifying delayed tree loss, understanding recovery trajectories, and guiding urban forest management after fire.

4.4.7 Conclusions

More broadly, this study shows why post-fire urban canopy recovery should be measured at the scale of individual trees and across time. A single post-fire canopy map can show where canopy remains or is absent, but it cannot distinguish trees that are returning to their own seasonal range from trees that remain present but persistently below baseline. By combining individual-tree canopy segments, PlanetScope time series, pre-fire baselines, burn severity, property context, and species information, this analysis provides an early assessment of urban forest condition one year after the Eaton and Palisades fires. Recovery was underway but uneven: many trees improved, many remained far below baseline, and recovery patterns differed by burn severity, foliage type, species, property type, and city. This approach cannot identify every mechanism behind low canopy condition, but it can document how post-fire urban tree condition changes through time as longer-term recovery, decline, and rebuilding continue.

4.5 References

Bär, A., Michaletz, S. T., & Mayr, S. (2019). Fire effects on tree physiology. *New Phytologist*, *223*(4), 1728–1741. https://doi.org/10.1111/nph.15871

Bastos, A., Gouveia, C. M., DaCamara, C. C., & Trigo, R. M. (2011). Modelling post-fire vegetation recovery in Portugal. *Biogeosciences*, *8*(12), 3593–3607. https://doi.org/10.5194/bg-8-3593-2011

Bousquet, E., Mialon, A., Rodriguez-Fernandez, N., Mermoz, S., & Kerr, Y. (2022). Monitoring post-fire recovery of various vegetation biomes using multi-wavelength satellite remote sensing. *Biogeosciences*, *19*(13), 3317–3336. https://doi.org/10.5194/bg-19-3317-2022

Burrows, G. E. (2002). Epicormic strand structure in *Angophora* , *Eucalyptus* and *Lophostemon* (Myrtaceae) – implications for fire resistance and recovery. *New Phytologist*, *153*(1), 111–131. https://doi.org/10.1046/j.0028-646X.2001.00299.x

Cansler, C. A., & McKenzie, D. (2012). How Robust Are Burn Severity Indices When Applied in a New Region? Evaluation of Alternate Field-Based and Remote-Sensing Methods. *Remote Sensing*, *4*(2), 456–483. https://doi.org/10.3390/rs4020456

Chi, D., Degerickx, J., Yu, K., & Somers, B. (2020). Urban Tree Health Classification Across Tree Species by Combining Airborne Laser Scanning and Imaging Spectroscopy. *Remote Sensing*, *12*(15), 2435. https://doi.org/10.3390/rs12152435

Clarke, P. J., Lawes, M. J., Midgley, J. J., Lamont, B. B., Ojeda, F., Burrows, G. E., Enright, N. J., & Knox, K. J. E. (2013). Resprouting as a key functional trait: How buds, protection and resources drive persistence after fire. *New Phytologist*, *197*(1), 19–35. https://doi.org/10.1111/nph.12001

Escobedo, F. J., Yadav, K., Ossola, A., Klein, R., & Drury, S. (2024). Urban forest cover and ecosystem service response to fire varies across California communities. *Urban Forestry & Urban Greening*, *101*, 128547. https://doi.org/10.1016/j.ufug.2024.128547

Ettinger, A. K., Bratman, G. N., Carey, M., Hebert, R., Hill, O., Kett, H., Levin, P., Murphy-Williams, M., & Wyse, L. (2024). Street trees provide an opportunity to mitigate urban heat and reduce risk of high heat exposure. *Scientific Reports*, *14*(1), 3266. https://doi.org/10.1038/s41598-024-51921-y

Falanga, V., Francini, S., Parisi, F., Cavalli, A., De Fioravante, P., Cucca, B., D'Amico, G., Chirici, G., Lasserre, B., Ottaviano, M., Munafò, M., & Marchetti, M. (2024). Near-Real-Time Detection of Insect Outbreaks in Urban Trees Using a PlanetScope Time Series. *Forests*, *15*(12), 2261. https://doi.org/10.3390/f15122261

Goetz, S. J., Fiske, G. J., & Bunn, A. G. (2006). Using satellite time-series data sets to analyze fire disturbance and forest recovery across Canada. *Remote Sensing of Environment*, *101*(3), 352–365. https://doi.org/10.1016/j.rse.2006.01.011

Gouveia, C., DaCamara, C. C., & Trigo, R. M. (2010). Post-fire vegetation recovery in Portugal based on spot/vegetation data. *Natural Hazards and Earth System Sciences*, *10*(4), 673–684. https://doi.org/10.5194/nhess-10-673-2010

Guirguis, K., Hatchett, B., Clemesha, R., Aguilera, R., Gershunov, A., Campbell, I., Cayan, D., & Merrifield, M. (2025). Compound atmospheric drivers of the catastrophic 2025 Los Angeles urban firestorm. *Npj Natural Hazards*, *2*(1), 103. https://doi.org/10.1038/s44304-025-00155-7

Hilbert, D., Roman, L., Koeser, A., Vogt, J., & Van Doorn, N. (2019). Urban Tree Mortality: A Literature Review. *Arboriculture & Urban Forestry*, *45*(5). https://doi.org/10.48044/jauf.2019.015

João, T., João, G., Bruno, M., & João, H. (2018). Indicator-based assessment of post-fire recovery dynamics using satellite NDVI time-series. *Ecological Indicators*, *89*, 199–212. https://doi.org/10.1016/j.ecolind.2018.02.008

Kenny, R., Johns, J., Pawlak, C., Fricker, A., Yost, J., & Ritter, M. (2026). Urban trees and structure loss in the 2025 Eaton and Palisades fires. *Urban Forestry & Urban Greening*, *121*, 129470. https://doi.org/10.1016/j.ufug.2026.129470

Key, C. H., & Benson, N. C. (2006). *Landscape Assessment (LA)*. United States Forest Service. https://research.fs.usda.gov/download/treesearch/24066.pdf

Lausch, A., Erasmi, S., King, D., Magdon, P., & Heurich, M. (2016). Understanding Forest Health with Remote Sensing -Part I—A Review of Spectral Traits, Processes and Remote-Sensing Characteristics. *Remote Sensing*, *8*(12), 1029. https://doi.org/10.3390/rs8121029

Leisenheimer, L., Wellmann, T., Jänicke, C., & Haase, D. (2024). Monitoring drought impacts on street trees using remote sensing—Disentangling temporal and species-specific response patterns with Sentinel-2 imagery. *Ecological Informatics*, *82*, 102659. https://doi.org/10.1016/j.ecoinf.2024.102659

Los Angeles County. (2025). *Palisades and Eaton Dissolved Fire Perimters (2025)* [Dataset]. https://data.lacounty.gov/maps/ad51845ea5fb4eb483bc2a7c38b2370c/about

Love, N. L. R., Nguyen, V., Pawlak, C., Pineda, A., Reimer, J. L., Yost, J. M., Fricker, G. A., Ventura, J. D., Doremus, J. M., Crow, T., & Ritter, M. K. (2022). Diversity and structure in California's urban forest: What over six million data points tell us about one of the world's largest urban forests. *Urban Forestry & Urban Greening*, *74*, 127679. https://doi.org/10.1016/j.ufug.2022.127679

McPherson, E. G., Xiao, Q., Van Doorn, N. S., De Goede, J., Bjorkman, J., Hollander, A., Boynton, R. M., Quinn, J. F., & Thorne, J. H. (2017). The structure, function and value of urban forests in California communities. *Urban Forestry & Urban Greening*, *28*, 43–53. https://doi.org/10.1016/j.ufug.2017.09.013

Minařík, R., Langhammer, J., & Lendzioch, T. (2020). Automatic Tree Crown Extraction from UAS Multispectral Imagery for the Detection of Bark Beetle Disturbance in Mixed Forests. *Remote Sensing*, *12*(24), 4081. https://doi.org/10.3390/rs12244081

Mitri, G. H., & Gitas, I. Z. (2013). Mapping post-fire forest regeneration and vegetation recovery using a combination of very high spatial resolution and hyperspectral satellite imagery. *International Journal of Applied Earth Observation and Geoinformation*, *20*, 60–66. https://doi.org/10.1016/j.jag.2011.09.001

Pausas, J. G., Keeley, J. E., & Schwilk, D. W. (2017). Flammability as an ecological and evolutionary driver. *Journal of Ecology*, *105*(2), 289–297. https://doi.org/10.1111/1365-2745.12691

Pawlak, C. C., Love, N. L. R., Yost, J. M., Fricker, G. A., Doremus, J. M., & Ritter, M. K. (2023). California's native trees and their use in the urban forest. *Urban Forestry & Urban Greening*, *89*, 128125. https://doi.org/10.1016/j.ufug.2023.128125

Peña-Molina, E., Moya, D., Marino, E., Tomé, J. L., Fajardo-Cantos, Á., González-Romero, J., Lucas-Borja, M. E., & De Las Heras, J. (2024). Fire Vulnerability, Resilience, and Recovery Rates of Mediterranean Pine Forests Using a 33-Year Time Series of Satellite Imagery. *Remote Sensing*, *16*(10), 1718. https://doi.org/10.3390/rs16101718

Planet Team. (2026). *Planet Application Program Interface: In Space for Life on Earth* [Dataset]. https://api.planet.com

Pysal Developers. (2018). *Spreg.GM_Error_Het* [Computer software]. https://spreg.readthedocs.io/en/latest/generated/spreg.GM_Error_Het.html

Rodrigues, M., De La Riva, J., Domingo, D., Lamelas, T., Ibarra, P., Hoffrén, R., & García-Martín, A. (2024). An empirical assessment of the potential of post-fire recovery of tree-forest communities in Mediterranean environments. *Forest Ecology and Management*, *552*, 121587. https://doi.org/10.1016/j.foreco.2023.121587

Ryu, J.-H., Han, K.-S., Hong, S., Park, N.-W., Lee, Y.-W., & Cho, J. (2018). Satellite-Based Evaluation of the Post-Fire Recovery Process from the Worst Forest Fire Case in South Korea. *Remote Sensing*, *10*(6), 918. https://doi.org/10.3390/rs10060918

SelecTree. (2025). *SelecTree: A Tree Selection Guide* [Web Application]. https://selectree.calpoly.edu/

Tanase, M., De La Riva, J., Santoro, M., Pérez-Cabello, F., & Kasischke, E. (2011). Sensitivity of SAR data to post-fire forest regrowth in Mediterranean and boreal forests. *Remote Sensing of Environment*, *115*(8), 2075–2085. https://doi.org/10.1016/j.rse.2011.04.009

U.S. Census Bureau. (2020). *Population, 2020, Dicennial Census* [Computer software].

Ventura, J., Pawlak, C., Honsberger, M., Gonsalves, C., Rice, J., Love, N. L. R., Han, S., Nguyen, V., Sugano, K., Doremus, J., Fricker, G. A., Yost, J., & Ritter, M. (2024). Individual tree detection in large-scale urban environments using high-resolution multispectral imagery. *International Journal of Applied Earth Observation and Geoinformation*, *130*, 103848. https://doi.org/10.1016/j.jag.2024.103848

Xiao, Q., & McPherson, E. G. (2005). Tree health mapping with multispectral remote sensing data at UC Davis, California. *Urban Ecosystems*, *8*(3–4), 349–361. https://doi.org/10.1007/s11252-005-4867-7

Ziter, C. D., Pedersen, E. J., Kucharik, C. J., & Turner, M. G. (2019). Scale-dependent interactions between tree canopy cover and impervious surfaces reduce daytime urban heat during summer. *Proceedings of the National Academy of Sciences*, *116*(15), 7575–7580. https://doi.org/10.1073/pnas.1817561116

4.6 Appendix

Appendix 4A. Distribution of dNBR values for all inside-perimeter trees, combining Altadena (Eaton Fire, green) and Pacific Palisades (Palisades Fire, blue). dNBR was calculated using Landsat 8/9 surface reflectance imagery acquired January 6 (pre-fire) and January 14, 2025 (post-fire) and scaled by a factor of 1000 (Key and Benson, 2006). Blue dashed lines indicate study-specific severity class boundaries, defined as the 20th, 40th, 60th, and 80th percentiles of the inside-perimeter dNBR distribution, producing five equal-frequency classes (low, moderate-low, moderate, moderate-high, and high severity). Quintile-based breaks were used in place of standard Key and Benson (2006) thresholds, which were calibrated for wildland fires and produced no high-severity classifications in this urban dataset despite both fires being among the most destructive in California history (Cansler and McKenzie, 2012).

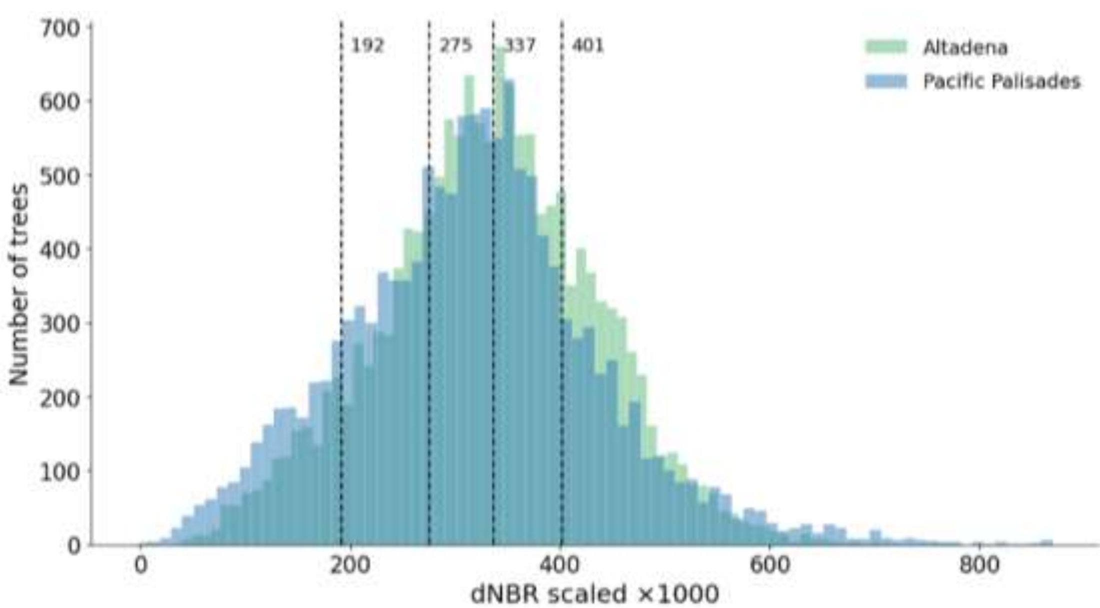

Appendix 4B. Sensitivity of burn-severity classification to dNBR window size. Single-pixel dNBR, 3×3 mean dNBR, and 6×6 mean dNBR were each divided into five study-specific quintile classes. Separation among severity classes was evaluated using Kruskal-Wallis tests on April 2025 and April 2026 anomaly z-scores, and by comparing the April 2026 mean anomaly z-score gap between the lowest- and highest-severity classes. The 3×3 mean dNBR metric produced the strongest separation at both timepoints and the largest April 2026 severity gap,

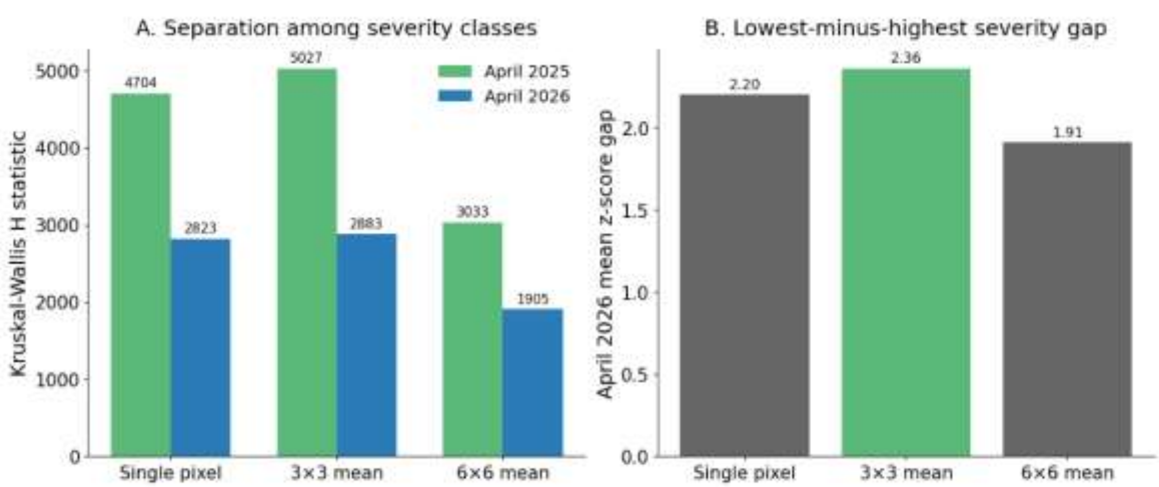

Appendix 4C. Sensitivity of spatial error model results to the k-nearest-neighbor spatial weights definition. Models were refit using k = 4, 8, 12, and 16 neighbors. The top row shows the estimated 3×3 dNBR coefficient and 95% confidence interval for each recovery outcome. The bottom row shows Moran’s I of the filtered residuals. Asterisks indicate significant residual spatial autocorrelation.

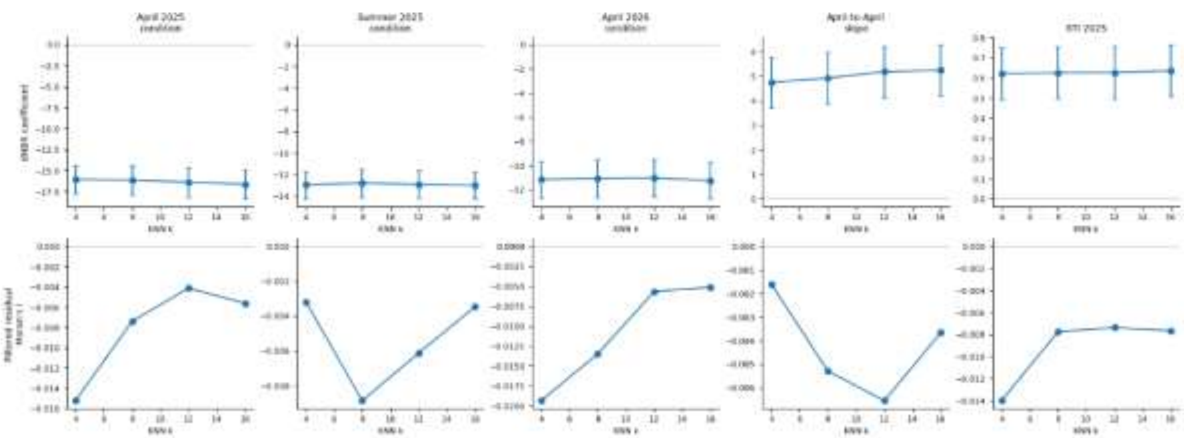

Appendix 4D. Holm-significant pairwise species contrasts for adjusted April 2026 recovery condition. Points show adjusted differences in April 2026 anomaly z-score between species pairs from the spatial species model, and horizontal bars show 95% confidence intervals. Only contrasts that remained significant after Holm correction are shown. Positive values indicate that species A had a higher adjusted April 2026 anomaly z-score than species B after accounting for 3×3 dNBR, UF_code, city, and spatial autocorrelation.

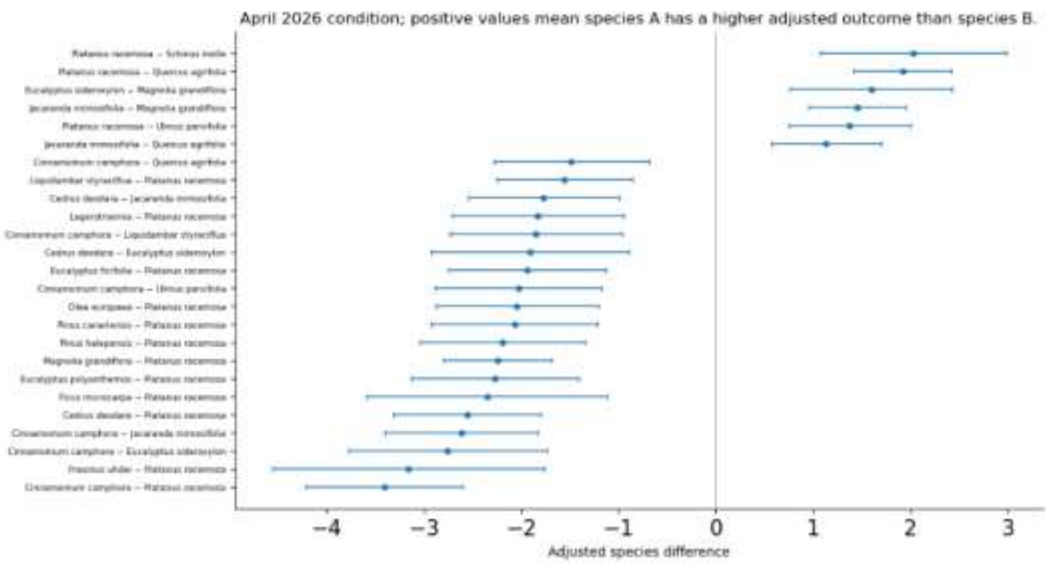

Appendix 4E. Relationship between dNBR burn severity and pre-fire canopy structure at three spatial window scales. Canopy cover fraction (bottom row) was computed from the 1-m binary canopy rasters developed in Chapter 2, using square windows centered on each tree centroid that match the Landsat footprints used to derive dNBR: 30 m (single pixel), 90 m (3x3), and 180 m (6x6). Tree detection counts (top row) reflect the number of individual crowns of trees used in this dataset (canopy area > 54m^2) from the same-scale windows. Each point is one tree inside the fire perimeter. Canopy cover shows a modest positive association with burn severity (r = 0.14 to 0.21), consistent with denser pre-fire canopy providing more combustible material, but the relationship is weak. Tree density shows no meaningful association with dNBR (r = -0.03 to -0.04).

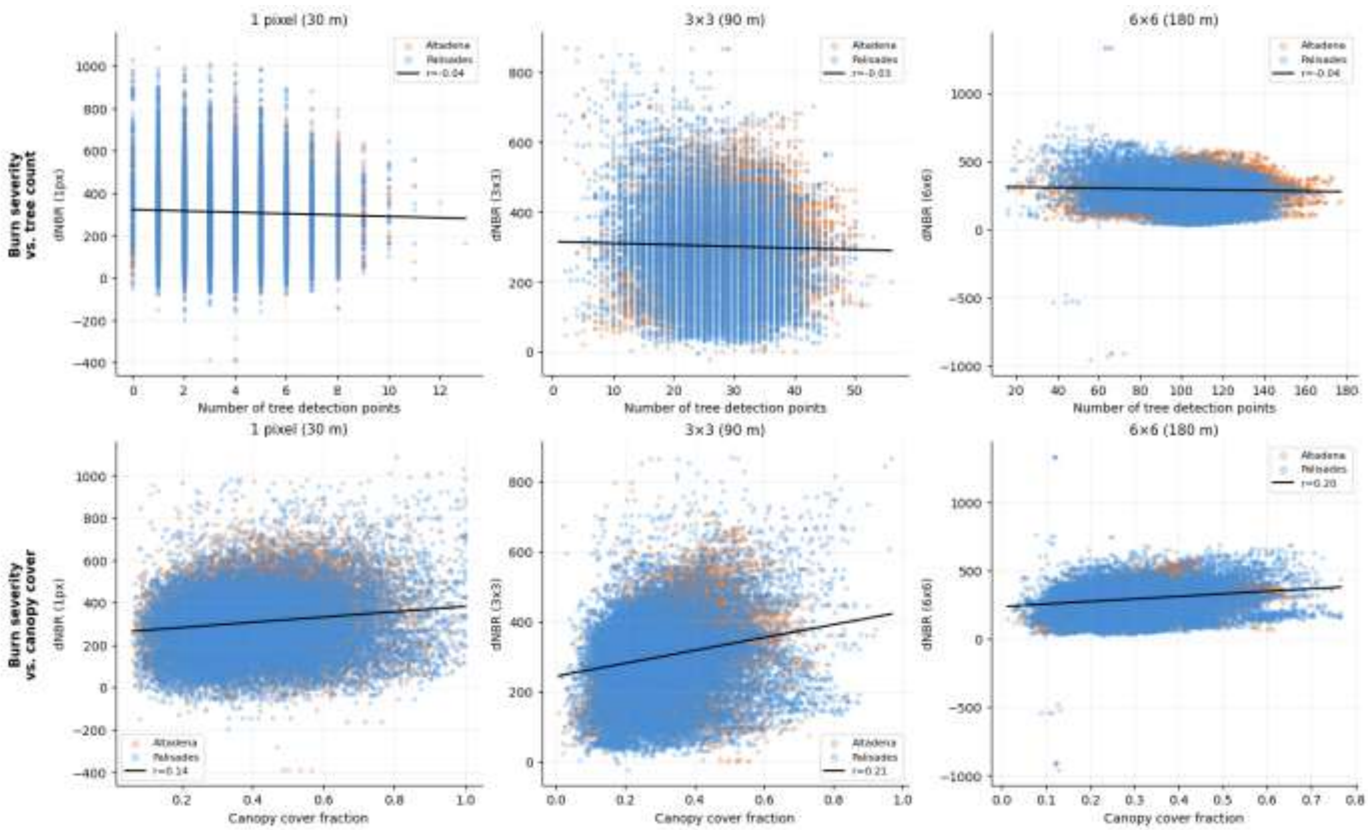

Chapter 5. Conclusion

Urban forest management depends on timely information about where canopy is changing, which trees are declining or being removed, and how forests respond to disturbance. Field-based monitoring remains essential, but it is costly, often limited to a subset of publicly managed trees, and difficult to repeat at the pace of urban development and canopy-goal reporting. Improving urban forest monitoring requires methods that can track change across public and private land, at both broad canopy and individual-tree scales, while providing information that is useful when management decisions are being made.

This dissertation addresses that need by combining high-spatial- and high-temporal-resolution datasets to track large-scale canopy change, detect tree loss at monthly scales, and monitor urban forest response to extreme stressors such as wildfire. Chapter 2 developed an error-adjusted canopy time series for California to evaluate broad canopy distribution and change while accounting for uncertainty in mapped estimates. Chapter 3 showed that repeated satellite imagery can be used to identify tree removals and phenology. Chapter 4 used repeated observations to track post-fire recovery of urban tree canopies and showed how recovery differed across burn severity, tree characteristics, cities, and property contexts after the Eaton and Palisades fires. The methods developed here support urban forest monitoring at scales that field assessment alone cannot reach. Used together, they help cities identify broad patterns of canopy change, separate real trends from mapping uncertainty, detect likely tree removals, and track recovery after disturbance. This information can support more realistic canopy goal tracking and help direct limited management resources. These approaches can be applied in other U.S. cities and more broadly where high-resolution imagery, repeated satellite observations, and tree-location data are available. The larger contribution is a shift in what urban forest monitoring can be: a continuous source of information that supports decisions as change occurs.